NASA/CR-97-206256

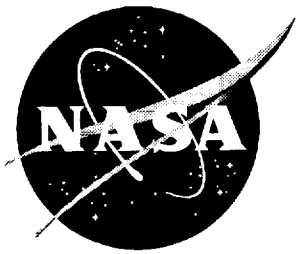

Novel Composites for Wing and Fuselage Applications

Speedy Nonlinear Analysis of Postbuckled Panels in Shear (SNAPPS)

Dave Sharp and Larry Sobel

October 1997

The NASA STI Program Office . . . in Profile

Since its founding, NASA has been dedicated to the advancement of aeronautics and space science. The NASA Scientific and Technical Information (STI) Program Office plays a key part in helping NASA maintain this important role.

The NASA STI Program Office is operated by Langley Research Center, the lead center for NASA's scientific and technical information. The NASA STI Program Office provides access to the NASA STI Database, the largest collection of aeronautical and space science STI in the world. The Program Office is also NASA's institutional mechanism for disseminating the results of its research and development activities. These results are published by NASA in the NASA STI Report Series, which includes the following report types:

- TECHNICAL PUBLICATION. Reports of completed research or a major significant phase of research that present the results of NASA programs and include extensive data or theoretical analysis. Includes compilations of significant scientific and technical data and information deemed to be of continuing reference value. NASA counter-part or peer-reviewed formal professional papers, but having less stringent limitations on manuscript length and extent of graphic presentations.

- TECHNICAL MEMORANDUM. Scientific and technical findings that are preliminary or of specialized interest, e.g., quick release reports, working papers, and bibliographies that contain minimal annotation. Does not contain extensive analysis.

- CONTRACTOR REPORT. Scientific and technical findings by NASA-sponsored contractors and grantees.

- CONFERENCE PUBLICATION. Collected papers from scientific and technical conferences, symposia, seminars, or other meetings sponsored or co-sponsored by NASA.

- SPECIAL PUBLICATION. Scientific, technical, or historical information from NASA programs, projects, and missions, often concerned with subjects having substantial public interest.

- TECHNICAL TRANSLATION. English-language translations of foreign scientific and technical material pertinent to NASA's mission.

Specialized services that help round out the STI Program Office's diverse offerings include creating custom thesauri, building customized databases, organizing and publishing research results . . . even providing videos.

For more information about the NASA STI Program Office, see the following:

- Access the NASA STI Program Home Page at ***http://www.sti.nasa.gov***

- Email your question via the Internet to help@sti.nasa.gov

- Fax your question to the NASA Access Help Desk at (301) 621-0134

- Phone the NASA Access Help Desk at (301) 621-0390

- Write to:
  NASA Access Help Desk
  NASA Center for AeroSpace Information
  800 Elkridge Landing Road
  Linthicum Heights, MD 21090-2934

NASA/CR-97-206256

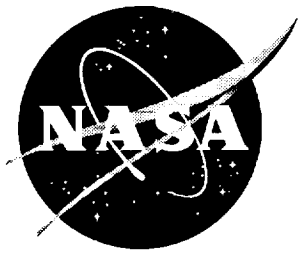

Novel Composites for Wing and Fuselage Applications

Speedy Nonlinear Analysis of Postbuckled Panels in Shear (SNAPPS)

Dave Sharp and Larry Sobel
Northrop Grumman Corporation, Bethpage, New York

National Aeronautics and
Space Administration

Langley Research Center
Hampton, Virginia 23681-2199

Prepared for Langley Research Center
under Contract NAS1-18784

October 1997

Available from the following:

NASA Center for AeroSpace Information (CASI)
800 Elkridge Landing Road
Linthicum Heights, MD 21090-2934
(301) 621-0390

National Technical Information Service (NTIS)
5285 Port Royal Road
Springfield, VA 22161-2171
(703) 487-4650

FOREWORD

This Final Technical Report covers work performed primarily under Contract No. NAS1-18784 in Task 6 — Computational Methods Testbed Validation. The work was completed by the Northrop Grumman Corporation under the sponsorship of NASA Langley Research Center, Hampton, Virginia 23681-0001. H. B. Dexter was the NASA LaRC Contracting Officer Technical Representative, and J. Housner was the Technical Advisor. J. Suarez was Northrop Grumman's Program Manager for most of the contract, and A. Pifko succeeded him. The bulk of the contract work for all six tasks was performed under the direction of S. Dastin, now a retired consultant to Northrop Grumman.

ACKNOWLEDGMENTS

This report describes work done in part by the Advanced Composite Group of the former Grumman Corporation in the years 1987 through 1993, and is dedicated to the members of that group.

The authors are especially indebted to J. Visconti who performed the initial sizing and stress analysis of the test panels, devised the test program, and wrote the test report; to W. Egensteiner for performing the exhaustive task of reducing the test data, and for developing an expression for Kuhn's diagonal tension factor in terms of panel stress resultants; to G. Flanagan for his valuable counsel and for furnishing material properties and thicknesses; to Bob Schwarz for his expertise in obtaining the moiré photographs of the test panels and deriving the out-of-plane displacement contours from them, and to E. Fiorelli of Cooper Union for his skillful assistance in preparing figures and tables.

We are also grateful to H. B. Dexter of NASA LaRC, who, on reviewing this report, directed our attention to the work of Minguet and O'Brien [1996], which gives some much-needed confirmation of the failure criterion used in this report.

ABSTRACT

This report presents a simple and rapid method for predicting the nonlinear response and stiffener separation of postbuckled, flat, composite, shear panels. The method uses modular, "strength-of-materials-type" models. The disbonding failure is hypothesized as being due to a stress concentration in the surface layer of the skin immediately under the toe of the attached flange. The highly local character of this stress, which renders a finite element analysis impractical, enables a simple analysis to be developed. The maximum principal tensile stress in the skin surface layer under the toe is determined, and failure is said to occur when this stress reaches the mean transverse tensile strength of the layer.

The analysis consists of a number of closed-form equations that have been programmed into a *preliminary design* code called SNAPPS [Speedy Nonlinear Analysis of Postbuckled Panels in Shear], which rapidly predicts the panel's postbuckling response and failure load. SNAPPS was applied to three test panels with widely different geometries, laminates and stiffnesses. At the test failure loads, the predictions of maximum principal tensile stress at the toe vary from 8% below to 20% above the transverse tensile strength. The predicted failure loads range from 18% below to 25% above the test failure loads.

Using the B-basis allowable stress, which is 62% of the mean transverse tensile strength, the predicted allowable load for each panel was consistently found to be about half the test failure load. In view of the scatter experienced in matrix-dominated modes of failure in composite materials, these are reasonable, but not excessively conservative predictions.

A new method was developed for determining experimental buckling loads for shear panels. The method uses the "diagonal tension factor", k, for which a closed-form expression was derived. An unambiguous estimate of the initial buckling load can be obtained by plotting k against load, and extrapolating back to the load at which k is zero.

The report also gives design recommendations for reducing the maximum principal tensile stress at the toe, thereby increasing the panel's load carrying capacity. Results from an approximate but accurate parametric analysis imply this is best accomplished by decreasing the skin thickness, increasing the flange width, and by decreasing the bending stiffness of the combined stack of the skin and attached flange.

CONTENTS

SECTION 1

INTRODUCTION

There is a need for a simple, rapid prediction of stiffener separation in postbuckled, flat, composite shear panels in which the stiffeners are bonded to the skin. Analysis and test evidence point to the failure being caused by a highly localized stress in the skin immediately under the toe of the attached flange of the stiffener. To locate and quantify this stress, a finite element model would have to be exquisitely detailed and may not be practical in real terms, particularly if it has to be re-done at each design change. Fortunately, the extreme localization of the stress enables the development of a simplified method of analysis.

1.1 Methodology

The analysis described in this report began with the premise that the physical behavior of a highly buckled, stiffened shear panel could be described by simple equations culled from standard texts. The challenge was to get a physical understanding of the panel behavior as it progressed into the postbuckled regime. Two key aids to this understanding came with a series of panels tested by Grumman [Visconti, 1988], followed by a detailed finite element analysis [Sobel and Sharp, 1994] of one test panel, denoted as C1. That analysis used the STAGS code [Almroth, et al., 1982] to perform a buckling analysis and then a nonlinear analysis up to the test failure load of fifteen times initial buckling.

The analysis developed here consists of a number of closed-form equations that can easily be used in a "hand analysis". For expediency, they have been programmed using the True Basic language into a code called SNAPPS [Speedy Nonlinear Analysis of Postbuckled Panels in Shear], which rapidly predicts the postbuckling response and failure load of the panel. The model used is similar to that of Tsai [1983], where strips of the skin and stiffener parallel to the diagonal tension field are idealized as beams and tie-rods. We depart from Tsai's analysis in the derivation of the out-of-plane displacement, in the idealization of the combined skin and flange, and in the failure criterion. For the latter, we compute a highly localized stress in the skin immediately under the toe of the flange and relate it to the transverse tensile strength of the skin ply, while Tsai uses an overall pull-off load which is geometry-dependent and has to be determined empirically for each configuration.

- **Development Phases**

The development of SNAPPS can be divided into three phases:

The first phase drew heavily on the methods of Kuhn [1952], Wagner (described in Kuhn [1952]), and Ranalli and Bunce [1977], for the analysis of stiffened aluminum panels in which the stiffeners were riveted to the panel. Ranalli and Bunce's analysis focused on overall pull-off loads between the skin and flange. This concept was carried over to a test program for stiffened composite panels, test coupons, and elements, as described by Visconti [1988]. Their analysis, when modified to include the twisting moment between the skin and flange in addition to the pull-off load [Sharp and Sobel, 1989] gave satisfactory agreement with test failure loads, but required element tests specific to the test panel, and these showed adhesive failures. In contrast, the panel tests revealed intra-ply failures of the skin immediately under the toe of the flange, as evidenced by the pull-out of fibers from the surface layer of the skin. This observation led to the realization that the flatwise tensile strength in the laminate was the key to the failure.

The second phase began with an analysis of the through-the-thickness tensile stress in the skin immediately under the toe (Sharp [1989] and Sobel [1990]). The model used was developed during Grumman's CTSA program [Cacho-Negrete, 1978], and consists of two beams, one representing the skin and the other the attached flange, joined by an elastic foundation. The analysis revealed peel stress concentrations under the heel and toe of the flange. These stresses die away within short distances, and do not significantly interact with each other, enabling a great simplification in the equations. In this second phase, the stress state in the postbuckled skin was assumed to be given by Kuhn's empirical theory of incomplete diagonal tension, and the width of the buckle was determined empirically from moire´ fringe patterns.

The third phase took account of the immense amount of data available from the STAGS analysis of panel C1, Sobel [1990], together with a more detailed interpretation of strain gauge readings and moire´ fringe patterns for the three test panels. From these, it was found that a reasonably accurate estimate of the stress resultants in the *flat* panel after buckling could be obtained by assuming (1) a diagonal tension angle of 45° and, (2) that the compressive stress resultant reaches a value equal to the buckling shear flow and does not increase further. The buckle width could now be determined analytically by isolating one buckle and imposing equilibrium on the out-of-plane components of the membrane stress

resultants. All of the empiricism in the earlier analysis was thereby removed.

- **Failure Criterion**

It is hypothesized that the failure is located in the skin layers immediately under the toe of the flange, and is caused by the maximum principal tensile stress in the layers (Sharp [1989] and Sobel [1990]). This stress is a combination of three stresses, all of which peak at the toe, in the outermost skin layer on the stiffener side of the panel whose fibers are normal to the diagonal tension fold. They are (1) an extremely localized peel stress, (2) an interlaminar shear stress, and (3) an inplane tensile stress in the direction of the diagonal tension fold. The combination of these three stresses makes the toe location critical: at the heel, the peel stress is higher, but the combination of the three stresses gives a lower principal stress there. The failure criterion adopted here equates the maximum principal tensile stress based on these three components to the transverse tensile strength of the skin layers.

- **Assessment of Method**

An assessment of the accuracy of the simplified method is achieved by applying the SNAPPS code, described in Appendix M, to the three panels manufactured and tested by Grumman [Visconti, 1988]. The predictions are compared to those of a nonlinear STAGS finite element analysis [Sobel & Sharp, 1994], and to strain gauge and moire´ fringe readings taken during the tests. SNAPPS predictions for the out-of-plane displacement, wavelengths, and skin stress resultants were found to agree well with both test measurements and STAGS results. While the intensely localized state of stress at the toe cannot be directly compared to the STAGS results, nor can it be determined from the test results, relating its predicted maximum principal tensile value to the transverse tensile strength of the skin layers provides estimations of the panel strength that are in reasonably good agreement with the test failure loads.

1.2 Structure of Report

This report consists of a number of sections and appendices, with details of the derivations of the governing equations used in SNAPPS being relegated to the appendices. The governing equations and computational procedure are summarized in Section 2, and coded in appendix M. Section 3 compares SNAPPS predictions for the three test panels with test

measurements and STAGS results, and Section 4 gives conclusions, lessons learned and recommendations.

The key elements of SNAPPS involve calculation of the following:

- The stress resultant state in the postbuckled skin (Appendix C),
- The buckle width and length (Appendix D),
- The maximum out-of-plane displacement (Appendix E),
- The "tie-rod" analysis of a strip of skin (Appendix F),
- The skin bending moment at the toe of the flange from compatibility of rotation between the tie-rod model and the combined skin and flange model at the toe of the flange (Appendix G),
- The maximum shear stress at the toe (Appendix H),
- The tensile peel stress between the skin and the toe of the flange, based on a simplified "coupled beams on an elastic foundation" analysis (Appendix I),
- The inplane transverse tensile stress in the critical ply, which is the outermost skin ply whose fibers are normal to the diagonal tension fold (Appendix K),
- The combining of the peel stress, the maximum shear stress and the transverse tensile stress under the toe to obtain the maximum principal tensile stress in the surface layer of the skin (Appendix L),
- Failure, which is identified as value of the applied shear flow at which the maximum principal tensile stress reaches the transverse tensile strength of the critical ply (Appendix L).

SECTION 2

DESCRIPTION OF ANALYSIS & COMPUTATIONAL PROCEDURE

2.1 Description of Analysis

The analysis described here is based on four major insights gained from the test results and the STAGS analysis:

(1) That the angle of the diagonal tension fold remained almost constant at between 45^{o} and 48^{o} to the normal to the stiffener.

(2) That the stress resultants in the skin after buckling could be simply described in the terms of the applied shear flow and the buckling shear flow without recourse to empiricism.

(3) That the buckles grew steadily in the skin as the load increased above buckling by narrowing the width of the buckle. This observation identified the aspect ratio and maximum out-of-plane displacement of the buckle as key parameters in the analysis.

(4) That the failure was localized under the toe of the attached flange of the stiffener, enabling a simplification of the CTSA [Cacho-Negrete 1978] analysis to be used to calculate the tensile peel stress in the skin under the toe.

Based on these insights, a simplified computational procedure was developed that uses strength-of-materials-type models. The first step in the procedure is to calculate the buckle width and length as a function of the applied shear flow. Next, the maximum out-of-plane displacement is computed. From this, the bending moment and transverse shear force in the skin immediately under the toe of the stiffener flange are determined. With these internal loads at the toe region, the analysis proceeds to the calculation of three stresses, τ_{xz}, σ_z and σ_x, all of which peak at the surface of the skin under the toe of the flange. They are defined in the xz plane, where x is in the direction of the diagonal tension fold and z is normal to the original plane of the skin. The shear stress, τ_{xz}, arises from the transfer of part of the diagonal tension load from the skin into the flange, σ_z is a tensile peel stress acting normal to the skin between the skin and the flange, and σ_x is a tensile stress in the outermost ply on the stiffener side of the panel whose fibers are normal to the direction of the diagonal tension fold. σ_x is induced by the membrane load and bending moment in the skin immediately under the toe. Combining these stresses

enables calculation of the maximum principal tensile stress in the critical ply. Comparing this to the transverse failure stress of the ply allows a prediction of failure to be made.

2.2 Governing Equations & Computational Procedure

In what follows, only the main equations are given. Detailed derivations of the equations are in the referenced appendices, and a flow chart of the various steps in the analysis procedure is given in Figure 1.

Note that the input to SNAPPS requires the membrane and bending stiffnesses of the skin, flange and the combined skin and flange (where they are bonded together to form a single stack). These have to be obtained from the layer properties and stacking sequences, using an independent computer code. We used MACLAMINATE [Flanagan, 1991], but any similar capability will serve.

- **Skin Stress Resultants**

Next, the principal stress resultants in the buckled skin, except under the toe of the flange, are determined from Appendix C as follows:

$$N_1 = 2q - q_{cr} \qquad \text{Eq. (7) of Appendix C}$$

$$N_2 = q_{cr} \qquad \text{Eq. (5) of Appendix C}$$

where N_1 and N_2 are principal tensile stress resultants parallel and normal, respectively to the direction of the diagonal tension folds. N_1 is positive when it is in tension and N_2 is positive when it is in compression. In these equations, q is the applied shear flow, and q_{cr} is the shear flow at which the skin buckles (q and q_{cr} are always positive in this report). The buckling shear flow q_{cr} may be estimated from standard procedures for orthotropic plates, such as the Grumman Advanced Composites Structures Manual (which is based on Seydel [1933]) or Housner and Stein [1975]. If available, the test buckling load or a STAGS (or similar) prediction can be used.

- **Buckle Kinematics**

The length, L, of the diagonal tension fold, measured along the fold between the toes of the attached flanges of the stiffeners, see Figure 1 of Appendix D, is given by

$$L = b_{tt}/\cos\alpha$$

where

b_{tt} = the toe-to-toe distance between the attached flanges of the stiffeners, measured normal to the stiffener direction.

and

α = the angle between the diagonal tension fold and the normal to the stiffener direction. It is assumed that α is constant at 45°.

The width of the buckle, c in Figure 1 of Appendix D, is calculated from

$$c = \sqrt{1.5}\, L \left(\frac{\sqrt{\frac{N_2}{N_1}}}{1+\sqrt{\frac{N_2}{N_1}}} \right) \qquad \text{Eq. (7) of Appendix D}$$

The projected length of the buckle along the stiffener axis, L_b, is then

$$L_b = \frac{c}{\cos \alpha} \qquad \text{Eq. (8) of Appendix D}$$

- **Maximum Out-of-Plane Displacement**

The amplitude of the out-of-plane displacement, δ_{max}, is next obtained from

$$\delta_{max} = \frac{2}{\pi} \sqrt{Lc \left(\frac{q-q_{cr}}{Gt} \right)} \qquad \text{Eq. (6) of Appendix E}$$

where Gt is the in-plane shear stiffness of the skin, referred to axes parallel and normal to the stiffener direction.

- **Loads in the Skin at the Toe of the Attached Flange**

The analysis now obtains the bending moment, M_{toe}, and the transverse shear, W_{toe}, in the skin immediately under the toe of the flange. To do this, a "tie-rod" model of the skin is connected to a beam model representing the combined flange and skin between the stiffener centerline and the toe of the flange. This is done by invoking rotational compatibility at the common ends of the models. Both models are of unit width and lie along the diagonal tension fold.

The "tie-rod" model of the skin is described in Appendix F. The beam model of the combined skin and flange, which contains the total stacking sequence of the flange, a layer of adhesive and the skin, is described in

Appendix G. It is assumed to be cantilevered at the stiffener centerline, and loaded at it's tip by W_{toe} and a moment given by $(M_{toe} - N_{1toe}z)$ The second term, $N_{1toe}z$, represents the moment due to the membrane load in the unbuckled skin at the toe being offset from the neutral axis of the combined section by an amount, z, (see Figure 1 of appendix G) and is calculated from

$$N_{1toe} = q \qquad \text{Eq. (10) of Appendix C}$$

and

$$z = \frac{Et_{fr}\left(t_s + t_a + \frac{t_f}{2}\right) + Et_{sr}\frac{t_s}{2}}{Et_{fr} + Et_{sr}} - \frac{t_s}{2} \qquad \text{Eq. (6) of Appendix G}$$

where

t_s = thickness of the skin
t_f = thickness of the flange
t_a = thickness of the adhesive layer between the skin and flange
Et_{sr} = membrane stiffness of the skin
Et_{fr} = membrane stiffness of the flange.

Et_{sr} and Et_{fr} are measured in the direction of the diagonal tension fold (as denoted by the subscript r).

M_{toe} is given by

$$M_{toe} = \frac{\frac{\pi \delta_{max}}{L}\left(1 - \frac{L_{fr}^2 N_1}{2 D_{totr}}\right) + \frac{L_{fr} q z}{D_{totr}}}{\left(\frac{\lambda - \pi/L}{N_1} + \frac{L_{fr}}{D_{totr}} + \frac{\pi}{2L}\frac{L_{fr}^2}{D_{totr}}\right)} \qquad \text{Eq. (10) of Appendix G}$$

and W_{toe} by

$$W_{toe} = \frac{\pi}{L}\left(N_1 \delta_{max} + M_{toe}\right) \qquad \text{Eq. (15) of Appendix G}$$

where

$$\lambda = \sqrt{\frac{N_1}{D_{sr}}}$$

and

$L_{fr} = L_f/\cos\alpha$, where L_f = the width of the attached flange of the stiffener, measured normal to the stiffener direction

D_{sr} = the bending stiffness of the skin about the inplane normal to the diagonal tension fold

D_{totr} = the bending stiffness of the combined skin and flange (where they are bonded together to form a single stack). D_{totr} is measured about the inplane normal to diagonal tension fold.

- **Calculation of Stresses in the Skin at the Toe**

The analysis now proceeds to the calculation of the three stresses which combine to give the maximum principal tensile stress at the surface of the skin under the toe. The stresses are defined in the xz plane, where x is in the direction of the diagonal tension fold and z is normal to the original plane of the skin, and are as follows:

The shear stress τ_{xz} at the interface between the skin and the flange is calculated first. It arises from the transfer of part of the membrane load from the skin into the flange and peaks in the surface ply under the toe. From Appendix H, the maximum shear stress, which occurs under the toe, is given by

$$\tau_{xz} = N_{1toe} K \frac{Et_{fr}}{Et_{fr} + Et_{sr}}$$ Eq. (5) of Appendix H

where

$$K = \sqrt{\phi_{xz}\left(\frac{1}{Et_{fr}} + \frac{1}{Et_{sr}}\right)}$$ Eq. (4) of Appendix H

and

$$\phi_{xz} = \frac{1}{\frac{1}{2}\left(\frac{t}{G_{13}}\right)_{flange} + \left(\frac{t}{G}\right)_{adhesive} + \left(\frac{t}{G_{13}}\right)_{face} + \frac{1}{2}\left(\frac{t}{G}\right)_{core}}$$ Eq. (2) of Appendix J

In the equation for ϕ_{xz}, G denotes the shear modulus for the isotropic adhesive and core materials. For the tape layers, it is simplest to use G_{13} for all layers regardless of orientation, while for fabric layers $G_{13} = G_{12}$.

The peel stress σ_z is a tensile stress acting normal to the skin face between the skin and the flange. This stress has peaks at the toe and heel of the flange, but we are concerned only with the peak at the toe in this analysis. As described in Appendix I, σ_z can be conveniently subdivided into two parts: the first, σ_{z1}, is due directly to the moment M_{toe} and the transverse shear W_{toe} applied from the skin; and the second, σ_{z2}, is caused by the shear along the interface between the skin and flange acting at half the laminate thickness away from the midplane of each laminate. The two parts of the peel stress are given by

$$\sigma_z = \sigma_{z1} + \sigma_{z2}$$

where

$$\sigma_{z1} = \frac{2\beta}{(1 + D_{sr}/D_{fr})}(W_{toe} + \beta M_{toe})$$ Eq. (21) of Appendix I

and

$$\sigma_{z2} = C_n t_f \phi_z (F_1 + F_2)$$ Eq. (22) of Appendix I

where

$$\beta = \left(\frac{\phi_z}{4}\frac{D_{sr} + D_{fr}}{D_{sr} D_{fr}}\right)^{1/4}$$

$$C_n = \frac{N_{1toe} K^2}{2\phi_z}\frac{Et_{fr}}{Et_{fr} + Et_{sr}}$$

$$F_1 = \left(1 - \frac{K^2}{2\beta^2} + \frac{K^3}{2\beta^3}\right)\left(\frac{m^* D_{fr} K^4}{\phi_z} - 1\right)$$

$$F_2 = \frac{2\beta D_{fr}}{K}\left(\frac{D_{sr}/D_{fr} - t_s/t_f}{D_{fr} + D_{sr}}\right)$$

$$m^* = \frac{\phi_z}{D_{sr} D_{fr} K^4}\left(\frac{D_{sr} K^4 + \phi_z(1 + t_s/t_f)}{K^4 + 4\beta^4}\right)$$

and

$$\phi_z = \frac{1}{\frac{1}{2}\left(\frac{t}{E_3}\right)_{flange} + \left(\frac{t}{E}\right)_{adhesive} + \left(\frac{t}{E_3}\right)_{face} + \frac{1}{2}\left(\frac{t}{E}\right)_{core}}$$ Eq. (1) of Appendix J

In these equations, D_{fr} is the bending stiffness of the flange, measured about the normal to diagonal tension fold, t denotes laminate thickness, E is Young's modulus for the isotropic adhesive and core materials, and E_3 is the out-of-plane modulus for the flange and skin layers (by assuming transverse isotropy for tape layers, we may take $E_3 = E_2$, where E_2 is the layer transverse modulus

The tensile stress σ_x in the skin face is induced by the membrane stress resultant and bending moment in the skin immediately under the toe

of the flange. It acts in the direction of the diagonal tension fold, in the "critical ply". The critical ply is defined by the following criteria: it has to be on the stiffener side of the skin; it has to be put into tension, along the diagonal tension fold, by the transverse shear W_{toe} and the moment M_{toe} and; it's fibers are normal to the diagonal tension fold, i.e. σ_x acts normal to the fibers, and in the plane of, the critical ply. To be conservative, by using the highest possible value of σ_x, the critical ply is assumed to be at the surface of the skin. The force and bending moment are analyzed in Appendix G. The derivation of σ_x is given in Appendix K, and results in the following equation for σ_x:

$$\sigma_x = \frac{E_2}{(1-\nu_{12}\nu_{21})}\left\{(1-\nu_{12})(1+\nu_{sr})\frac{q}{Et_{sr}} + \frac{t_s}{2}\frac{M_{toe}}{D_{sr}}\right\} \quad \text{Eq. (7) of Appendix K}$$

where

ν_{sr} = the Poisson's ratio of the skin in the xy axis system ($\nu_{sr} = \nu_{xy}$ is defined according to $\nu_{xy} E_y = \nu_{yx} E_x$, where E_x and E_y are the engineering constants for the skin laminate),

and

E_1, E_2, and ν_{12} are the in-plane Young's moduli and Poisson's ratio for the face ply of the skin. (The subscript 1, when affixed to a material property, pertains to the fiber direction, and ν_{12} is defined according to $\nu_{21} E_1 = \nu_{12} E_2$).

- **Maximum Principal Tensile Stress**

The three stress components τ_{xz}, σ_z and σ_x are combined to give the following expression for the maximum principal tensile stress in the surface ply immediately under the toe:

$$\sigma_{mpt} = \left(\frac{\sigma_z+\sigma_x}{2}\right) + \sqrt{\left(\frac{\sigma_z-\sigma_x}{2}\right)^2 + (\tau_{xz})^2} \quad \text{Eq. (1) of Appendix L}$$

- **Failure Criterion**

Examination of photomicrographs of ply cross sections shows that for graphite/epoxy the placing of the fibers within such a section is random, and it is impossible to discern the orientation of the photographed section within the ply without other, external, clues. We may therefore assume transverse isotropy, and that the tensile strength at any orientation in the xz plane is equal to the transverse tensile strength F_2^{tu} of the layer.

Failure is assumed to occur when the maximum principal tensile stress in the skin immediately under the toe reaches the transverse tensile strength of the layer, i.e., when

$$\sigma_{mpt} = F_2^{tu} \qquad \text{Eq. (2) of Appendix L}$$

Failure of this layer constitutes failure of the joint, because cracking of the matrix allows fibers to be pulled out of the skin surface. This type of failure was observed on all of the panels tested.

The following values used in the analysis of the test panels are based on statistical analysis of 19 coupon test results for transverse tension of IM6/3501-6 graphite/epoxy tape, in the room temperature, ambient, moisture ("dry") condition [Shyprykevich, 1988]:

F_2^{tu} = Mean strength = 7150 psi
Standard Deviation = 1180 psi
"B-basis" allowable stress = 4460 psi

where the B-basis allowable strength is such that at least 90% of the transverse tensile strengths are expected to exceed the B-basis allowable value, with a confidence of 95%.

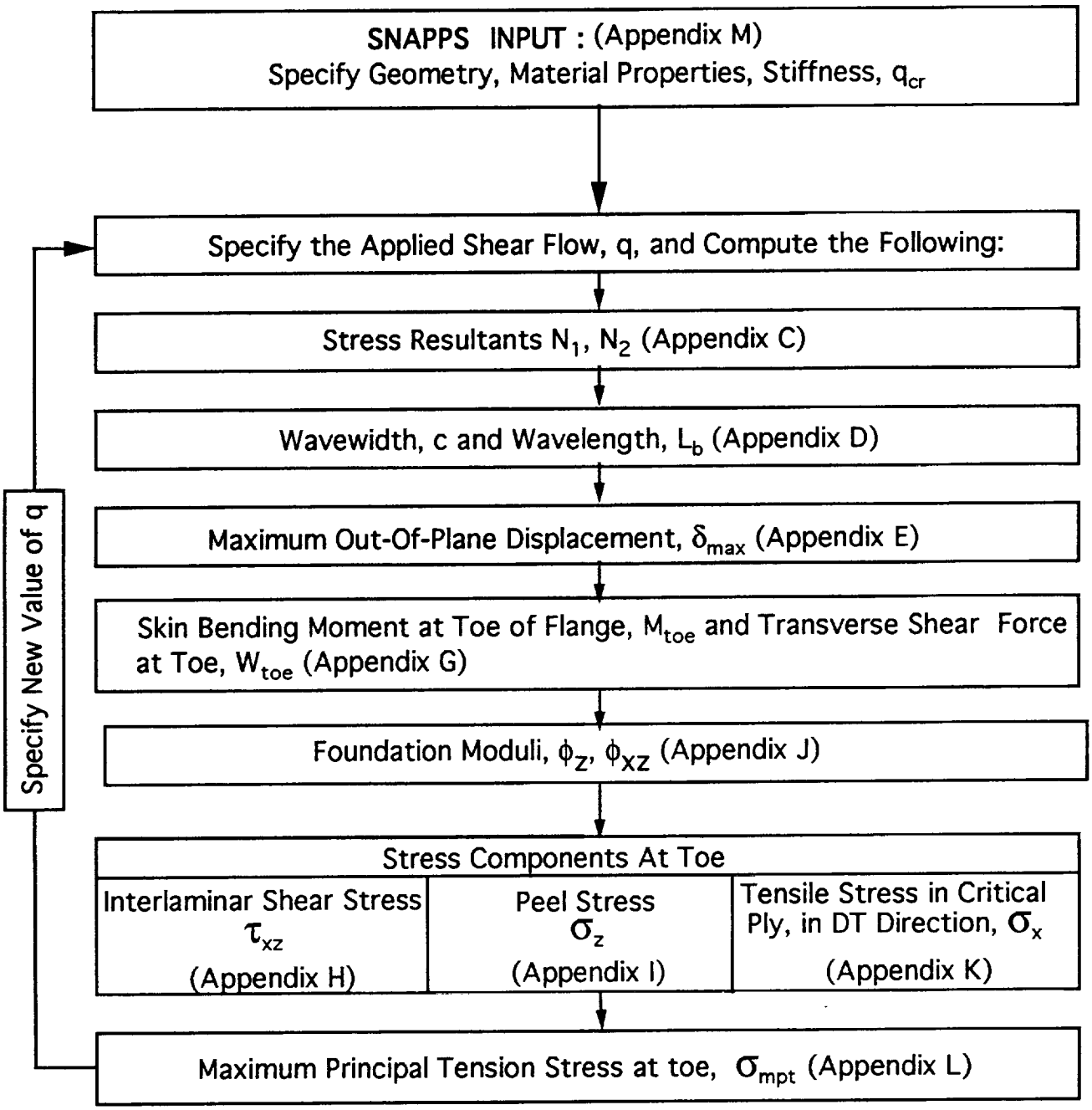

FIGURE 1 COMPUTATIONAL PROCEDURE

SECTION 3

RESULTS AND ASSESSMENT OF METHODOLOGY

The computational procedure described in Section 2 has been programmed, using the True Basic language, into a code called SNAPPS, (Appendix M), which has been applied to three, flat, stiffened, composite panels (A1, B1 and C1) tested at Grumman, as described in Appendix A. The current section presents results pertaining to the SNAPPS methodology, and assesses the accuracy of the SNAPPS predictions by comparing them to the panel test results and STAGS predictions for panel C1 [Sobel and Sharp, 1994].

3.1 Assessment of Basic Premises

The SNAPPS analysis is built around two basic premises: that the angle of diagonal tension, α, is 45° (for *flat* panels), and that the compressive stress resultant normal to the diagonal tension fold reaches a value equal to the buckling shear flow, q_{cr}, but does not increase beyond that value as the panel is loaded into the postbuckling regime. The first assumption implies that the principal stress tensile and compressive resultants, N_1, and N_2, line up with the diagonal tension folds at all load levels, with N_1 acting in the direction of the fold and N_2 normal to it, and the second assumption stems from the use of Wagner's model of the buckled panel, see Kuhn [1952]. Inplane equilibrium then dictates the value of N_1, which is derived in Appendix C. The validity of these assumptions is assessed by comparing SNAPPS values for α, N_1 and N_2 with test and STAGS results for the three panels. This is done in Figures 1 through 4, with the caption of Figure 1 defining the location of the strain gauges, and how the gauge measurements at these locations were averaged to obtain the test values of α, N_1 and N_2. (The values of the test failure loads and q_{cr} appearing in the abscissas in the figures are given in Appendix A).

Figure 1 compares the $\alpha = 45°$ assumption with measured and STAGS results. The measured and predicted values of α all lie between 45° and 48° degrees from the normal to the stiffener, thereby justifying this assumption.

Figures 2, 3 and 4 plot the principal stress resultants for the three panels against q/q_{cr}. Test results are given together with predictions based on the SNAPPS model and STAGS (for C1 only). Also included are

results from Kuhn's [1952] model based on an empirical expression for the diagonal tension factor, k, obtained from tests on *aluminum* panels. The figures reveal that the simplified SNAPPS approach gives stress resultants that are in reasonable agreement with the measured and STAGS results.

From Figures 1 through 4 it is concluded that the basic premises used in the SNAPPS analysis correlate well with the test and STAGS results. SNAPPS results stemming from these basic premises are compared next with test and STAGS for both global (kinematic) and local (stress) response variables.

3.2 Assessment of Global Predictions (Kinematic Variables)

SNAPPS computes the buckle (half) wavelength projected along the stiffener direction, L_b, (Appendix D) and the maximum out-of-plane displacement, δ_{max} (Appendix E). Normalized values of these kinematic variables are compared next with test and STAGS results to provide a "global" check on the SNAPPS methodology.

Figure 5 gives the variation of L_b with the dimensionless load level q/q_{cr}. L_b, is normalized with respect to the toe-to-toe distance, b_{tt}, measured normal to the stiffener direction. This distance is shown in Figure 1 of Appendix D, and the SNAPPS expression for L_b/ b_{tt} is given by Eq. (10) of that appendix. Included in the figure are wavelengths measured from moire´ photographs taken during the loading to failure for panels A1 and C1, and wavelengths predicted by the STAGS analysis for C1, and Timoshenko's [1961] "end point (q/q_{cr} =1)" buckling solution through which the SNAPPS prediction was forced to pass (see Appendix D). The figure demonstrates that the simple SNAPPS model used to determine the wavelength gives results that agree quite well with the measured and STAGS results.

Figure 6 shows the variation with q/q_{cr} of δ_{max}, which is normalized with respect to $L\sqrt{\gamma_{cr}}$, where L is the toe-to-toe distance between flanges, measured along the length of the diagonal tension fold (see Figure 1 of Appendix E), and γ_{cr} is the critical shear strain corresponding to q_{cr}. The SNAPPS expression for $L\sqrt{\gamma_{cr}}$ is given by Eq. (8) of Appendix E. The test results in the figure are based on moire´ fringe patterns photographed at various load levels during the tests of panels A1 and C1 (panel B1 was the earliest tested and was not instrumented for moire´ fringe measurements). The test set-up for the Shadow Moiré' Method of obtaining out-of-plane displacements in the buckled panel is described in Visconti

[1988]. The SNAPPS predictions based on the simple model of Appendix E somewhat overpredict δ_{max}, but this discrepancy is judged acceptable within the framework of a simplified, preliminary design, analysis tool.

Taken together, Figures 1 through 6 engender a sense of confidence that the basic premises underlying the SNAPPS procedure are physically realistic, and are valid even at postbuckling load levels of fifteen times initial buckling (which corresponds to the failure load level for panel C1).

3.3 Assessment of Local Predictions (Stress Variables)

The final check involves using SNAPPS to predict the maximum principal tensile stress, σ_{mpt}, immediately under the toe of the flange, and comparing this stress to the transverse tensile failure stress of the skin ply. This stress is highly localized and cannot be verified, either by the tests or STAGS results. However, if we get reasonable predictions for the failure loads for the three panels, then we may reasonably conclude that the methodology is valid, at least within the range of parameters for the tested panels, for the purpose of providing a preliminary design tool. The comparisons are made in two ways, the results of which are summarized in Tables 1 and 2.

Corresponding to the test failure load for each of the three tested panels, Table 1 compares σ_{mpt} with the mean transverse tensile strength, F_2^{tu}, which is taken as the failure criterion, as described Section 2 and Appendix L. For the IM6/3501-6 Graphite/Epoxy material in the room temperature, ambient moisture content condition, F_2^{tu} = 7150 psi (see Appendix L). Table 1 shows that σ_{mpt} differs from the mean strength by an average of 12.9%. It can be shown that the calculated values of σ_{mpt} are approximately within one standard deviation from the mean value of F_2^{tu}.

The SNAPPS code can also be used to predict the failure shear flow. To do this, the code is run with a succession of values of the applied shear flow until the predicted maximum principal tensile stress at the toe reaches the mean strength of 7150 psi. The results so obtained are displayed in Table 2, from which it is seen that the predicted failures differ from the test failures by an average of 18.3% (based on absolute differences, using algebraic differences gives -2%). This is a higher percent difference than the 12.9% obtained in the previous table, because σ_{mpt} varies nonlinearly with q.

Table 2 also gives SNAPPS predictions of the allowable load for each panel based on the "B-basis" allowable of 4460 psi, (which is 62% of the mean failure stress of 7150 psi, see Appendix L). It is observed that the predicted allowable loads for the three panels are consistently about half the test failure load. These predicted allowable loads are reasonably but not excessively conservative, in light of the nonlinear nature of the problem, and the variability in the matrix-dominated strength.

Tables 1 and 2 give SNAPPS results for σ_{mpt} for two load levels, one corresponding to the test failure load for each panel, and the other corresponding to the load level at which SNAPPS predicts failure to occur. The SNAPPS predictions for σ_{mpt} for a range of load levels, are displayed in Figures 7 to 9 for the three panels, which also serve to summarize the foregoing results of Tables 1 and 2. The SNAPPS predictions for the maximum principal tensile stress under the toe are seen to vary nonlinearly with load, thereby demonstrating that the simple models used in SNAPPS capture the basic geometric nonlinear behavior of the postbuckled shear panels.

TABLE 1 SNAPPS PREDICTIONS FOR THE MAXIMUM PRINCIPAL TENSILE STRESS AT THE TEST FAILURE LOAD FOR EACH OF THE THREE TESTED PANELS.

Panel	Predicted Max Prin Stress at toe, psi	% Diff Relative to Mean Strength (7150 psi)
A1	8597	20.2
B1	7893	10.4
C1	6580	-8.0
	Avg % Diff of Absolute Values of σ_{mpt} Relative to Mean Strength	12.9

TABLE 2 SNAPPS FAILURE AND ALLOWABLE LOAD PREDICTIONS FOR EACH OF THE THREE TESTED PANELS.

Panel	Test Failure Load, ppi	Predicted Failure Load, ppi	% Diff of Predicted Load w.r.t Test Failure Load	Allowable Shear Flow (B-basis), ppi	Ratio of Allowable Load to Test Failure Load
A1	1403	1149	-18.1	791	.56
B1	838	735	-12.3	451	.54
C1	962	1199	24.6	468	.49
		Avg % Diff of Absolute Values of Predicted Failure Load w.r.t to Test Failure Load	18.3		

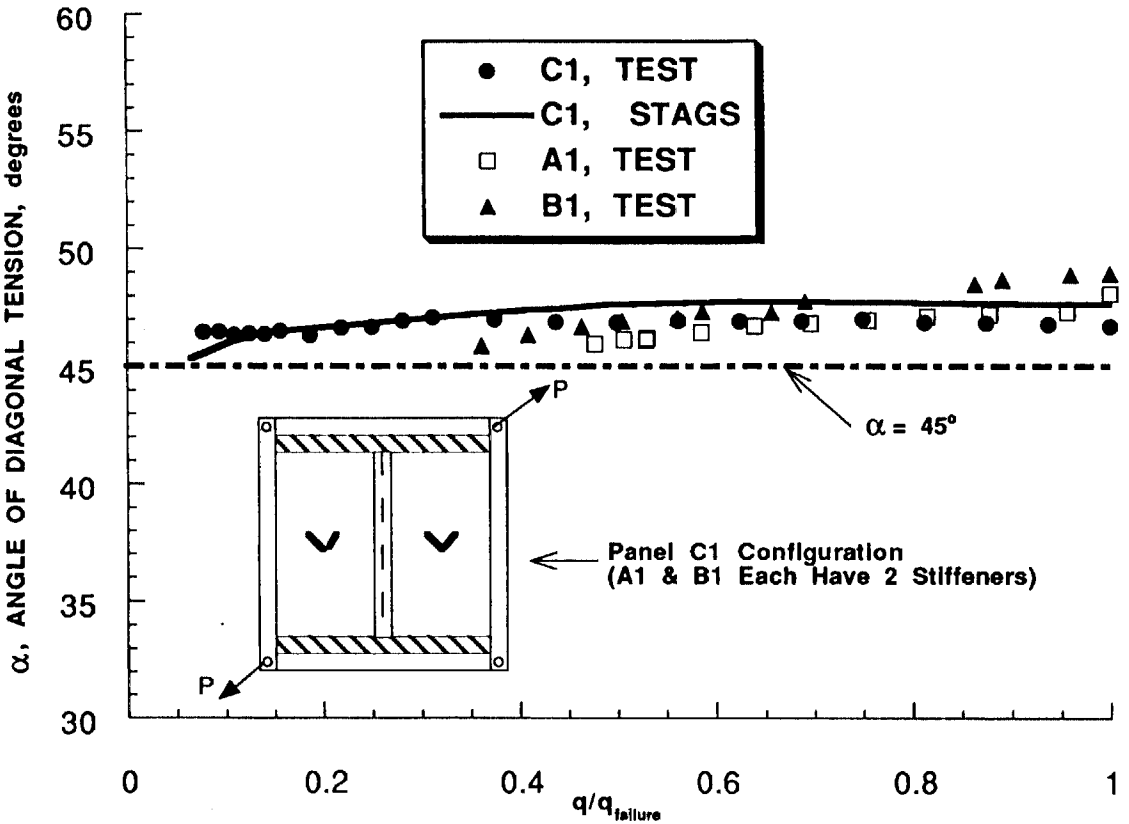

FIGURE 1 VARIATION OF ANGLE OF DIAGONAL TENSION WITH APPLIED SHEAR LOAD FOR C1, A1, B1

Note: The Angle of Diagonal Tension is Computed From Strain Gage Values at the Gage Locations in Each Bay. These Values are Then Averaged at the Following Locations:

- **For C1 (see Inset): Center of the Left and Right Bays.**
- **For A & B1: 1/4 and Center Points in Center Bay, and 1/4 Point in End Bay.**

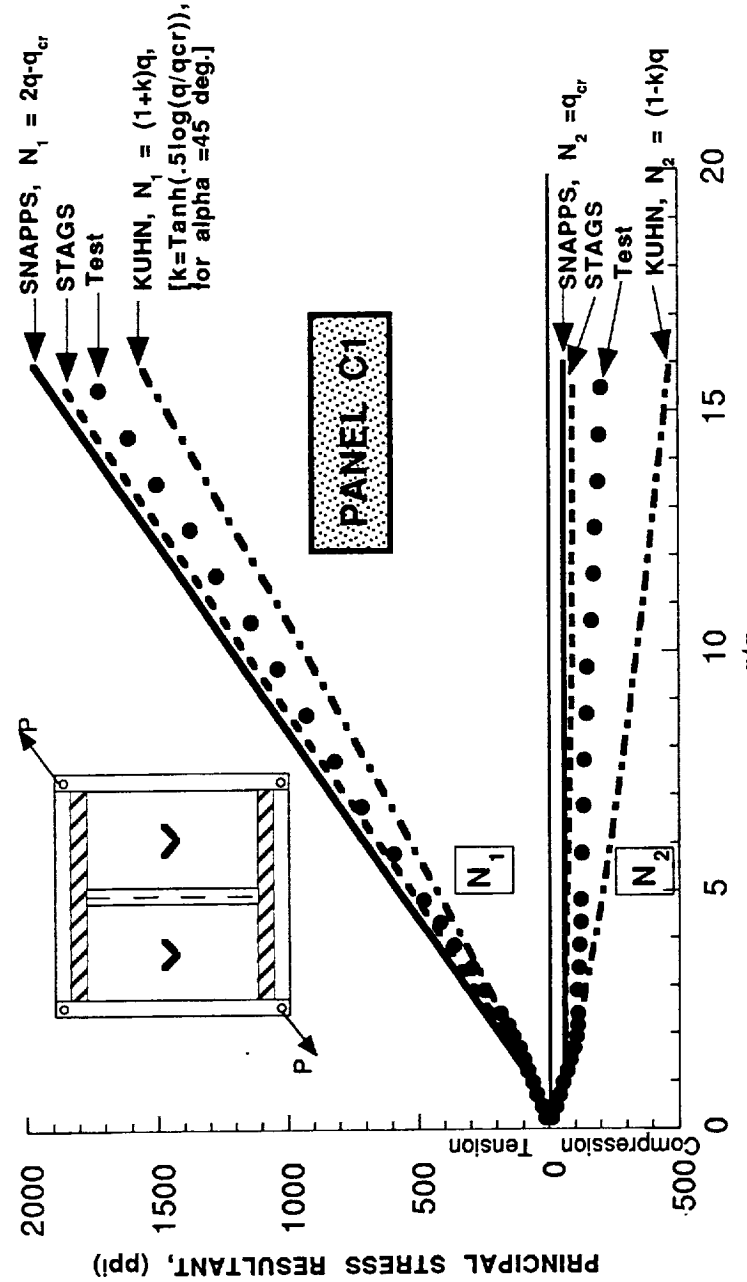

FIGURE 2 VARIATION OF PRINCIPAL STRESS RESULTANTS WITH APPLIED SHEAR LOAD FOR PANEL C1 (q_{cr}=63.5 ppi FROM STAGS)

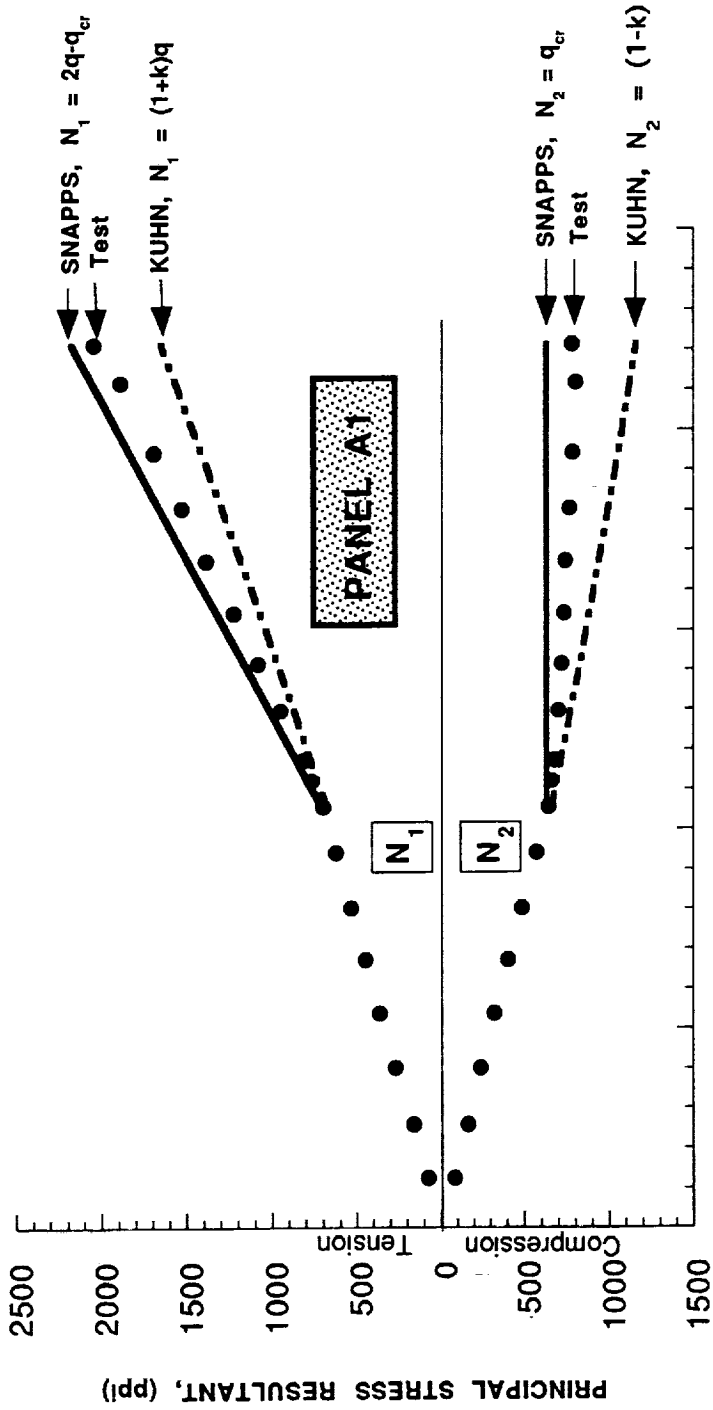

FIGURE 3 VARIATION OF PRINCIPAL STRESS RESULTANTS WITH APPLIED SHEAR LOAD FOR PANEL A1 (q_{cr}=634 ppi FROM TEST)

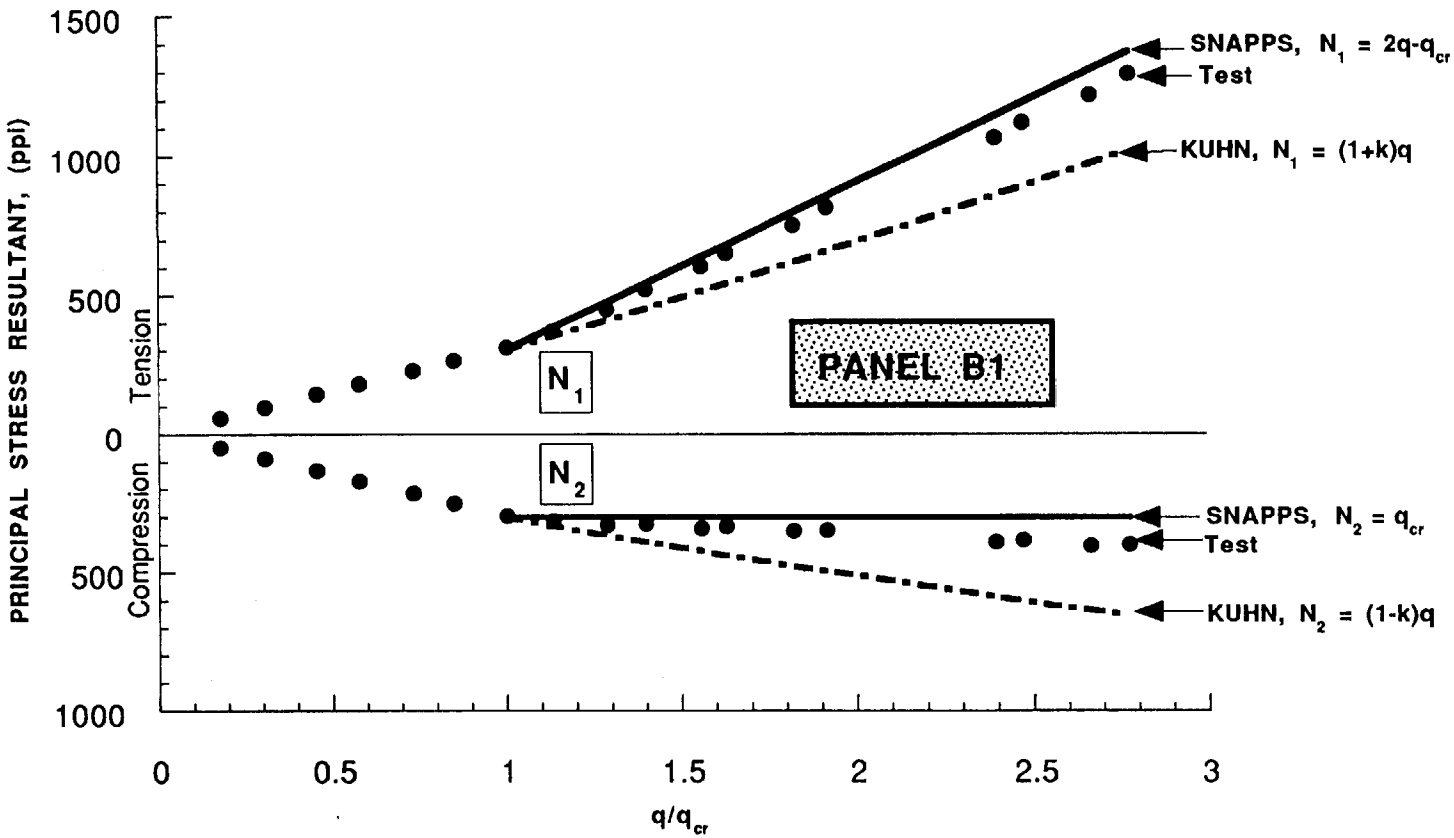

FIGURE 4 VARIATION OF PRINCIPAL STRESS RESULTANTS WITH APPLIED SHEAR LOAD FOR PANEL B1 (q_{cr}=302 ppi FROM TEST)

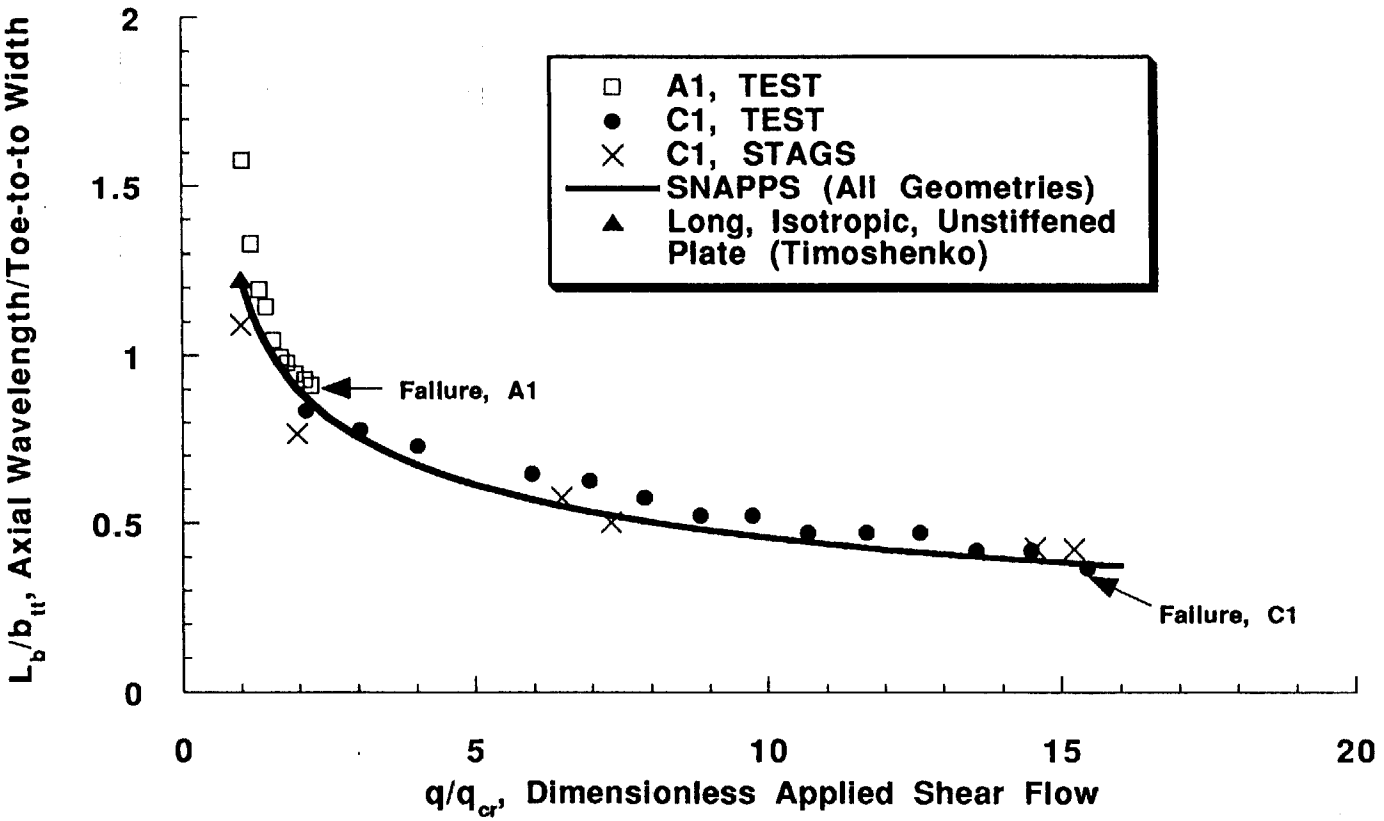

FIGURE 5 VARIATION OF AXIAL WAVELENGTH OF BUCKLE WITH APPLIED SHEAR FLOW IN SKIN

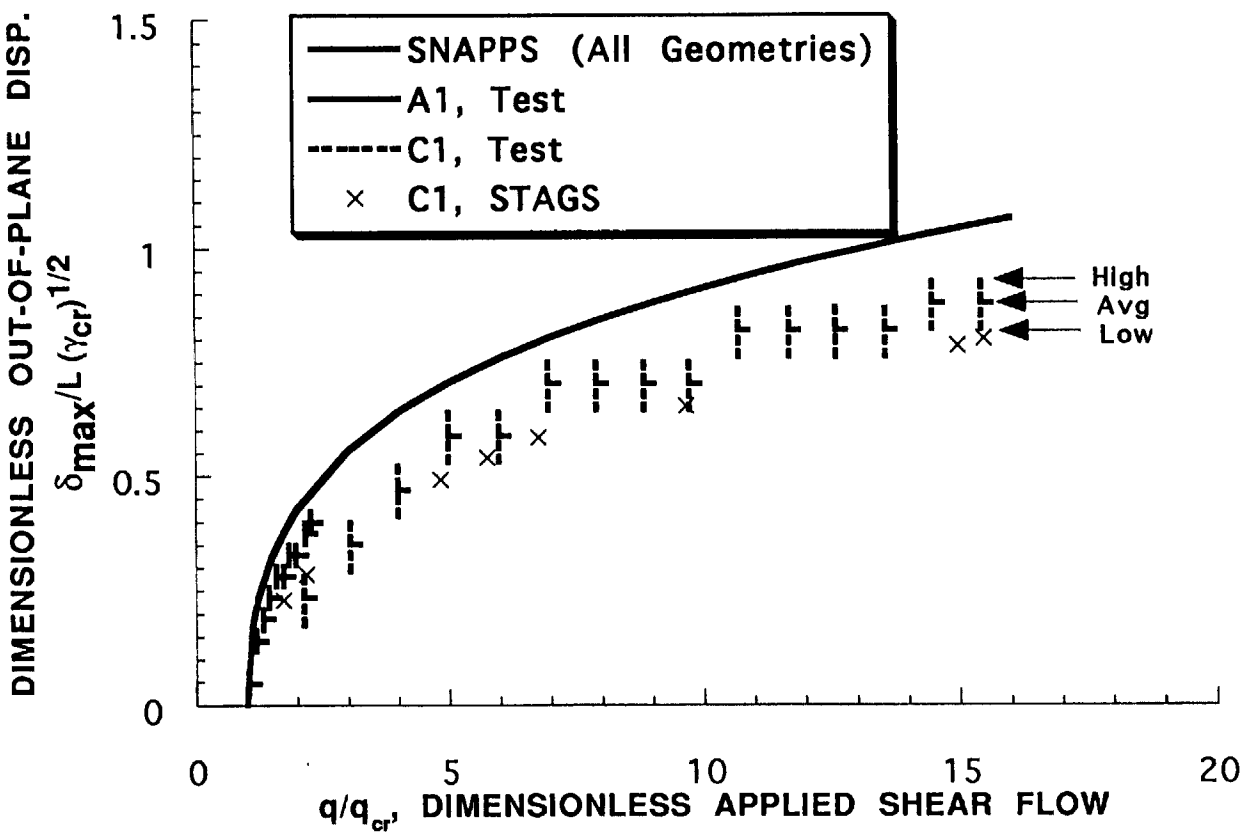

FIGURE 6 VARIATION OF MAXIMUM OUT-OF-PLANE DISPLACEMENT OF BUCKLE WITH APPLIED SHEAR FLOW IN SKIN

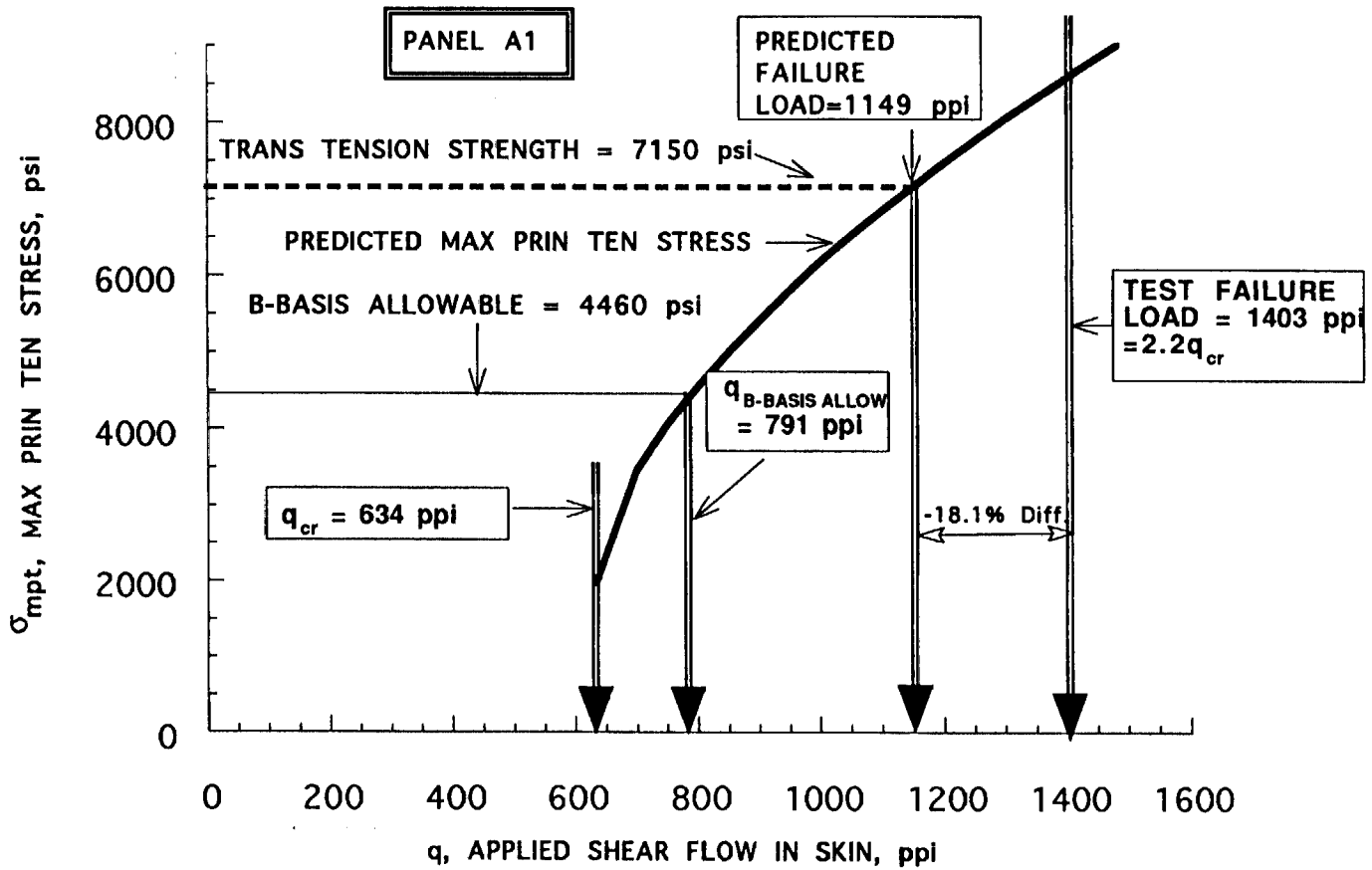

FIGURE 7 MAXIMUM PRINCIPAL TENSILE STRESS AT TOE, & PREDICTED FAILURE LOAD. PANEL A1.
Note the nonlinear variation of predicted stress with load.

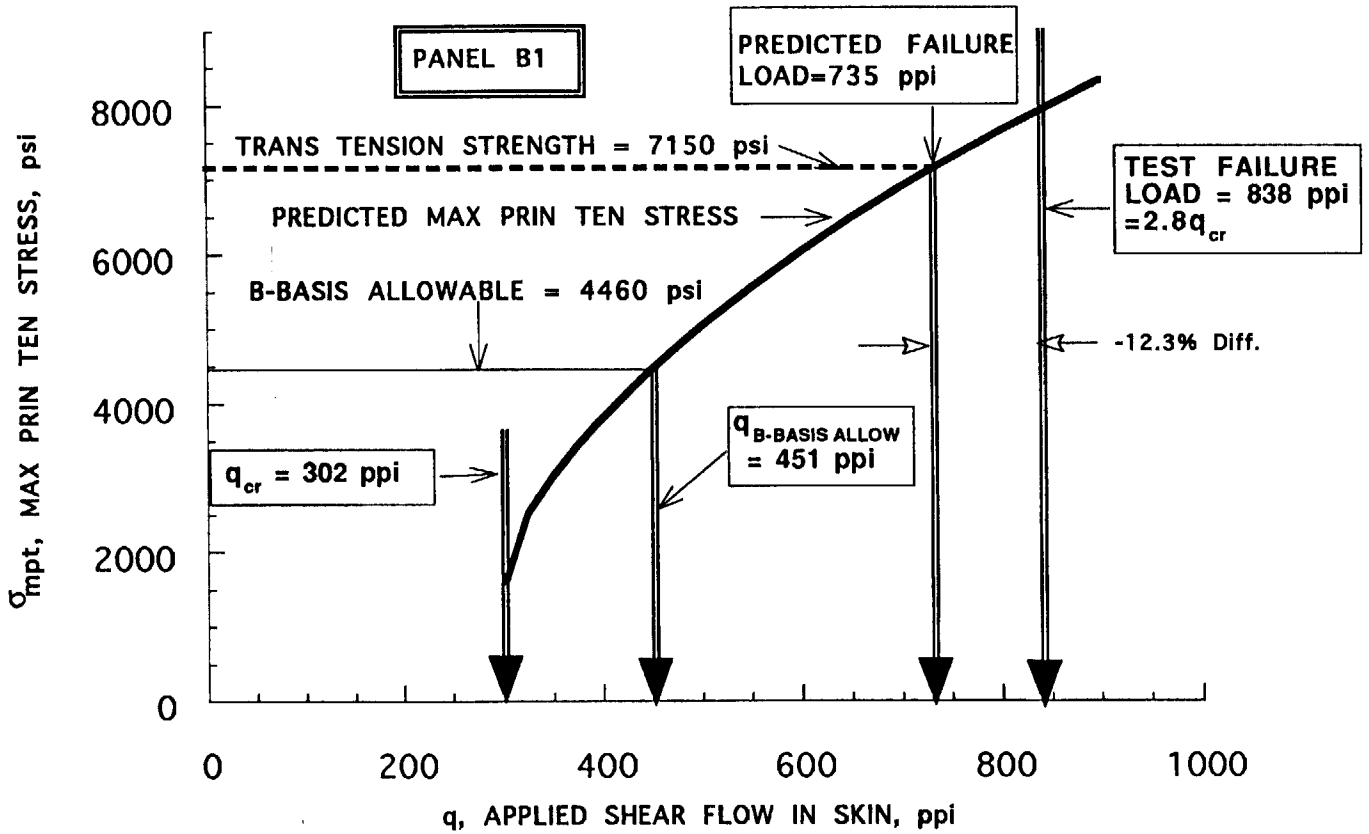

FIGURE 8 MAXIMUM PRINCIPAL TENSILE STRESS AT TOE, & PREDICTED FAILURE LOAD. PANEL B1.

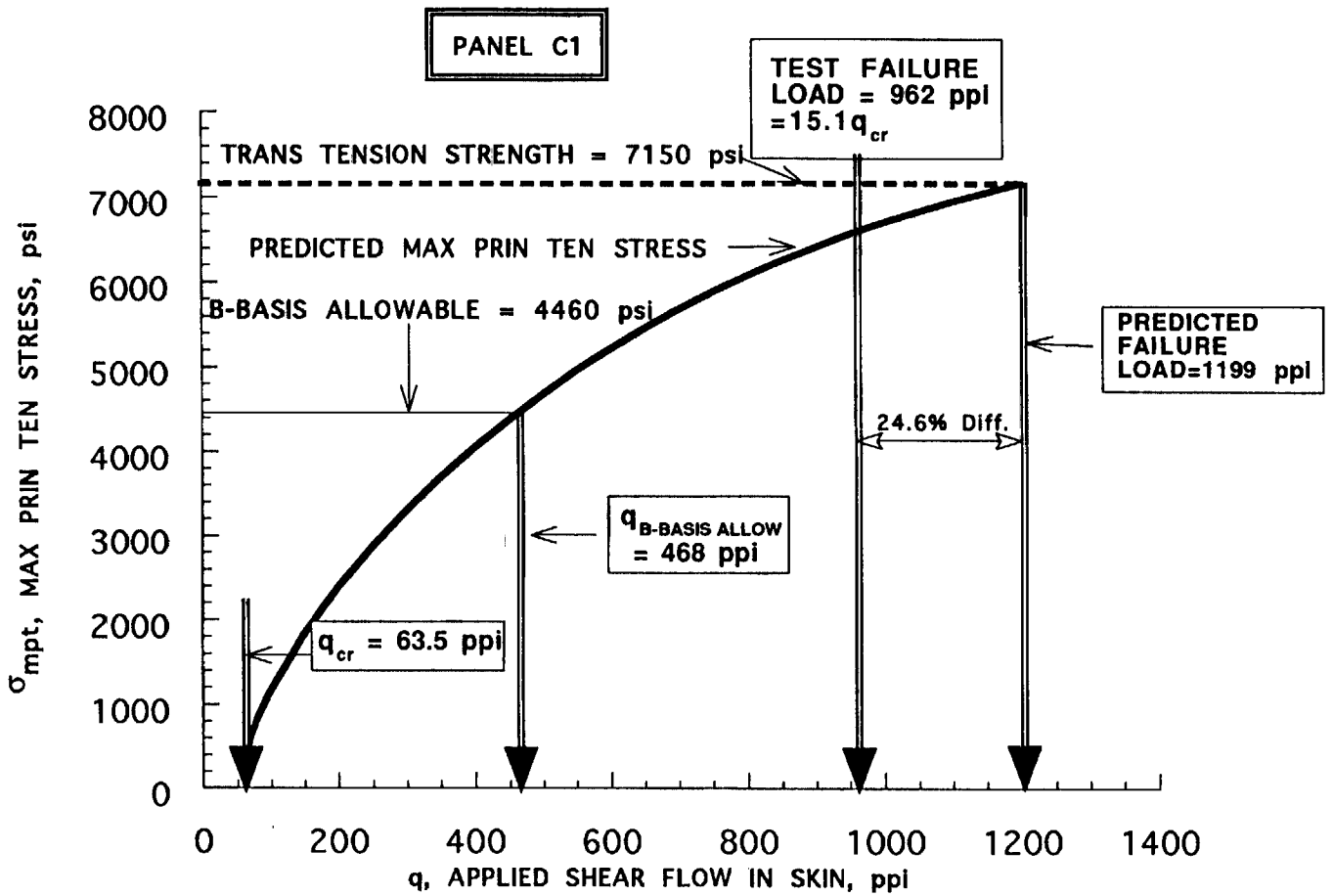

FIGURE 9 MAXIMUM PRINCIPAL TENSILE STRESS AT TOE, & PREDICTED FAILURE LOAD. PANEL C1.

SECTION 4

CLOSING REMARKS

4.1 Summary and Conclusions

We have attempted, using a simple "strength-of-materials" approach, to develop a preliminary design tool for rapidly analyzing the very complex nonlinear problem of the postbuckling behavior and failure of flat, stiffened, composite shear panels.

The analysis is based on the premise that the physical behavior of a highly buckled, stiffened shear panel can be described by simple, closed-form, equations using the insights gained from a series of panels tested by Grumman, and the subsequent correlation of the test results with STAGS nonlinear finite element results for one of the panels.

The analysis method has been programmed, using the "True Basic" language, into a code called SNAPPS ("Speedy Nonlinear Analysis of Postbuckled Panels in Shear"), which is a simple and fast preliminary design tool for predicting failure and postbuckling behavior of composite shear panels with bonded stiffeners. The code is written in a modular form so that it may be easily modified by the user if new test data or physical insight makes modification desirable. Each module of the code is the subject of an Appendix in this report.

Confirmation of the validity of the basic premises of the method has been gained by comparing its predictions with test results for the three panels, A1, B1, and C1, and with the nonlinear finite element analysis results obtained from STAGS for panel C1 only. We are encouraged that the SNAPPS predictions for the skin's diagonal tension stress resultants and out-of-plane deflections (i.e., the large-scale behavior of the panel) agree well with test results for these panels of widely different geometries and stiffnesses, and with the STAGS predictions.

However, the failure criterion adopted - that failure occurs when the maximum principal tensile stress in the skin under the toe of the stiffener flange exceeds the transverse tensile strength of the surface plies - cannot be confirmed, either by test measurements or by finite element analysis. Indirectly, it is judged by comparing the test failure loads of the A1, B1 and C1 panels with SNAPPS predictions based on the

mean strength of 19 transverse tensile test coupons. The predictions of failure for the two-stiffener panels, A1 and B1, are 18% and 12% below the test failures respectively, i.e. on the conservative side. For panel C1, the predicted failure load is about 25% above the test failure load, i.e., unconservative. The mean (algebraic) error is 2%. We contend that the failure criterion is physically realistic, and that the failure mode is correctly identified, and feel this conclusion is confirmed by Minquet and O'Brien [1996] in their analysis of stiffener pull-off specimens. It is worthy of note that their analysis of the maximum principal tensile stress at failure for four different specimens gave values ranging from 6600 psi to 7300 psi for the same IM6/3501-6 graphite/epoxy material used in our tested panels and for which we used an average transverse tensile strength of 7150 psi. Never the less, we must admit that our data base is too small for comfort because of the large amount of scatter, although this is typical of matrix dominated failures.

The B-basis allowable transverse tensile strength is 4460 psi, much lower than the mean value of 7150 psi (allowable = 62% of mean), reflecting the wide scatter of a matrix-dominated failure in graphite/epoxy, which is made worse by the small sample size. The prediction of allowable shear flows for all three panels is consistent, at 56%, 54% and 49% of the test failure loads for A1, B1 and C1 respectively. We feel that these are reasonably, but not excessively, conservative in view of the matrix-dominated nature of the failure, and the small data base.

SNAPPS requires much more work for its complete validation. Its predictions need to be compared with test results for other panels. A larger, statistically significant, data base of transverse tensile strengths needs to be acquired, and applied to a wider range of test panels. Meanwhile, SNAPPS should be useful in performing trade studies, with the understanding that any design obtained from the trade studies should be verified by test and/or a detailed analysis.

4.2 Limitations

The method was developed for flat, stiffened, composite panels loaded in shear only. The skin is assumed to be a balanced and symmetric laminate.

There must be a sufficient number of stiffeners so that the aspect ratio of a skin-bay between the toes of the stiffener flanges is large enough to allow a number of buckles to develop, ensuring that end effects

do not dominate the buckle pattern, and that the out-of-plane deformation of the diagonal tension fold is symmetric about the midlength of the fold, as is assumed in the SNAPPS analysis (the STAGS results for panel C1 show that such symmetry is not the case for this single stiffener panel — see Figure 2 of Appendix G).

The stiffeners are assumed to have sufficient bending stiffness to prevent the diagonal tension folds from progressing across the stiffener centerlines. The user is alerted that the analysis assumes zero rotation of the skin at the stiffener centerline in the diagonal tension direction (see Figure 1 of Appendix G). This is correct for stiffeners made up of back-to-back channels or angles, and may reasonably apply to sturdy "hat"-sections. The applicability of the code to unsymmetric sections such as single angles or Z-section stiffeners has not been verified, nor has it been applied to non-sandwich composite skins, or metallic panels with bonded-on stiffeners.

The Wagner model [see Kuhn 1952] for the principal stress resultants in the diagonal tension folds has been used in this analysis because it gave good agreement with the measured and STAGS skin stress resultants, and it enabled the removal of undesirable empiricism from the analysis. This model should be checked against other test results.

Further, because of the assumption that the principal stress resultants line up with the diagonal tension folds, and that the angle of diagonal tension is 45°, the method cannot be applied to curved panels.

It is to be recalled that the allowable and mean transverse tensile strength values for the graphite/epoxy face ply material for the tested panel's are based on a limited data base (see Appendix L). Thus, the values of the SNAPPS predictions for the allowable and failure loads may suffer accordingly.

4.3 Lessons Learned & Design Implications

Particular care needs to be taken with sign conventions, stacking sequence "clocks" on drawings, and load directions with respect to the structural axes (parallel and normal to stiffeners). Changes in stacking sequence or load direction relative to the structural axes on the drawing, resulting from manufacturing errors or changes in load spectrum, may have significant effects on initial buckling and failure. For thin skins, the initial buckling load is markedly effected by the sign of the shear load,

and by orthotropy and/or anisotropy in the skin, as is well illustrated in Figure 17 of Nemeth [1997].

While the stiffener must be sturdy enough to prevent the diagonal tension folds from progressing across the stiffener centerlines, the resistance to stiffener disbonding can be improved by reducing the moment in the skin immediately under the toe of the flange, thereby lowering the value of the maximum principal tensile stress. The moment is lower when the entire attached flange is flexible, but, because the stress components which make up the maximum principal tensile stress die away rapidly from the toe, the same effect may be achieved by tapering the flange locally at the toe, instead of the square edge we tested. Minquet and O'Brien [1996] have shown that trimming the flange edge to a 20° wedge angle at the toe gives a significant improvement in the load-carrying capability of the skin-stiffener joint. The taper may also be achieved by dropping internal plies in the stacking sequence of the flange, but this may cause problems in tooling because a terminated ply has to be prevented from moving during the cure cycle and because a resin pocket is created at it's end.

4.4 Recommendations

To further verify SNAPPS and to suggest possible refinements to it, SNAPPS should be applied to other test panels, particularly those without sandwich skins, those with many stiffeners and those tested in different fixtures.

The models used in the various steps in the computational procedure are quite simple. Further development should concentrate on refinement of some of these models, particularly those associated with the transition region at the nose of the buckle where the diagonal tension field stress resultants in the buckled panel have to be transformed into a complex set of internal loads, both inplane and out-of-plane, at the toe of the flange. The refinement would be based on insights gained from a detailed finite element modeling of the area around the nose of the buckle where it meets the toe of the flange, and the model would have to include the shear deformation of the skin. The model would be bounded by adjacent nodal lines in the skin and should also include a portion of the attached flange bounded by the nodal lines, and the toe and heel of the stiffener. From the results of the model it would be possible to determine the redistribution of load and moment in the flange and the skin at the nose of the buckle, and thereby refine the current models used in SNAPPS.

Although the above model would have to be super-detailed, it is still unlikely to accurately determine the concentrated stresses in the vicinity of the toe. In order to quantify the critical through-the-thickness maximum principal tensile stress in a one inch wide stiffener pull-off specimen, Minquet and O'Brien [1995 and 1996] used 2273 elements with 13908 degrees of freedom. The size of the element was of the order of one-third of a ply thickness (i.e. about 0.002 inches) in the critical region. This was essentially a two-dimensional plane strain analysis where the location of the critical stress was known. Similar models of equal complexity were used by Wang, et al. [1994] and Li, et al. [1996]. Imagine, then, the complexity of the same finely detailed analysis in the present problem, where the analysis has to be three-dimensional. The critical stress is in the skin under the toe of the stiffener, but it's location could be anywhere along the length of the stiffener. Further, because of the changing wave-pattern in the postbuckled state, the location of the maximum stress will move with increasing load until, at some point and some load level, it reaches either the allowable stress for a design analysis, or the average strength for a failure analysis. Therefore, we should explore the possibility of using a code such as SUBLAM [Flanagan, 1993] to investigate the stresses at the interface between the skin and the flange, using loads from the finite element model as boundary conditions in a global-local approach.

The "diagonal tension factor method" (Appendix B) of obtaining the initial buckling shear load from experimental results needs additional verification.

For panel C1, which failed deep in the postbuckling range at a load about 15 times initial buckling, the predicted moment in the skin at toe, M_{toe}, reached a maximum before the test failure load was reached and then decreased with increasing load (see Figure 3 of Appendix G). Further study is required to ascertain whether or not this behavior reflects physical reality or a limitation of the basic SNAPPS methodology.

Finally, it is emphasized that only one failure mode is considered here, based on the observation that failure originated in the plies of the face sheet immediately under the toe of the flange for the three tested panels. Other failure locations and modes need to be investigated, such as those associated with the sandwich core for which the deformation of the skin at the nose of the buckle can be extreme at high postbuckling loads. Such an investigation is beyond the current scope of SNAPPS. However, the modular approach used in SNAPPS enables the user to estimate the

transverse shear force and bending moment in the skin at the toe of the flange, and add more failure criteria to the code.

APPENDIX A

DESCRIPTION OF TEST PANELS A1, B1, and C1

Comparisons are made throughout this report between SNAPPS predictions and test results for three shear panels tested by Grumman. This appendix briefly describes these panels: complete descriptions are given in the test report [Visconti, 1988], and a STAGS analysis report [Sobel and Sharp, 1994].

The panels (Figures 1 to 3) were tested in the room temperature "dry" condition (i.e. stabilized at the ambient moisture condition of the test laboratory). The test frame was designed to allow the diagonal tension field to be reacted by the compressive load in the stiffener(s), rather than in the test frame members. This is accomplished through the use of a "breather joint", as described below. The skin of each panel consists of two identical thin composite faces separated by SynCore to form a sandwich (Figure 2). SynCore is an epoxy resin filled with glass micro-balloons to reduce its density by approximately one half. The face material is IM6/3501-6 graphite/epoxy tape. The panels all have the same overall dimensions, so as to fit into the test frame, but the face layups and thicknesses differ, as does the thickness of the SynCore. Panels A1 and B1 have two stiffeners at approximately 11 inches spacing, but differ in the skin faces, the SynCore thickness and in the stiffener thickness. Panel C1 had a single stiffener, dividing the skin into two bays of approximately 17 inches width, and also differs from both A1 and B1 in its SynCore and stiffener thicknesses. The stiffeners (Figure 2) are built up from back-to-back channel sections of AS4/3501-6 graphite/epoxy fabric, with straps of the same layup as the channels. Because the longitudinal and transverse modulii are almost equal in a fabric, see Table 1, the stiffener web and flanges are, as far as is possible with a wrapped shape, balanced and symmetric laminates. Warping in the curing process is thereby minimized. The stiffeners have the same overall dimensions, being formed on common tools, but are of different layups and thicknesses for the three panels. The laminate nominal thicknesses and layups are given in Tables 2 to 4. The stiffeners are cured first and then the "green" skin is cured and bonded to the stiffeners in one operation ("cocured") on a flat tool. A single layer of FM300 adhesive is used between the skin and the flange of the stiffener.

The test frame is 38-in.-square fixture built up from heavy steel bars pinned at the frame corners. The test load P is applied through two

of these pins on opposite corners of the test frame, as shown in Figure 1. Parallel to the stiffener(s), the thickened edges of the panel skin are sandwiched between the steel bars, and normal to the stiffener(s) the skin is attached to the steel bars through a breather joint. The breather joint (Figure 3) is intended to ensure that the diagonal tension field load in the buckled skin is reacted by compression loads in the stiffener(s) rather than in the test frame members. The breather joint consists of thin steel angles bolted to the thickened laminate at the edge of the skin, and these, in turn, are bolted to similar angles attached to the test frame. The joint acts as a bellows, capable of transmitting the applied shear load in the plane of the frame but not permitting significant axial load to develop across the joint. While the breather joint did induce axial compression in the stiffeners, it also contributed to the nonuniformity of shear stress near the panel edges, as illustrated in Figure 11 of Sobel and Sharp [1994]. Fortunately, the shear stress concentrations in the skin are well away from the disbond failures experienced between the skin and the attached flanges of the stiffener(s), and did not influence the test results.

The panels were instrumented with strain gauges, using rosettes on both skin faces, and axial gauges on the stiffener web and flanges Layouts of the gauge positions for each panel are given in the test report. The moiré fringe technique, described in Volume III of Visconti [1988], was used to obtain both wavelengths and out-of-plane displacements in the buckled skin for Panels A1 and C1. Examination of a series of photographs of the moiré fringes taken during the tests enabled the progression of the buckle waves to be recorded as the load increased. A major finding of the test program was the slow growth of new buckles progressing in from the ends of the panel, i.e. the buckle wavelength reduces continuously as the shear load is increased without sudden "snap-throughs".

The mode of failure observed for all the test panels was not a failure of the bondline between the flange of the stiffener and the skin, but rather an intra-ply failure of the epoxy matrix of the skin immediately under the toe of the flange. This was evidenced by the pull-out of fibers from the surface layer of the skin. It was this observation that led to the realization that the flatwise tensile strength of the skin face material was the key to the failure. The test failure loads (from Visconti [1988]) and buckling loads (from Appendix B) are given in Table 5.

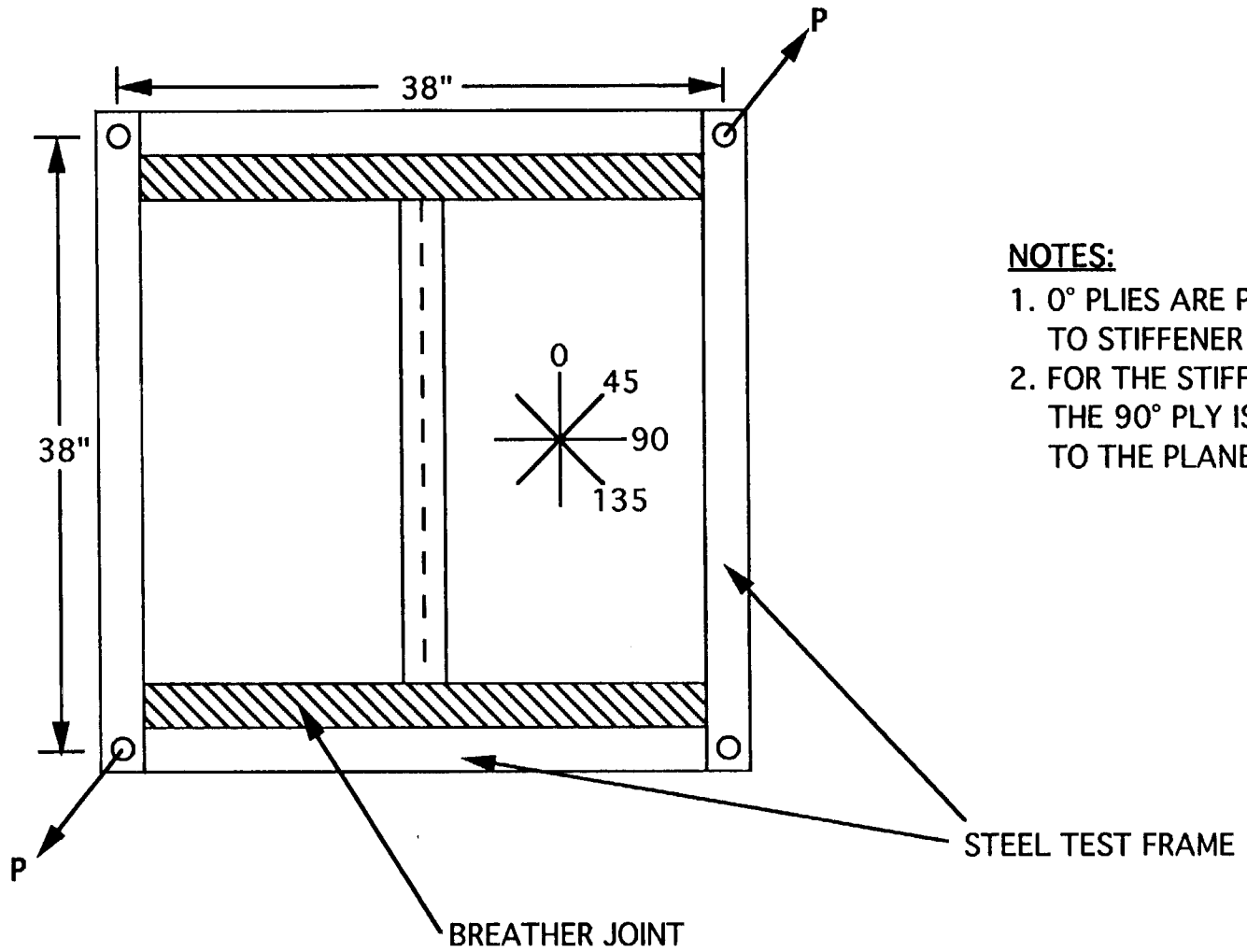

NOTES:

1. 0° PLIES ARE PARALLEL TO STIFFENER AXIS
2. FOR THE STIFFENER WEB, THE 90° PLY IS NORMAL TO THE PLANE OF THE SKIN

FIGURE 1 PLAN VIEW OF THE STIFFENER SIDE OF THE PANAL (ILLUSTRATED FOR THE SINGLE STIFFENER PANAL C1).

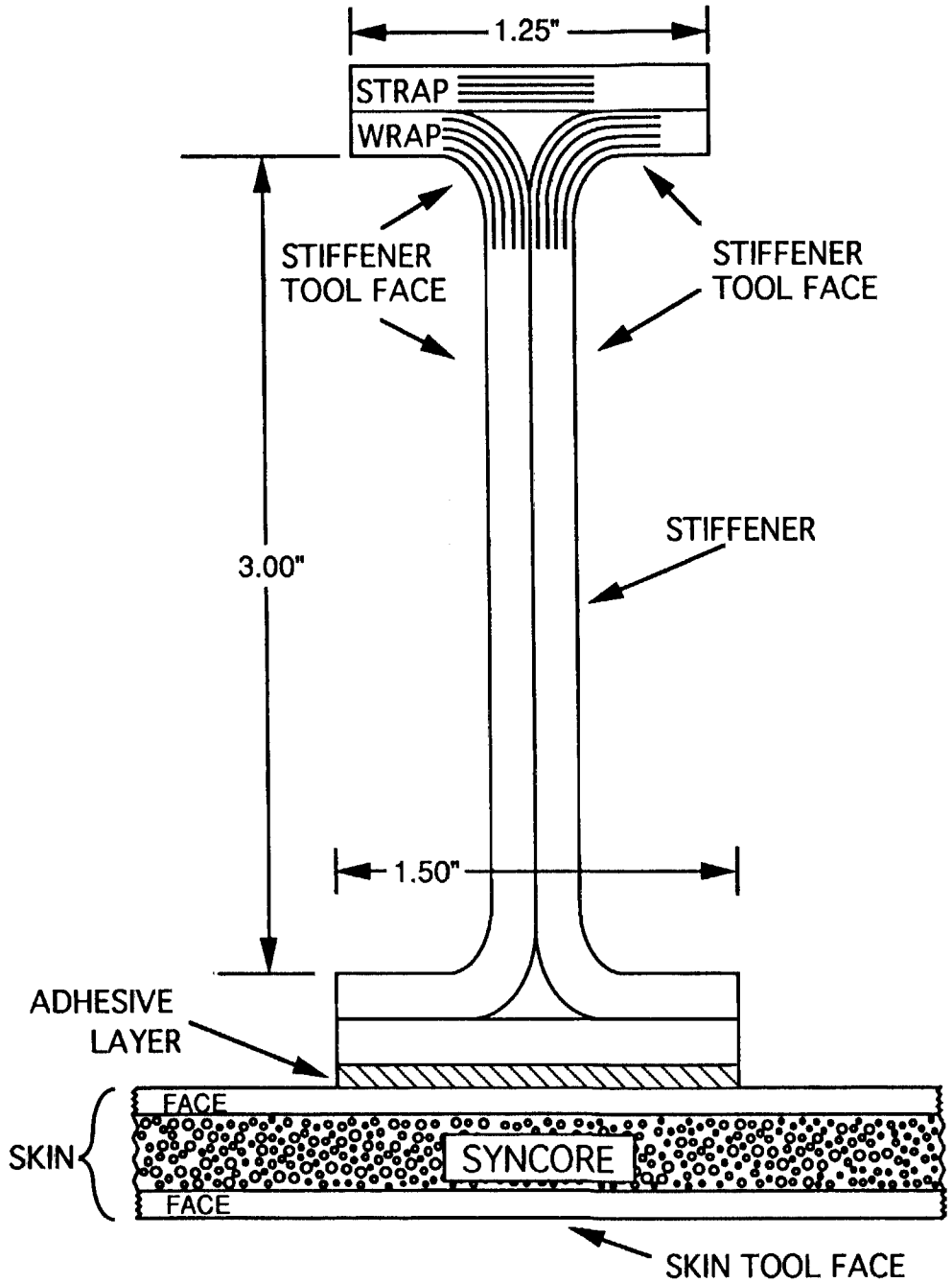

FIGURE 2 SKIN AND STIFFENER FOR PANELS A1, B1, AND C1

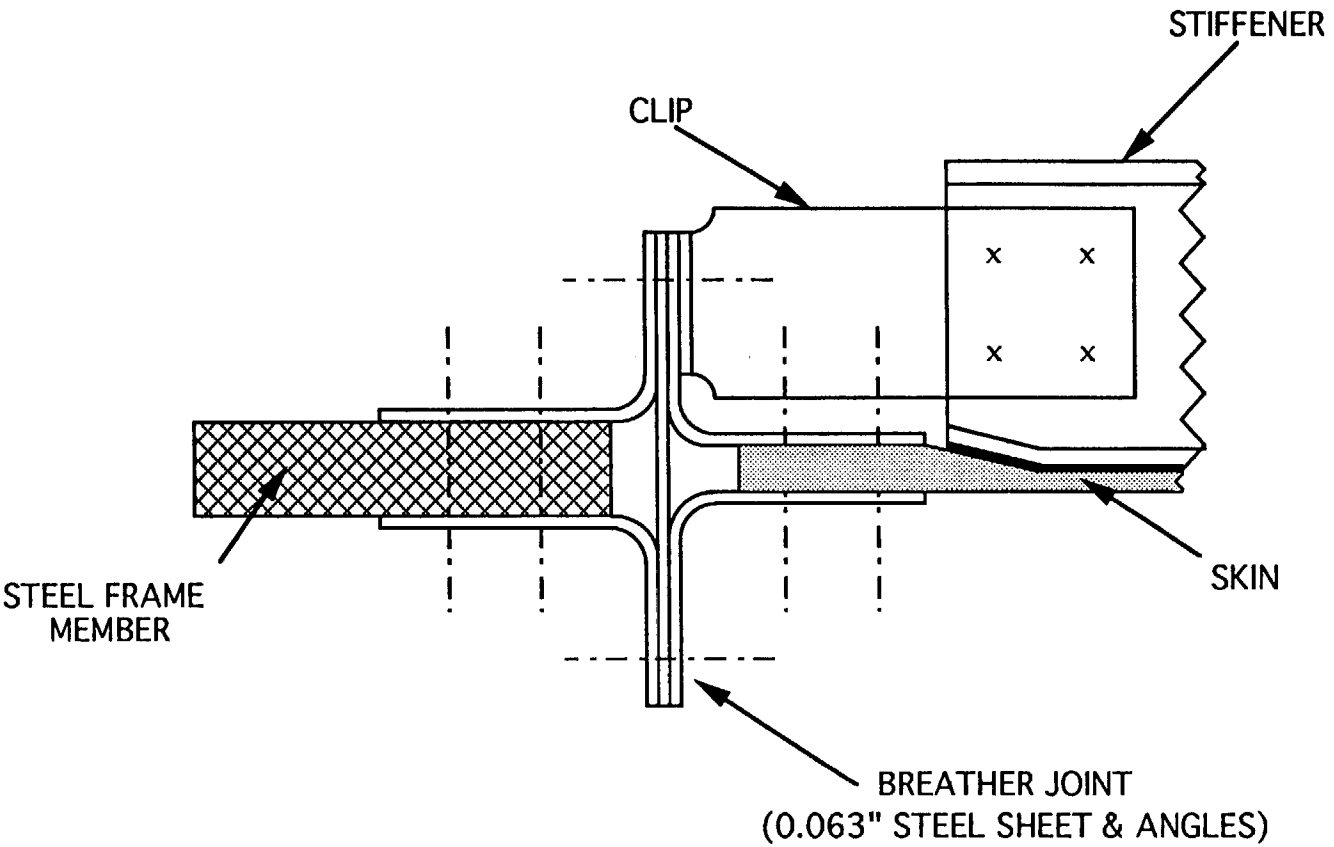

FIGURE 3 BREATHER JOINT ON A COMPLIANT EDGE OF TEST FRAME NORMAL TO DIRECTION OF STIFFENER.

TABLE 1 PLY MATERIAL PROPERTIES AND THICKNESSES (Room Temperature "Dry")

PROPERTY	DESCRIPTION	STIFFENER	FACE SHEET	CORE	ADHESIVE
		AS4/3501-6 FABRIC	IM6/3501-6 TAPE [1]	SynCore[1] HG9872	FM300[3]
E_1, Msi	YOUNG'S MODULUS IN FIBER DIRECTION	9.70[1]	20.50	0.38	0.30
E_2, Msi	YOUNG'S MODULUS IN TRANSVERSE DIRECTION	9.30[1]	1.30	0.38	0.30
E_3, Msi	YOUNG'S MODULUS IN THICKNESS DIRECTION	1.60[2]	1.30[4]	0.38	0.30
G_{12}, Msi	IN-PLANE SHEAR MODULUS	1.00[1]	0.80	0.15	0.12
G_{13}, Msi	OUT-OF-PLANE SHEAR MODULUS	0.64[2]	0.80	0.15	0.12
G_{23}, Msi	OUT-OF-PLANE SHEAR MODULUS	0.64[2]	0.50	0.15	0.12
ν_{12}[5]	POISSON'S RATIO	0.09[1]	0.35	0.25	0.25
t, in.	PLY THICKNESS	0.0072[1]	0.0056	0.0100	0.0080

Notes
(1) [Flanagan, 1988]
(2) [Cox and Flanagan, 1997]
(3) [Dastin, 1996]
(4) $E_3=E_2$ assuming transverse isotropy for tape
(5) ν_{12} is defined according to $\nu_{12}E_2 = \nu_{21}E_1$

TABLE 2 NOMINAL LAMINATE THICKNESSES (inches) OF TEST PANELS

LAMINATE	PANEL		
	A1	B1	C1
EACH FACE	.0336	.0224	.0224
SYNCORE	.050	.040	.020
TOTAL SKIN	.1172	.0848	.0648
ADHESIVE	.008	.008	.008
STRAP	.036	.0288	.0216
WRAP	.036	.0288	.0216
TOTAL FLANGE (WRAP+STRAP)	.0720	.0576	.0432
TOTAL WEB (WRAP+WRAP)	.0720	.0576	.0432

TABLE 3 LAMINATE LAYUPS FOR TEST PANELS

(a) Skin Layup (M6/3501-6 Tape)

LAMINATE	PANEL		
	A1	B1	C1
Free Surface			
SKIN FACE	45		
	135		
	0	45	45
	90	135	135
	135	90	90
	45	0	0
SynCore Surface			

(b) Stiffener Layup (AS4/3501-6 Fabric)

LAMINATE	PANEL		
	A1	B1	C1
Stiffener Tool Face			
WRAP	45		
	90	45	
	0	90	45
	90	0	90
	135	135	135
STRAP (inner & outer)	135	135	45
	90	0	90
	0	90	135
	90	45	
	45		
Free Surface			

NOTES:
1. 0° plies are parallel to stiffener direction (See Figure 1).
2. The cross section and tool surfaces are shown in Figure 2.

TABLE 4 STACKING SEQUENCE FOR SKIN & ATTACHED FLANGE OF TEST PANELS. Stacking Sequences Are From Skin Tool Surface (See Figure 2), And Are Used In The Maclaminate Code To Obtain Stiffnesses For Input To Snapps.

LAMINATE (Material)	PANEL		
	A1	B1	C1
FACE (IM6/3501-6 Tape)	45 135 90 0 135 45	 45 135 90 0	 45 135 90 0
SYNCORE (HG 9872)	5 Plies	4 Plies	2 Plies
FACE (IM6/3501-6 Tape)	45 135 0 90 135 45	0 90 135 45	0 90 135 45
ADHESIVE (FM300)	1 Ply	1 Ply	1 Ply
STRAP (AS4/3501-6 Fabric)	45 90 0 90 135	 45 90 0 135	 45 90 135
WRAP (AS4/3501-6 Fabric)	135 90 0 90 45	135 0 90 45	45 90 135

NOTE : 0° plies are parallel to stiffener direction (See Figure 1).

TABLE 5 BUCKLING & TEST FAILURE LOADS FOR TEST PANELS

LOAD	PANEL		
	A1	B1	C1
Buckling Load P_{cr}, Kips	37.5	17.6	4.13
Failure Load $P_{failtest}$, Kips	85.0	50.0	64.0
Buckling Shear Flow q_{cr}, ppi	634.	302.	63.5
Failure Shear Flow $q_{failtest}$, ppl	1403.	838.	962.

APPENDIX B

BUCKLING SHEAR FLOW q_{cr} FOR THREE TEST PANELS, AND DEVELOPMENT OF A NEW METHOD OF OBTAINING EXPERIMENTAL BUCKLING LOADS FOR FLAT SHEAR PANELS

The SNAPPS code input requires the value of the buckling shear flow, q_{cr}. This appendix describes methods used to obtain the buckling shear flow for the three panels A1, B1, and C1 (see Appendix A) analyzed here.

B.1 Buckling Load for Panel C1

Sobel and Sharp [1994] performed a STAGS [Almroth, et al., 1982] analysis for one of the panels, panel C1. The detailed finite element model includes the skin, stiffener, breather joint and loading frame. The STAGS results for C1 are as follows:

- **C1**: $P_{cr,STAGS} = 4.13$ Kips, $q_{cr,STAGS} = 63.5$ ppi (1)

where P is the load applied at two opposite corners of the test frame (see Figure 1 of Appendix A). A new method, described next, was developed here for obtaining the buckling loads for the other two panels.

B.2 Description of a Method of Obtaining Experimental Buckling Loads For Flat Shear Panels — Based on the Diagonal Tension Factor, k

As is well known, the determination of buckling loads for flat panels from test results is notoriously difficult because the buckles initially develop slowly with little out-of-plane distortion and it is hard to recognize the load at which they first appear. This is particularly so if the stiffeners are on one side of the skin only, so that bending out of the original flat plane of the skin occurs immediately upon application of load, and is aggravated if the as manufactured skin is not perfectly flat. Usually, the buckling load is estimated from plots of measured skin strains by finding the load at which the strains bifurcate or begin to grow. Such estimates are sensitive to the location of the strain gauges relative to the nodal lines of the initial buckle pattern. This, together with variations in user judgment, can lead to ambiguous answers.

A method is presented here for determining experimental buckling loads for *shear* panels. The method employs the "diagonal tension factor", k, which is a measure of the amount of diagonal tension developed in the buckled skin. Following the model of Kuhn [1952 & 1956], which is also

described by Perry [1950], and referring to Figure 1, which is adapted from Figure 8 of Kuhn [1952], the applied shear flow q is assumed to be divided into two parts, a portion (1-k)q carried by shear resistant (SR) action of the skin, and the remainder kq carried by diagonal tension (DT) action in the (post)buckled skin, i.e. by a tensile stress in the direction of the folds of the buckled skin. The objective of the method is to derive an expression for k as a function of membrane stress resultants $N_{x'}$, $N_{y'}$ and $N_{x'y'}=q>0^*$, where x' is normal to the stiffener direction, and y' is parallel to the stiffener (or axial) direction. These resultants are calculated from strain gauge readings (a considerable effort in itself) and analytically determined skin stiffnesses. Because k is a measure of the amount of diagonal tension developed in the skin, a zero value of k infers initial buckling. Therefore, an unambiguous estimate of the experimental buckling load can be obtained by plotting k against load to determine the load at which k is zero. The expression relating k to $N_{x'}$, $N_{y'}$ and q is derived next.

From standard stress resultant transformation equations (or use of Mohr's circle, see Perry [1950]), the following expressions for the skin stress resultants, N_x, N_y, and N_{xy}, in the diagonal tension axis system x, y (where, see Figure 1, x is parallel to the direction of the diagonal tension fold, and y in normal to it in the plane of the skin) can be written in terms of the applied skin shear flow q:

$$\begin{Bmatrix} N_x \\ N_y \\ N_{xy} \end{Bmatrix} = \begin{Bmatrix} N_x \\ N_y \\ N_{xy} \end{Bmatrix}_{SR} + \begin{Bmatrix} N_x \\ N_y \\ N_{xy} \end{Bmatrix}_{DT}$$

$$= \begin{Bmatrix} (1-k)\, q\, \sin(2\alpha) \\ -(1-k)\, q\, \sin(2\alpha) \\ (1-k)\, q\, \cos(2\alpha) \end{Bmatrix}_{SR} + \begin{Bmatrix} 2kq/\sin(2\alpha) \\ 0 \\ 0 \end{Bmatrix}_{DT}$$

$$= \begin{Bmatrix} (1-k)\, q\, \sin(2\alpha) + 2kq/\sin(2\alpha) \\ -(1-k)\, q\, \sin(2\alpha) \\ (1-k)\, q\, \cos(2\alpha) \end{Bmatrix} \qquad (2),\ (3),\ (4)$$

In these equations, the diagonal tension angle, α, is the angle the diagonal folds make relative to the normal to the stiffener direction (i.e., α is measured from the structural axis, x', to the diagonal tension fold axis, x). Equations (2) and (3) are given in Kuhn [1952 & 1956] and Perry [1950], and

---

* Throughout this work, q is taken to be positive, as is its buckling value, q_{cr}.

Eq. (4) stems directly from the stress resultant transformation equations. From Eq. (4) it may be concluded that the direction of the diagonal tension fold is generally not the same as the principal stress direction unless all the shear is carried by diagonal tension (k=1), or if $\alpha = 45°$.

To relate k to the stress resultants in the structural axis system, we invoke the first stress invariant, namely, that the sum of normal stress resultants is invariant with respect to an orthogonal transformation of coordinates, i.e.,

$$N_x + N_y = N_{x'} + N_{y'} \tag{5}$$

and we substitute N_x and N_y from Eqs. (2) and (3) into this equation to obtain

$$k = \frac{(N_{x'} + N_{y'})}{2q} \sin(2\alpha) \tag{6}$$

To express k as a function of the three stress resultants only, we need a relationship between α and the resultants. To obtain this relationship, we equate the maximum principal stress resultant expressed in the structural (x', y') and diagonal tension (x, y) axis systems to get

$$\frac{(N_{x'} + N_{y'})}{2} + \sqrt{\frac{(N_{x'} - N_{y'})^2}{4} + q^2} = \frac{(N_x + N_y)}{2} + \sqrt{\frac{(N_x - N_y)^2}{4} + N_{xy}^2}$$

Eliminating the sum of the resultants on each side of this equation by virtue of Eq. (5,) and then squaring the radical gives

$$\frac{(N_{x'} - N_{y'})^2}{4} + q^2 = \frac{(N_x - N_y)^2}{4} + N_{xy}^2$$

which is also recognizes as being the square of the radius in the x and x' directions of Mohr's circle for stress resultants. To eliminate the stress resultants N_x, N_y and N_{xy} in the diagonal tension axis system, we substitute Eq. (1), (2) and (3) into this equation to get

$$(N_{x'} - N_{y'})^2 = \left[\frac{2kq}{\sin(2\alpha)} + 2(1-k)q \sin(2\alpha)\right]^2 + 4(1-k)^2 q^2 \cos^2(2\alpha) - 4q^2$$

$$= \left[\frac{2kq}{\sin(2\alpha)}\right]^2 + 8k(1-k)q^2 + 4(1-k)^2q^2 - 4q^2$$

$$= \left[\frac{2kq}{\sin(2\alpha)}\right]^2 - 4k^2q^2 \qquad (7)$$

q on the right hand side of this equation may be expressed in terms of $N_{x'}$ and $N_{y'}$ by summing Eq. (1) and (2), and using Eq. (5) to give

$$(N_{x'} - N_{y'})^2 = \left[\frac{2kq}{\sin(2\alpha)}\right]^2 \qquad (8)$$

so that Eq. (7) becomes

$$(N_{x'} - N_{y'})^2 = (N_{x'} + N_{y'})^2 - (N_{x'} + N_{y'})^2 \sin^2(2\alpha) = (N_{x'} + N_{y'})^2 \cos^2(2\alpha)$$

Thus, the angle of diagonal tension is

$$\alpha = \frac{1}{2}\cos^{-1}\left(\frac{N_{x'} - N_{y'}}{N_{x'} + N_{y'}}\right) \qquad (9)$$

To get the final expression for k in terms of the stress resultants in the structural axis system, we square Eq. (6) for k to get

$$k^2 = \frac{(N_{x'} + N_{y'})^2}{4q^2}\sin^2 2\alpha = \frac{(N_{x'} + N_{y'})^2}{4q^2}(1-\cos^2 2\alpha)$$

and substitute α from Eq. (9) to yield

$$k^2 = \frac{(N_{x'} + N_{y'})^2}{4q^2}\frac{(4N_{x'}N_{y'})}{(N_{x'} + N_{y'})^2}$$

from which, finally

$$k = \frac{\sqrt{N_{x'}\,N_{y'}}}{q} \qquad (10)$$

Experimental values of k, as a function of load level, are obtained from this equation by calculating the stress resultants $N_{x'}$, $N_{y'}$ and q from strain gauge readings and analytically determined skin stiffnesses. As mentioned earlier, the parameter k is a measure of the amount of diagonal tension developed in the skin. Therefore, by plotting k against the load P and extrapolating the plot back to the load at which k is zero (which infers buckling), an unambiguous estimate of the buckling load, P_{cr}, can be obtained. The corresponding value of the buckling shear flow, q_{cr}, is obtained from a (very nearly linear) plot of the skin shear flow, q (also calculated from the measured strains), against P, and determining the value of q corresponding to P_{cr}.

B.3 Buckling Results Based on the "Diagonal Tension Factor Method"

Panel A1 was instrumented with back-to-back rosette gauges on the skin at the center of the center bay between the two stiffeners, and at the quarter points of the center and one side bay, see Visconti [1988]. The measured strains recorded during loading to failure were averaged for each pair of back-to-back gauges. Using calculated skin stiffnesses, the stress resultants $N_{x'}$, $N_{y'}$ and q were obtained, and these were then averaged for the three locations The factor k was then calculated from Eq. (10) and plotted against load, as shown in Figure 3. By linear extrapolation back to the load at which k is zero, the estimated buckling load P_{cr} and the corresponding value of q_{cr} are

- **A 1**: P_{cr} = 37.5 Kips, q_{cr} = 634 ppi (11)

The same procedures were applied to panel B1, as shown in Figure 3, resulting in the following values:

- **B 1**: P_{cr} = 17.6 Kips, q_{cr} = 302 ppi (12)

Panel C1 was instrumented with back-to-back rosette gauges at the center of each bay of this one-stiffener panel. The recorded strains were averaged for each pair of back-to-back gauges. The value of the diagonal tension factor k was then calculated. This procedure was performed for three test runs: a preliminary run to 16 Kips in increments of 2 Kips; a second run to 10 Kips in 1 Kip increments to more accurately record the buckling behavior, and the final run in 4 Kips increments to failure (see Visconti [1988]). The plots of k versus load for each test are shown in Figure 4, together with a linear curve fit to the combined set.

The results for panel C1 are:

- **C1**: $(P_{cr})_{k=0}$ = 3.96 Kips, $(q_{cr})_{k=0}$= 60.8 ppi (13)

The subscript "k=0" is appended to these results for C1 to distinguish them from the STAGS results given in Eq. (1). Comparison of Eqs. (13) and (1) for C1 shows that the method developed here gives a value of q_{cr} that is within 4% of the STAGS prediction. Either of the two close value of q_{cr} for C1 can be used as input to SNAPPS with inconsequential differences in results. We choose to use the STAGS value (Eq. (1)).

B.4 Closing Comment

Although the above favorable correlation between values of q_{cr} obtained by the "diagonal tension factor method" and STAGS is encouraging for panel C1, it is to be emphasized that more work is required to verify the adequacy of this new method.

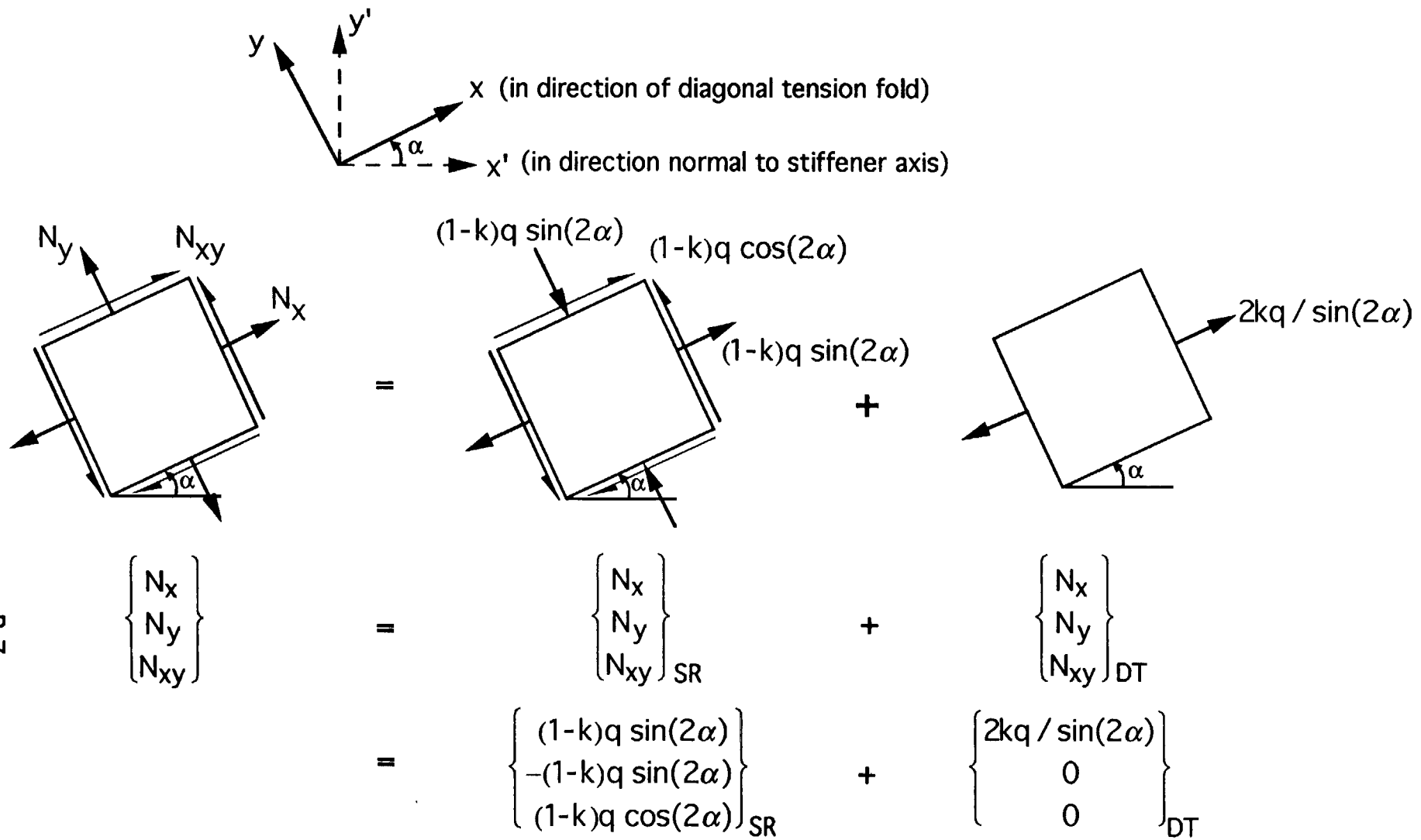

FIGURE 1 DIAGONAL TENSION STRESS RESULTANTS (ADAPTED FROM KUHN, [1952]). THE APPLIED SHEAR FLOW q IS DIVIDED INTO TWO PARTS, A PORTION (1-k)q CARRIED BY SHEAR RESISTANT ACTION, WHERE k IS THE "DIAGONAL TENSION FACTOR", AND THE REMAINDER kq IS CARRIED BY DIAGONAL TENSION ACTION. THIS FIGURE SHOWS THE STRESS RESULTANTANTS DUE TO EACH PART.

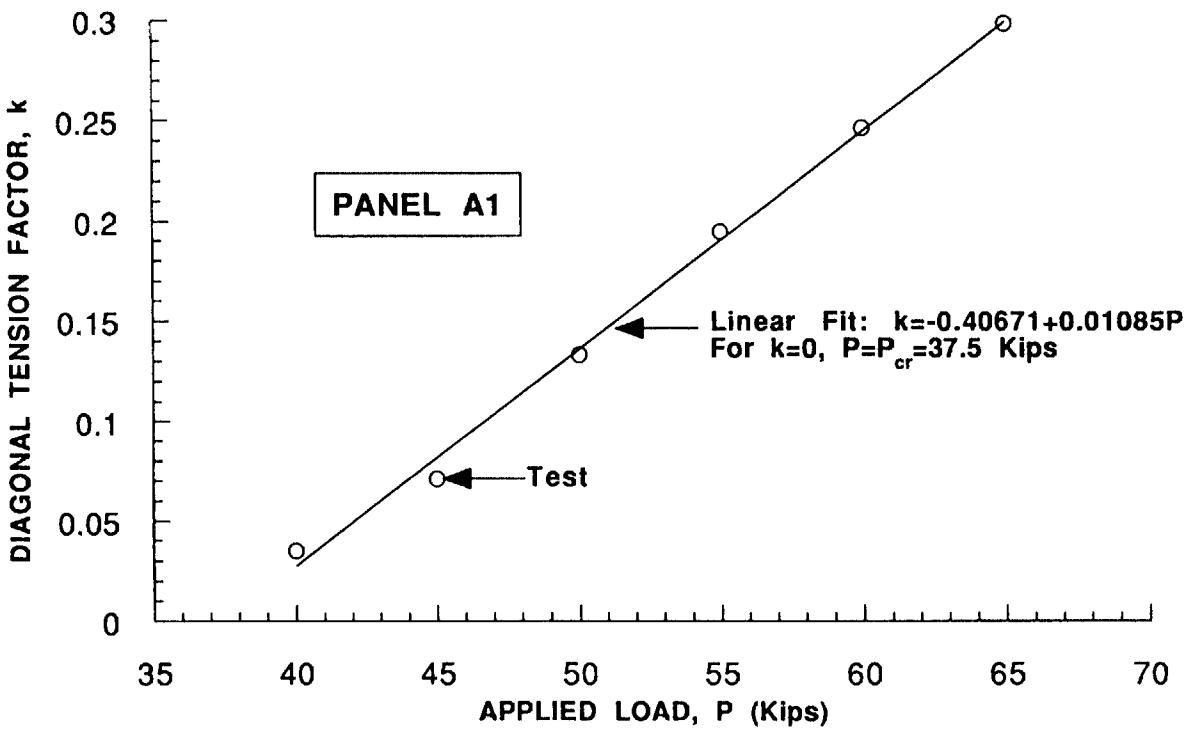

FIGURE 2 DETERMINATION OF THE EXPERIMENTAL VALUE OF THE BUCKLING LOAD FOR PANEL A1

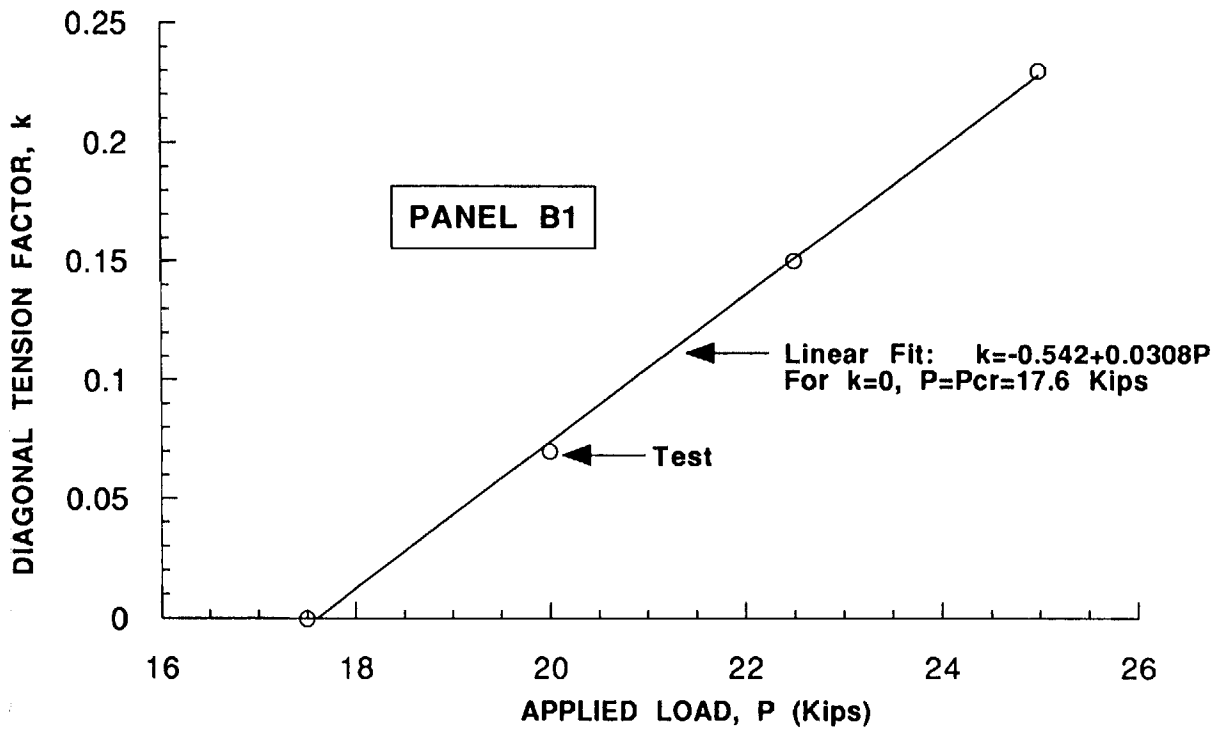

FIGURE 3 DETERMINATION OF THE EXPERIMENTAL VALUE OF THE BUCKLING LOAD FOR PANEL B1

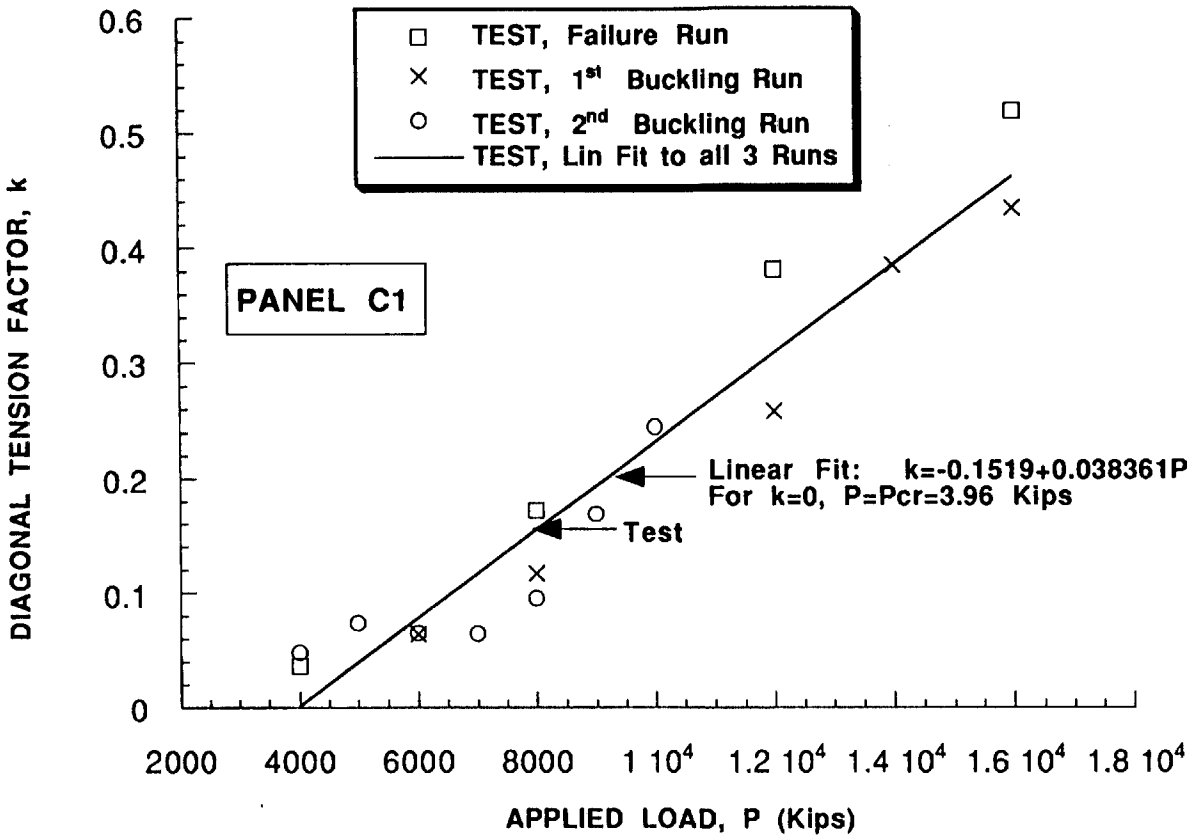

FIGURE 4 DETERMINATION OF THE EXPERIMENTAL VALUE OF THE BUCKLING LOAD FOR PANEL C1

APPENDIX C

PRINCIPAL STRESS RESULTANTS IN SKIN

C.1 Introduction

This appendix presents expressions for the principal inplane membrane stress resultants N_1 and N_2 as a function of the shear load. N_1 is positive when it is in tension, and N_2 is taken to be positive when it is in compression. Expressions are also given for the inplane stress resultants $N_{x'}$ and $N_{y'}$, which are, respectively, normal to the stiffener direction, which is the global x' direction, and parallel to the stiffener direction, which is the global y' direction. The global (x', y') axis system is also referred to as the structural axis system. The skin is loaded by an applied inplane shear flow q relative to the structural axis system. The shear flow can be applied in either of two directions for a fixed stacking sequence. Throughout this work, q is taken to be positive, as is its buckling value, q_{cr}.

Prior to buckling, the principal stress resultants equal q and make an angle of 45° relative to the global axes. The objective here is to determine their values after buckling. The expressions for the stress resultants are based on two simplifying assumptions (Eqs. (1) and (5)) that are reasonable for the objective of developing a simplified postbuckling method. The validity of these assumptions is confirmed by comparing predictions based on them with test results for the three test panels A1, B1, C1 described in Appendix A.

C.2 Principal Stress Resultants

The angle of diagonal tension (see Figure 1 of Appendix B) for *flat* shear panels is assumed to be

$$\alpha = 45°. \tag{1}$$

Figure 1 of Section 3 shows that this is a good approximation for the three tested. The experimental values of α in this figure are based on Eq. (9) of Appendix B, which is repeated below for completeness:

$$\alpha = \frac{1}{2} \cos^{-1} \left(\frac{N_{x'} - N_{y'}}{N_{x'} + N_{y'}} \right)$$

For this assumed value of α, Eq. (4) of Appendix B states that the shear stress resultant, N_{xy}, in the diagonal tension axis system vanishes. Hence, the direct stress resultants, N_x and N_y, are in fact principal resultants, N_1 and N_2, i.e., the principal stress resultants line up with the diagonal tension folds at all load levels. Noting that N_2 is assumed to be positive when it is in compression, Eqs. (2) and (3) of Appendix B give

$$N_1 = (1+k)q \tag{2}$$

and

$$N_2 = (1-k)q \tag{3}$$

where k is the diagonal tension factor described in Appendix B. Based on test results for *aluminum* panels, Kuhn [1952] gives the following empirical expression for k:

$$k_{Kuhn\text{-}DT} = \text{Tanh}[0.5\log(q/q_{cr})] \tag{4}$$

For the three panels considered in the present work, Figures 2 through 4 of Section 3 compares principal stress resultants obtained from Kuhn's diagonal tension (DT) model based on k from Eq. (4) with results from tests and STAGS (for C1 only). The STAGS results agree well with those from test, but the Kuhn-DT model slightly under-predicts the maximum principal diagonal tension stress resultant, N_1, but considerably over-predicts the minimum principal stress resultant, N_2, in the buckled panels. Furthermore, as may be observed from Figure 1, the Kuhn-DT model predicts a significant degradation in shear stiffness with increasing load in comparison with the measured and STAGS results for C1. For example, at the test failure load, the shear strain predicted by the Kuhn-DT model is about 30% higher than that of the test and STAGS for C1. Also, examination of the STAGS and test results in the figure reveals that the overall shear stiffness of the panel is constant*, and is equal to the initial shear stiffness (c.f., the linear and nonlinear STAGS analysis results.), a result that we use in Appendix E, where we calculate the maximum out-of-plane displacement as a function of load. In view of these findings, we decided not use Kuhn's empirical expression for k. Besides, we want the

* Note, however, that there is a reduction in *overall* stiffness at the bifurcation buckling point, of course, as is evidenced from a plot of the overall corner displacement, δ, at the loaded corner against the fixture load, P, as shown in Figure 7 of Sobel and Sharp [1994]. The slope of the P-δ curve is a measure of the overall stiffness of the panel and therefore represents all stiffnesses, including out-of-plane bending stiffnesses, as is evident from the energy consideration that $P\delta/2$ equals the panel's total strain energy (bending plus membrane).

SNAPPS methodology to be devoid of all empiricism. To obtain k, and hence N_1 and N_2 via Eqs. (2) and (3), we make a further assumption; namely, that the compressive principal resultant after buckling, N_2, is constant for all values of q and equal to the buckling shear flow, q_{cr}, i. e.,

$$N_2 = q_{cr}, \text{ (for } q \geq q_{cr}) \tag{5}$$

With this assumption, Eq. (3) gives

$$k = 1 - q_{cr}/q \tag{6}$$

Inserting Eq. (6) into Eq. (2) provides the following expression for the tensile principal resultant after buckling:

$$N_1 = 2q\text{-}q_{cr}, \text{ (for } q \geq q_{cr}) \tag{7}$$

This view of events is similar to that proposed by Wagner in the "frame analogy", as described by Kuhn [1952] and illustrated in Figures 3a and 3b of Kuhn. It is noted that Kuhn first gives an expression for k (Kuhn's Eq. (26)) that is the same as the "Wagner-type" expression for k ((Eq. (6) above), but later abandoned it in favor of an empirically determined diagonal tension factor, Eq. (4).

It is important to point out that if N_2 was assumed to increase (in an absolute sense) above its value at buckling, then N_1 would have to decrease by the same amount in order for the sum of (N_1+ N_2) to remain constant (in accord with the first stress invariant principle), and this would lead to a higher predicted failure load, q_{fail}. Thus, the assumption that $N_2 = q_{cr}$ after buckling is conservative. On the other hand, it would be unrealistic to assume that N_2 is zero for all values of q, i.e., to assume a state of pure diagonal tension.

C.3 Direct Stress Resultants in Structural Axis System

Using standard equations for transformation of stresses from one orthogonal axis system to another, we readily obtain from the expressions for the stress resultants in the diagonal tension axis system (Eqs. (5) and (7)), the following expressions for the stress resultants in the structural axis system:

$$N_{x'} = N_{y'} = q\text{-}q_{cr}, \text{ (for } q \geq q_{cr}) \tag{8}$$

As a check we substitute these equations into the general expression for k, (Eq. (10)) of Appendix B, repeated below for convenience,

$$k = \frac{\sqrt{N_{x'} N_{y'}}}{q} \tag{9}$$

to obtain

$$k = 1 - q_{cr}/q$$

which is Eq. (6).

C.4 Closing Comments

The principal stress resultants described by Eqs. (5) and (7) are averages over the extent of the buckle. However, they can be used to approximate integrated quantities such as the buckle wavewidth, c (Appendix D); the maximum out-of-plane displacement, δ_{max} (Appendix E); and the rotation at the end of the tie-rod, $\bar{\theta}$ (Appendix F).

Postbuckling values of the principal stress resultants are also needed for *local* considerations at the toe of the flange. There the skin is flat and can be assumed to be in a state of pure shear. This means that the stress resultants in the skin under the toe in the diagonal tension field direction are given by

$$N_{1toe} = N_{2toe} = q, \text{ (for all q)} \tag{10}$$

It is to be recalled that N_{2toe} is taken to be positive when it is in comression, and that q>0. Equation (10) is used in Appendices H, I, and K to describe local stresses in the unbuckled skin under the toe of the flange.

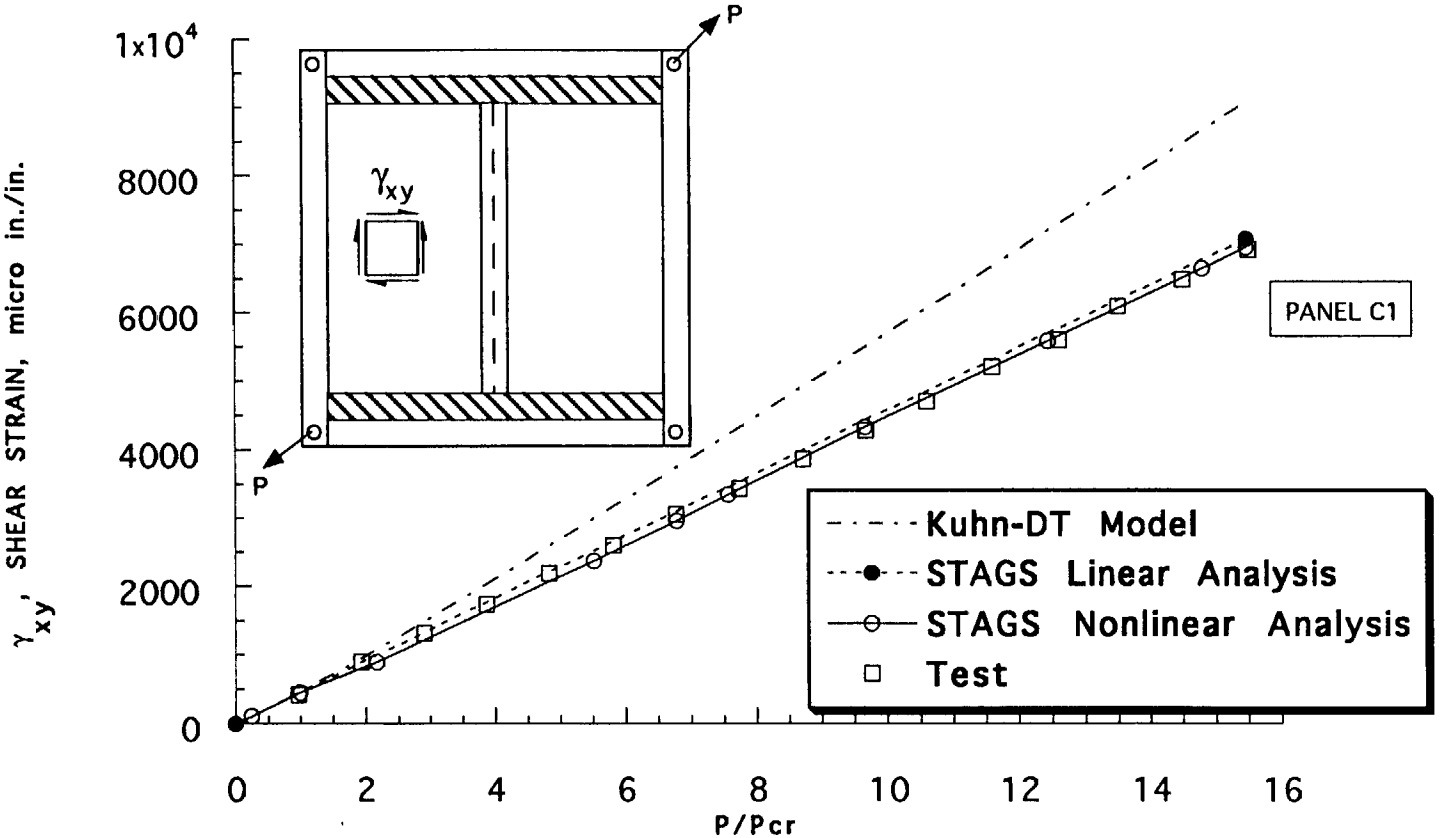

FIGURE 1 AVERAGE MEMBRANE SHEAR STRAIN AT MIDBAY FOR PANEL C1

APPENDIX D

BUCKLE WIDTH & LENGTH

D.1 Buckle Width

Figure 1 depicts a buckle bounded by adjacent nodal lines and the stiffener flanges. The buckle width c is determined next from considerations of out-of-plane equilibrium. If we assume that the buckle may be approximated by the rectangle ABCD of length ℓ and width c, then we may take the out-of-plane displacement δ as

$$\delta(\xi,\eta)=\delta_{max}\sin\frac{\pi\xi}{\ell}\sin\frac{\pi\eta}{c} \qquad (1)$$

where the axis system has its origin at B; ξ is measured from B to C, η is measured from B to A. The stress resultant in the ξ direction is tensile and is denoted by N_1; that in the η direction is compressive and is denoted by N_2 (a positive N_2 is compressive). As discussed in Appendix C, they are assumed to be constant throughout the area bounded by the rectangle ABCD. This piece of the buckled sheet has to be put into equilibrium normal to its original flat plane, under the components of N_1 and N_2 acting through the slopes along the edges of the distorted shape.

The total out-of-plane force due to the tensile stress resultant N_1 acting at the angle $d\delta/d\xi$ along one edge of the buckle (such as AB in Figure 1) is then given by

$$\int_0^c N_1\left(\frac{d\delta}{d\xi}\right)_{\xi=0}d\eta = 2\,N_1\,\delta_{max}\frac{c}{\ell}$$

This must be balanced by the following out-of-plane force due to the compressive stress resultant N_2 acting at the angle $d\delta/d\eta$ along a nodal edge of the buckle (such as BC in Figure 1):

$$\int_0^\ell N_2\left(\frac{d\delta}{d\eta}\right)_{\eta=0}d\xi = 2\,N_2\,\delta_{max}\frac{\ell}{c}$$

By equating these two forces, we obtain

$$2\,N_1\,\delta_{max}\,\frac{c}{\ell} = 2\,N_2\,\delta_{max}\,\frac{\ell}{c}$$

It is seen that δ_{max} in this equation conveniently cancels out (δ_{max} is determined in the next appendix) thereby providing the following expression for the buckle aspect ratio:

$$\frac{c}{\ell} = \sqrt{\frac{N_2}{N_1}} \tag{2}$$

In terms of known quantities, and assuming that the diagonal tension angle α is 45°, the length ℓ can be written as

$$\ell = \left(\frac{b-2L_f}{\cos\alpha}\right) - c$$

From Figure 1, $\frac{b-2L_f}{\cos\alpha}$ is the length OC, denoted by L, the known toe-to-toe distance between flanges measured in the diagonal tension axis system, i.e.,

$$L = \left(\frac{b-2L_f}{\cos\alpha}\right) \tag{3}$$

Thus

$$\ell = L - c$$

so that Eq. (2) yields the following expression for the buckle wavewidth:

$$c = L\left(\frac{\sqrt{\frac{N_2}{N_1}}}{1+\sqrt{\frac{N_2}{N_1}}}\right) \tag{4}$$

in which (see Appendix C)

$$N_1 = 2q - q_{cr}, \quad (q>q_{cr}), \tag{5}$$

$$N_2 = q_{cr}, \quad (q>q_{cr}). \tag{6}$$

It is to be recalled that positive N_1 is tensile, and positive N_2 is compressive.

At buckling, for which $N_1 = N_2$, Eq. (4) yields

$$\left(\frac{c}{L}\right)_{cr} = \frac{1}{2}$$

whereas, from Timoshenko and Gere's [1961, page 383] buckling analysis of a long, simply supported, isotropic plate under shear, it may be shown that

$$\left(\frac{c}{L}\right)_{cr,Timo} = \frac{1}{2}\sqrt{1.5}$$

It is proposed that Eq. (4) be modified to pass through this buckling point to give

$$c = \sqrt{1.5}\, L \left\{ \frac{\sqrt{\frac{N_2}{N_1}}}{1+\sqrt{\frac{N_2}{N_1}}} \right\} = 1.225\, L \left\{ \frac{\sqrt{\frac{N_2}{N_1}}}{1+\sqrt{\frac{N_2}{N_1}}} \right\} = 1.225\, L \left\{ \frac{\sqrt{\frac{q_{cr}}{2q-q_{cr}}}}{1+\sqrt{\frac{q_{cr}}{2q-q_{cr}}}} \right\} \tag{7}$$

From the last term on the right, it is seen that the wavewidth c is expressed as a function of the load level q. Effectively, we determined the shape of the c vs. q curve from equilibrium considerations, and adjusted the amplitude (by 22.5%) of the curve to have the curve pass through the buckling point.

D.2 Buckle Length

The axial wavelength, L_b, which is the projected length of the wavewidth along the stiffener axis, is used in Section 3 for correlating SNAPPS results with those from test and STAGS. From Figure 1, it is seen to be given by

$$L_b = \frac{c}{\cos \alpha} \tag{8}$$

From Eqs. (3) and (7), and with the angle of diagonal tension equal to 45°, the wavelength may be written in the following dimensionless form:

$$\frac{L_b}{b_{tt}} = 2\sqrt{1.5}\,\frac{\sqrt{\frac{N_2}{N_1}}}{1+\sqrt{\frac{N_2}{N_1}}} = 2.45\,\frac{\sqrt{\frac{N_2}{N_1}}}{1+\sqrt{\frac{N_2}{N_1}}} \tag{9}$$

where

$$b_{tt} = b - 2L_f \tag{10}$$

is the toe-to-toe width of the skin, measured normal to the stiffener direction (see Figure 1). Note that this form for the wavelength is valid for all panel geometries. A comparison of predicted and measured wavelengths based on Eq. (9) is given in Section 3.

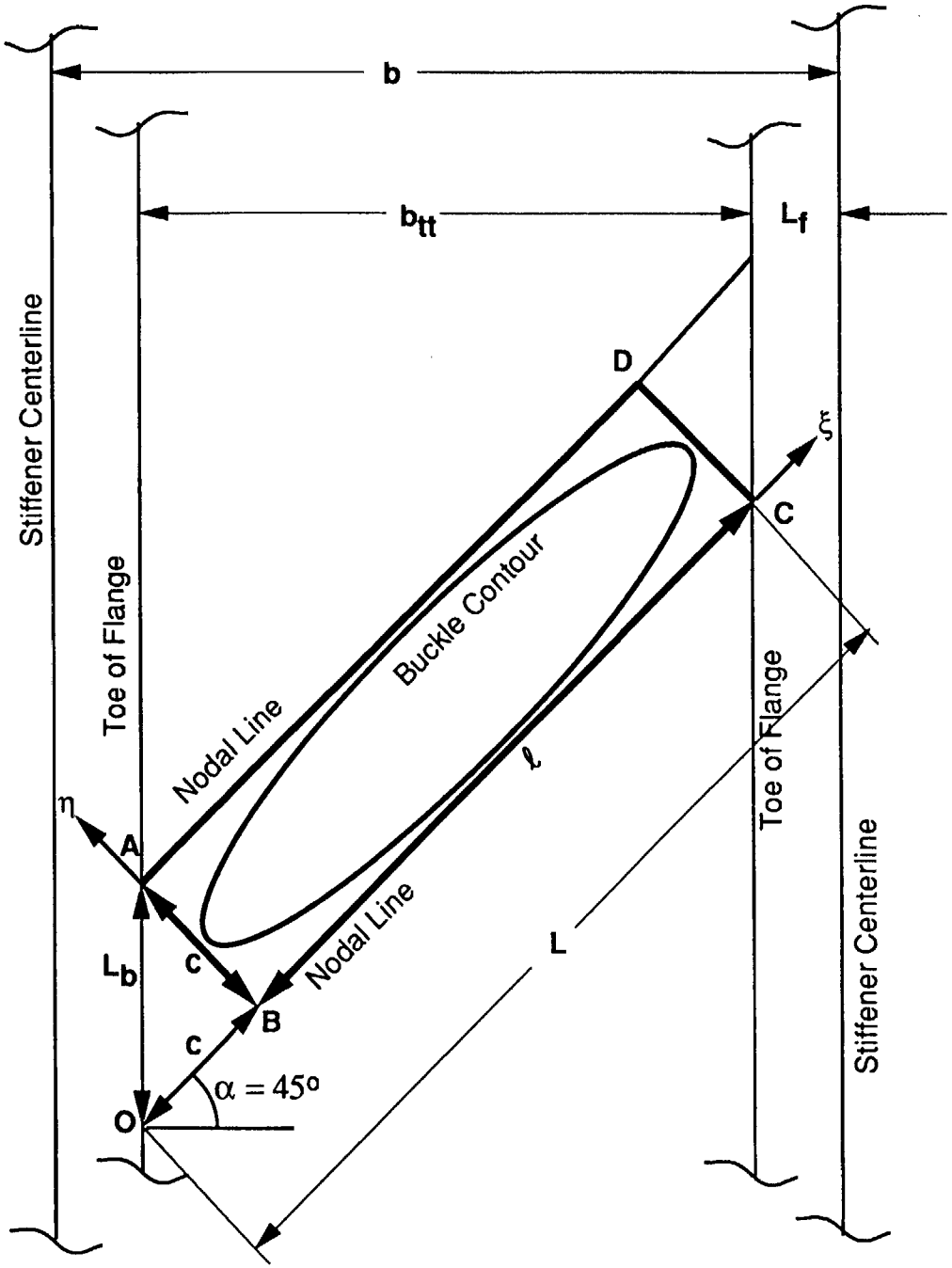

FIGURE 1 THE ANALYSIS FOR THE WAVEWIDTH, c, CONSIDERS A SINGLE BUCKLE BOUNDED BY ADJACENT NODAL LINES AND BY THE TOES OF THE STIFFENER FLANGES.

APPENDIX E

MAXIMUM OUT-OF-PLANE DISPLACEMENT

As we saw in the preceding appendix, the out-of-plane displacement, δ, through its effect on the slopes at the boundaries of the buckle, governs the out-of-plane equilibrium of the buckle, from which we were able to determine the buckle width c. Now we need to find an expression for the maximum value of the displacement, δ_{max}. The following derivation is based on the kinematic argument that the buckled sheet must fit into the distorted shape imposed by the nodal lines and the stiffeners, and that, after buckling, it does this by moving out of its original flat plane into the characteristic shear buckling pattern.

Figure 1 shows a single buckle, bounded by adjacent nodal lines and by the toes of the stiffener flanges. The length of the nodal line OC is assumed to remain unchanged in a shear distortion, and the length d of the shorter diagonal AC is given by

$$d_i^2 = L^2 + L_b^2 - 2LL_b\cos(\pi/2-\phi)$$

$$= L^2 + L_b^2 - 2LL_b\sin\phi \text{ for small values of } \gamma.$$

Imposing a shear strain γ, such that ϕ becomes $\phi+\gamma$, the new length of the diagonal AC is given by

$$d_n^2 = L^2 + L_b^2 - 2LL_b\sin(\phi+\gamma)$$

$$= (L^2 + L_b^2 - 2LL_b\sin\phi) - (2LL_b\gamma\cos\phi) \text{ for small values of } \gamma.$$

Increasing the shear strain from the buckling value γ_{cr} to γ, and expressing the change in the length of the diagonal AC as a strain ε_d [i.e. where ε_d = (new length - old length)/old length] gives

$$\varepsilon_d = (d_n-d_i)/d_i$$

$$\varepsilon_d = \frac{\left[L^2+L_b^2-2LL_b\sin\phi\ -2LL_b\gamma\cos\phi\right]^{1/2} - \left[L^2+L_b^2-2LL_b\sin\phi\ -2LL_b\gamma_{cr}\cos\phi\right]^{1/2}}{\left[L^2+L_b^2-2LL_b\sin\phi\ -2LL_b\gamma_{cr}\cos\phi\right]^{1/2}}$$

By expanding the radicals, and neglecting terms in γ^2 or higher powers, the expression for ε_d can be approximated by

$$\varepsilon_d = \frac{-LL_b(\gamma-\gamma_{cr})\cos\phi}{L^2 + L_b^2 - 2LL_b\sin\phi}$$

But $L = b_{tt}\sec\phi$ (see Figure 1) and $d^2 = (L^2 + L_b^2 - 2LL_b\sin\phi)$ so that the approximation for ε_d may be written as

$$\varepsilon_d = -\frac{L_b b_{tt}}{d^2}(\gamma-\gamma_{cr}) \qquad (1)$$

where the minus sign denotes compression.

Now, to obtain an alternate expression for ε_d in the postbuckled panel, define an axis χ along the diagonal AC, and assume the out-of-plane displacement to be

$$\delta(\chi) = \frac{\delta_{max}}{2}\left(1 - \cos\frac{2\pi\chi}{d}\right)$$

It is straightforward to show that this assumed displacement variation along the diagonal d is consistent with the double-sine displacement shape (Eq. (1) of Appendix D) used in the preceding analysis for the determination of the wavewidth c. Later we will show that δ_{max} is insensitive to the assumed displacement shape. Integrating the length ds along the curve from $0 < \chi < d$, using

$$\frac{ds}{d\chi} = \sqrt{1 + \left(\frac{d\delta}{d\chi}\right)^2} = 1 + \frac{1}{2}\left(\frac{\pi\delta_{max}}{d}\right)^2 \sin^2\left(\frac{2\pi\chi}{d}\right) \quad \text{for small } \frac{\pi\delta_{max}}{d}$$

gives the length the total S measured along the curve as

$$d\left(1 + \frac{1}{4}\left(\frac{\pi\delta_{max}}{d}\right)^2\right)$$

Expressing the change of length as a strain ε_d [= (d-S)/d] yields

$$\varepsilon_d = \frac{d - d\left(1 + \frac{1}{4}\left(\frac{\pi\delta_{max}}{d}\right)^2\right)}{d} = -\left(\frac{\pi\delta_{max}}{2d}\right)^2 \qquad (2)$$

Equating the two expressions for ε_d, Eqs. (1) and (2), provides the following closed-form expression for the maximum out-of-plane displacement:

$$\delta_{max} = \frac{2}{\pi}\sqrt{L_b b_{tt}(\gamma-\gamma_{cr})} \tag{3}$$

It may be noted that the precise shape of the out-of-plane distortion is not very critical, because we are integrating along a curve and expressing the result as an average (ε_d). In a study in which different expressions for the assumed shape were used, such as circular arcs, parabolas, fourth-order polynomials, sine and sine squared waves, Eq. (3) retained the same form and the multiplier in front of the radical changed by less than 7% from the higher and hence more conservative value of $2/\pi$.

Because the STAGS analysis and test results for panel C1 [Sobel & Sharp, 1994] and the test results for panels A1 and B1 [Visconti, 1988] revealed that the skin shear stiffness Gt did not change with applied load level (see Figure 1 of Appendix C, and discussion therein), Eq. (3) can be written as

$$\delta_{max} = \frac{2}{\pi}\sqrt{L_b b_{tt}\left(\frac{q-q_{cr}}{Gt}\right)} \tag{4}$$

In this expression, b_{tt} is the toe-to-toe distance measured normal to the stiffener direction, i. e.,

$$b_{tt} = b-2L_f \tag{5}$$

where b is the stiffener spacing, L_f is width of the flange measured from stiffener centerline to toe, and L_b is the buckle wavelength projected along the stiffener axis. An expression for L_b is given in the preceding Appendix.

An alternative form for the maximum out-of-plane displacement may be obtained by inserting

$L_b = c\sec\phi$ and $b_{tt} = L\cos\phi$ (see Figure 1),

into Eq. (4). This yields the following formula, written in terms of diagonal tension axes:

$$\delta_{max} = \frac{2}{\pi}\sqrt{Lc\left(\frac{q-q_{cr}}{Gt}\right)} \tag{6}$$

In this equation, L is the toe-to-toe length of the diagonal tension fold, and c is the buckle width for which the following expression is derived in the preceding Appendix:

$$c = \sqrt{1.5}\, L \left\{ \frac{\sqrt{\frac{N_2}{N_1}}}{1+\sqrt{\frac{N_2}{N_1}}} \right\} = \sqrt{1.5}\, L \left\{ \frac{\sqrt{\frac{q_{cr}}{2q-q_{cr}}}}{1+\sqrt{\frac{q_{cr}}{2q-q_{cr}}}} \right\} \tag{7}$$

The form for the maximum out-of-plane displacement given by Eq. (6) is used in the SNAPPS code of Appendix N.

From the last two equations, the maximum out-of-plane displacement may be written in the following dimesionless form:

$$\frac{\delta_{max}}{L(\gamma_{cr})^{1/2}} = \frac{2}{\pi}(1.5)^{.25} \sqrt{\left\{ \frac{\sqrt{\frac{1}{2\frac{q}{q_{cr}}-1}}}{1+\sqrt{\frac{1}{2\frac{q}{q_{cr}}-1}}} \right\} \left\{ \frac{q}{q_{cr}} - 1 \right\}} \tag{8}$$

$$= 0.7045 \sqrt{\left\{ \frac{\sqrt{\frac{1}{2\frac{q}{q_{cr}}-1}}}{1+\sqrt{\frac{1}{2\frac{q}{q_{cr}}-1}}} \right\} \left\{ \frac{q}{q_{cr}} - 1 \right\}}$$

This dimensionless form for δ_{max} is used in Section 3 to compare predicted and measured values of the maximum out-of-plane displacement. Note that form is valid for all panel geometries

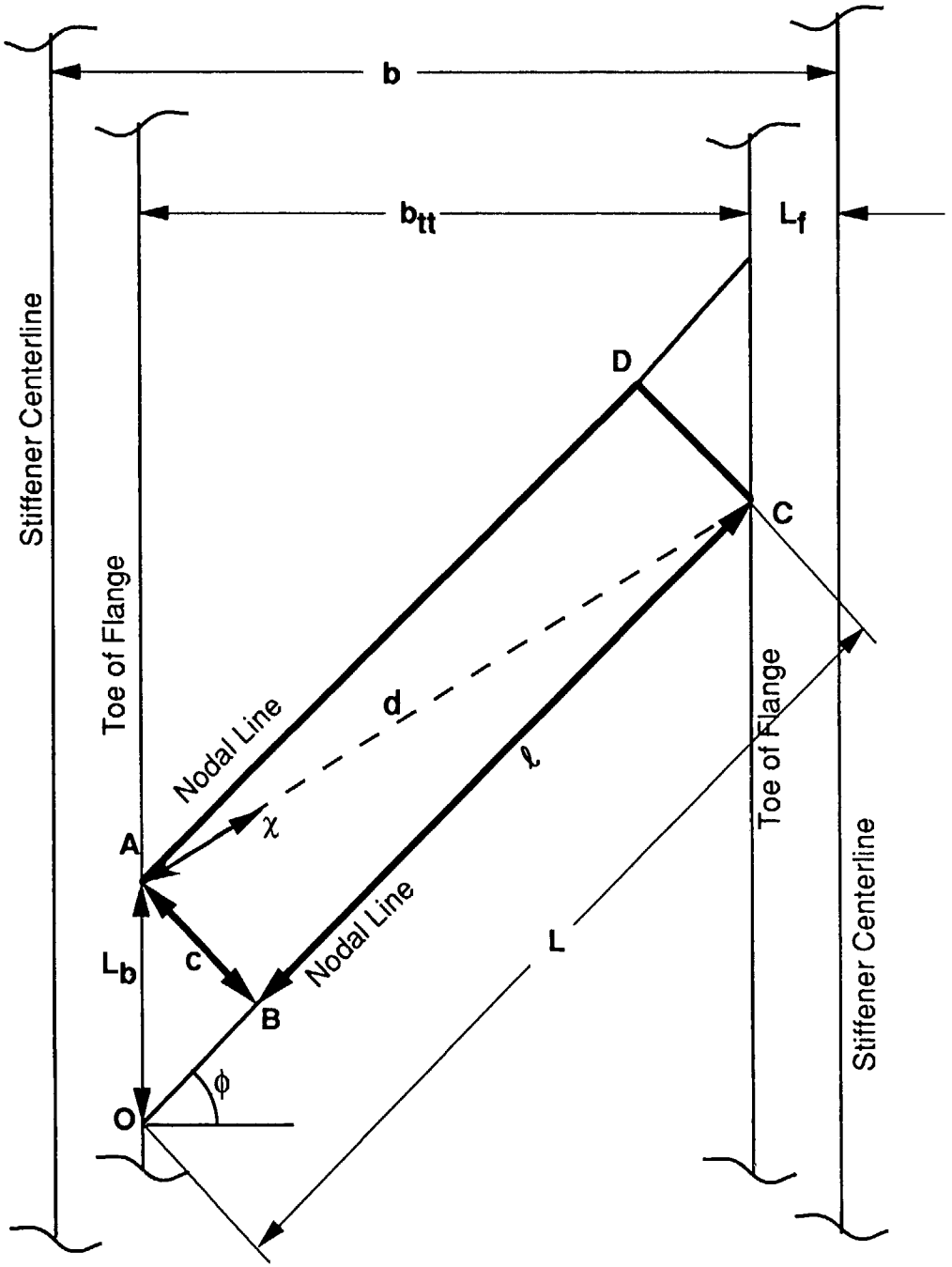

FIGURE 1 THE ANALYSIS FOR THE MAXIMUM OUT-OF-DISPLACEMENT, δ_{max}, CONSIDERS THE KINEMATICS OF A SINGLE BUCKLE, BOUNDED BY ADJACENT NODAL LINES AND BY THE TOES OF THE STIFFENER FLANGES.

APPENDIX F

TIE-ROD ANALYSIS

F.1 Introduction

The development of the simplified analysis now proceeds to the "tie-rod" analysis in which a unit width of skin parallel to the long axis of the diagonal tension buckle is assumed to be loaded axially by the tensile stress resultant, N_1, and by a lateral load p, which is normal to the original unbuckled plane of the skin and which represents the out-of-plane component of the compressive stress resultant N_2. For this simplified analysis, it suffices to assume that N_1 and N_2 are constant along the length of the tie-rod, but, in fact, both stress resultants vary along the length and fall to the unbuckled values at the toe of the flange. Because the angle through which N_2 acts varies, the lateral load p is assumed to vary sinusoidally along the length of the nodal line, a variation consistent with those used in the wavewidth (Appendix D) and maximum out-of-plane displacement (Appendix E) analyses. The objective of the tie-rod analysis is to obtain a closed-form expression for the rotation $\bar{\theta}$ at the end of the tie-rod in terms of the axial load N_1, the maximum out-of-plane displacement δ_{max}, and the moment $\bar{M}$ at the end of the tie-rod.

Figure 1 shows the tie-rod model. The upper half of Figure 1a depicts the assumed bi-sinusoidal buckle pattern in a typical diagonal tension fold, and the shaded strip in the lower half represents one-half of the tie-rod model, which extends along the entire length, L, of the buckle*. The tie-rod model is further displayed in Figures 1b to 1d. From Figure 1c it is seen that the vertical (out-of-plane) component of the compressive membrane force, N_2, produces transverse shear forces at the edges of the tie-rod. As just mentioned, these edge forces are assumed to vary sinusoidally in the direction of the fold (Figures 1b and 1d) and are represented by a lateral (out-of-plane) running load, p (Figures 1b and 1c).

---

* The stiffener is not shown in the figure, to avoid excessive clutter. However, the downward deformation of the buckle, implies that the stiffener is on the top surface of the skin (on the surface with the negative y coordinate.

The running load p is reacted by the edge forces R (Figure 1d). Thus, R balances the vertical component of N_2 that varies along the longitudinal edges of the strip.

For simplicity, the tensile axial load in the tie-rod model is held constant at it's average value (i.e. $N_1 = 2q\text{-}q_{cr}$, see Appendix C) and the solution is then tractable. In fact, the axial load must be slightly above the average value over most of the length of the tie-rod, but must fall, over an undefined—but assumed small—distance at each end, to the value in the unbuckled sheet (i.e. $N_{1toe} = q$, see Appendix C)

F.2 Solution Of Tie-Rod Problem

Figure 2 displays the notation and sign conventions. The x axis is in the direction of the diagonal tension fold, and it's origin is at mid-length of the fold. The y axis is normal to the plane of the skin. Because the solution of the tie-rod problem is straightforward, it is presented in more-or-less outline form.

- Relate Reaction R to Magnitude (p_o) of the Pressure p

$$R = \frac{1}{2}\left[2\int_0^{\frac{L}{2}} p_o \cos\left(\frac{\pi x}{L}\right)\right] = \frac{L}{\pi} p_o \qquad (1)$$

- Differential Equation (DE), [Timoshenko, 1956]

$$D_{sr}w'''' - N_1 w'' = p_o \cos\left(\frac{\pi x}{L}\right) \qquad (2)$$

where $(\,)' = \frac{d}{dx}(x)$ and D_{sr} is the bending stiffness of the skin (subscript "s" for "skin", subscript "r" for "rotated" in the direction of the diagonal tension fold).

Letting:

$$\lambda^2 = \frac{N_1}{D_{sr}} \qquad (3)$$

The DE becomes:

$$w'''' - \lambda^2 w'' = \frac{p_o}{D_{sr}} \cos\left(\frac{\pi x}{L}\right) \tag{4}$$

- Complementary Solution, w_c

  The solution of the homogenous form of Eq. (2) is

  $$w_c = A\text{Cosh}(\lambda x) + B\text{Sinh}(\lambda x) + C + Dx$$

- Particular Solution, w_p

  A particular solution of Eq. (2) is easily shown to be:

  $$w_p = r \frac{R}{N_1} \cos\left(\frac{\pi x}{L}\right) \tag{5}$$

where r, which has dimensions of length, is given by

$$r = \frac{\frac{L}{\pi}}{1 + \left(\frac{\pi}{\lambda L}\right)^2} \tag{6}$$

- Total Solution, $w = w_c + w_p$

  $$w = A\text{Cosh}(\lambda x) + B\text{Sinh}(\lambda x) + C + Dx + r \frac{R}{N_1} \cos\left(\frac{\pi x}{L}\right) \tag{7}$$

Because the displacement must be symmetric about the midlength, $x = 0$, the two asymmetrical terms (B Sinh (λx) and Dx) must vanish.

Therefore,

$$w = A\text{Cosh}(\lambda x) + C + r \frac{R}{N_1} \cos\left(\frac{\pi x}{L}\right) \tag{8}$$

The arbitrary constants (A and C) in this equation are determined from the following boundary conditions (BC) at $x = \pm \frac{L}{2}$):

BC1: $M\left(\pm \frac{L}{2}\right) = \overline{M}$, (where $\overline{M}$ is depicted in Figure 1d)

BC2: $w\left(\pm \frac{L}{2}\right) = 0$

Using $M = -D_{sr}w''$ (see Figure 2b) and Eq. (3), BC1 becomes:

$$w''\left(\pm \frac{L}{2}\right) = -\frac{\overline{M}}{D_{sr}} = -\lambda^2 \frac{\overline{M}}{N_1}$$

Substituting Eq. (8) for w into the above expression yields the arbitrary constant A:

$$A = -\text{Sech}\left(\frac{\lambda L}{2}\right)\frac{\overline{M}}{N_1} \tag{9}$$

The constant C is obtained from BC2 and Eq. (9):

$$C = -A\text{Cosh}\left(\frac{\lambda L}{2}\right) = +\text{Sech}\left(\frac{\lambda L}{2}\right)\text{Cosh}\left(\frac{\lambda L}{2}\right)\frac{\overline{M}}{N_1} = \frac{\overline{M}}{N_1} \tag{10}$$

Substitution of these constants into Eq. (8) provides the solution for w:

$$w(x) = \left[1 - \frac{\text{Cosh}(\lambda x)}{\text{Cosh}\left(\frac{\lambda L}{2}\right)}\right]\frac{\overline{M}}{N_1} + r\frac{R}{N_1}\cos\left(\frac{\pi x}{L}\right) \tag{11}$$

- Rotation at Left End $\left(x = -\frac{L}{2}\right)$, $\overline{\theta}$

Differentiating Eq. (11) once gives:

$$w'(x) = -\lambda\frac{\overline{M}}{N_1}\frac{\text{Sinh}(\lambda x)}{\text{Cosh}\left(\frac{\lambda L}{2}\right)} - r\frac{R}{N_1}\frac{\pi}{L}\sin\left(\frac{\pi x}{L}\right) \tag{12}$$

Therefore, the rotation, $\bar{\theta}$, at the left end $x = -\frac{L}{2}$, see Figure 1d, is:

$$\bar{\theta} = +w'\left(\frac{-L}{2}\right) = +\lambda \text{Tanh}\left(\frac{\lambda L}{2}\right)\frac{\bar{M}}{N_1} + r\frac{R}{N_1}\frac{\pi}{L} \tag{13}$$

- Maximum Displacement, δ_{max}

$$\delta_{max} = w(0) = \left[1 - \text{Sech}\left(\frac{\lambda L}{2}\right)\right]\frac{\bar{M}}{N_1} + r\frac{R}{N_1} \tag{14}$$

- Simplification of Eqs. (13) and (14) for Large Values of λL

  - $\text{Tanh}\left(\frac{\lambda L}{2}\right)$ term in $\bar{\theta}$

    $\text{Tanh}\left(\frac{\lambda L}{2}\right) \rightarrow 1$ for $\frac{\lambda L}{2} > 2$, or $\lambda L > 4$

  - $\left[1 - \text{Sech}\left(\frac{\lambda L}{2}\right)\right]$ term in δ_{max}

    Assuming a 10% error in neglecting $\text{Sech}\left(\frac{\lambda L}{2}\right)$ in comparison with unity gives

    $\text{Sech}\left(\frac{\lambda L}{2}\right) = 0.1 \Rightarrow \text{Cosh}\left(\frac{\lambda L}{2}\right) = 10$

    $\Rightarrow \frac{\lambda L}{2} = 3 \Rightarrow \lambda L > 6$

  - $1 + \left(\frac{\pi}{\lambda L}\right)^2$ term in denominator of r (Eq. (6))

    Assuming a 10% error in neglecting $\left(\frac{\pi}{\lambda L}\right)^2$ in comparison with unity gives

    $\left(\frac{\pi}{\lambda L}\right)^2 = 0.1 \Rightarrow \lambda L = \frac{\pi}{\sqrt{0.1}} = 9.9$, or $\lambda L > 10$

$$\Rightarrow r = \frac{L}{\pi}$$

With the above approximations, the equations for the rotation and maximum out-of-displacement simplify to

$$\bar{\theta} \approx \lambda \frac{\bar{M}}{N_1} + \frac{R}{N_1} \tag{18}$$

$$\delta_{max} \approx \frac{\bar{M}}{N_1} + \frac{L}{\pi} \frac{R}{N_1} \tag{19}$$

In view of the above discussion the simplified equations for $\bar{\theta}$ and δ_{max} are valid for:

$$\lambda L > 10 \tag{20}$$

The simplified expressions given by Eqs. (18) and (19) are used in this report.

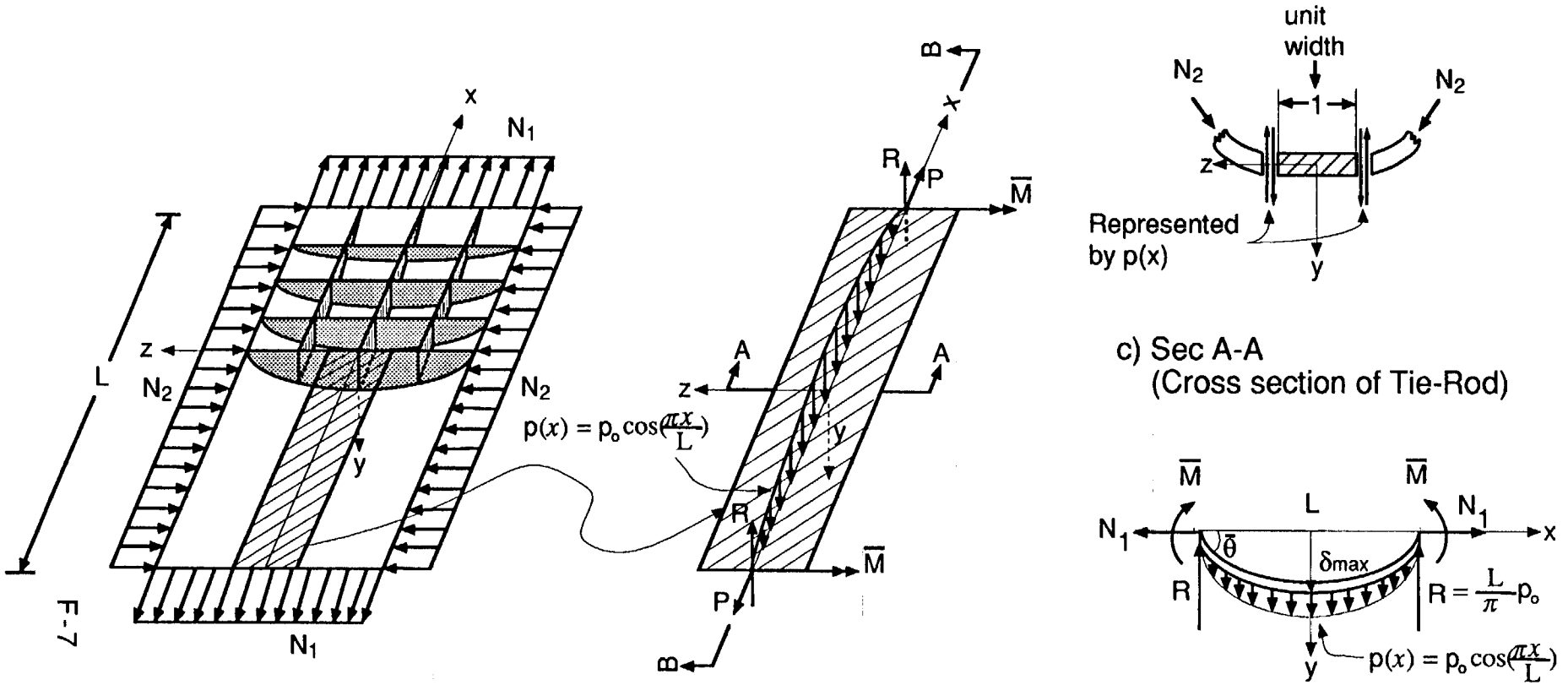

FIGURE 1 TIE-ROD MODEL: THE VERTICAL (OUT-OF-PLANE) COMPONENT OF THE COMPRESSIVE MEMBRANE FORCE, N_2, PRODUCES TRANSVERSE SHEAR FORCES AT THE EDGES OF THE TIE-ROD. THESE EDGE FORCES ARE ASSUMED TO VARY COSINUSOIDALLY IN THE DIRECTION OF THE FOLD (FIGURES b AND d) AND ARE REPRESENTED BY A LATERAL (OUT-OF-PLANE) RUNNING LOAD, p (FIGURES b & c). THE RUNNING LOAD p IS REACTED BY THE EDGE FORCES R (FIGURE d). THUS, R BALANCES THE VERTICAL COMPONENT OF N_2 THAT VARIES ALONG THE LONGITUDINAL EDGES OF THE STRIP.

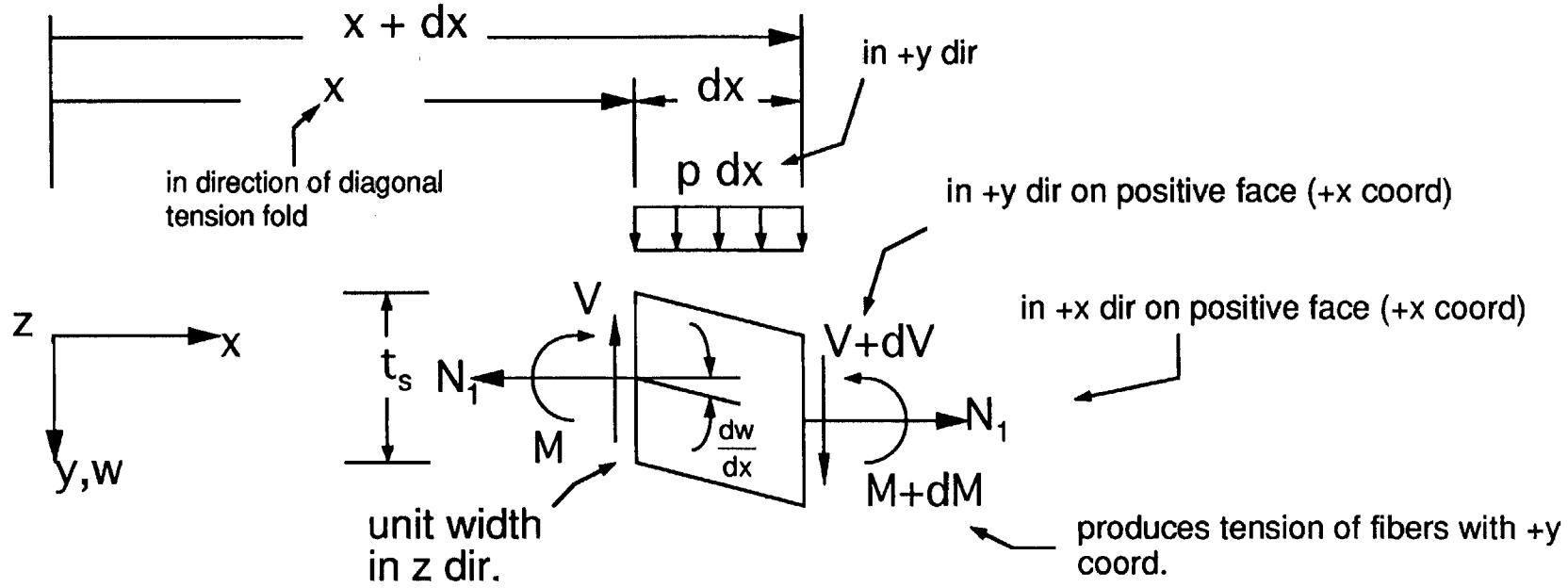

a) Free Body Diagram of Typical Beam Element

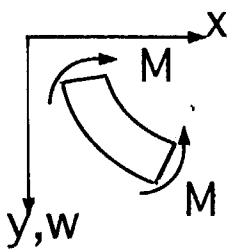

- pos M produces neg curvature

$$M = -D_{sr}\frac{d^2w}{dx^2}$$

- moment equilibrium

$$V = \frac{dM}{dx} + N_1\frac{dw}{dx}$$

D_{sr}=bending stiffness about neutral axis

b) Constitutive Equations

FIGURE 2. NOTATION AND SIGN CONVENTION FOR TYPICAL BEAM ELEMENT

APPENDIX G

SKIN BENDING MOMENT AT TOE, M_{toe}

G.1 Introduction

The purpose of this appendix is to determine the bending moment in the skin immediately under the toe. This is done by linking the "tie-rod" model, described in the previous Appendix F, to a model of the combined stack of the skin, flange and adhesive layers between the toe of the flange and the heel (or stiffener centerline). The latter model is based on that of Tsai [1983] in that it is cut from the stiffener in the same diagonal axis as the tie-rod model of the skin, but departs from Tsai's model in that it includes the entire stack of layers, adhesive and SynCore of the skin and the flange (for this reason, properties of the total stack have the subscript "tot" and, because they are in the diagonal tension or rotated axis system, "totr"). The model of the combined skin and flange is represented by a cantilever in the diagonal tension direction, clamped at the stiffener centerline and loaded at its tip by the transverse shear force and bending moment from the end of the tie-rod. The moment is determined by requiring rotational compatibility between the tie-rod end and the tip of the cantilever. Because the transverse shear force is related to the moment through the maximum out-of-plane displacement δ_{max} of the tie-rod, the only unknown in the equations for the rotations is the moment.

G.2 Rotation at End of Tie-rod (see Figure 1 of Appendix F)

From Eq. (18) of Appendix F, the rotation at the left end of the tie-rod, is given by

$$\bar{\theta} = \lambda \frac{\bar{M}}{N_1} + \frac{R}{N_1} \tag{1}$$

and from Eq. (19) of the same appendix, the transverse shear force at the end of the tie-rod is

$$\frac{R}{N_1} = \frac{\pi}{L}\left(\delta_{max} - \frac{\bar{M}}{N_1}\right) \tag{2}$$

In these equations,

$$\lambda = \sqrt{\frac{N_1}{D_{sr}}} \qquad \text{(from Eq. (3) of Appendix F)} \quad (3)$$

and

L is the toe-to-toe length of the buckle, see Figure 1 of Appendix E,
δ_{max} is the out-of-plane displacement at the center of the tie-rod, as described in Appendix E,
N_1 is the membrane stress resultant in the buckled skin in the diagonal tension direction,
D_{sr} is the bending stiffness of the skin about it's neutral axis normal to the long axis of the buckle.

Eliminating R/N_1 from these equations gives

$$\bar{\theta} = \lambda \frac{\bar{M}}{N_1} + \frac{\pi}{L}\left(\delta_{max} - \frac{\bar{M}}{N_1}\right) \qquad (4)$$

G.3 Rotation of "Flange and Skin" Cantilever Model

Figure 1 shows the beam model of the combined skin and flange. The beam is assumed to be clamped at the heel, an assumption justified by the STAGS results of Figure 2. Any elementary strength of materials text provides

$$\theta_{totr} = \frac{1}{2}\frac{W_{toe} L_{fr}^2}{D_{totr}} + (M_{toe} - qz)\frac{L_{fr}}{D_{totr}} \qquad (5)$$

where

W_{toe} = the transverse shear at the tip of the cantilever,
M_{toe} = the bending moment at the tip of the cantilever,
D_{totr} = the bending stiffness of the combined stack of skin, adhesive and flange,
L_{fr} = the heel-to-toe width of the flange measured in the direction of the diagonal tension fold,
qz = the moment due to the offset of the skin stress resultant from the midplane of the combined stack, as described below.

As described in Appendix F, the tensile axial load in the tie-rod model is held constant at it's average value (i.e. $N_1 = 2q\text{-}q_{cr}$, see Appendix C) . In fact, the axial load must be slightly above the average value over most of the length of the tie-rod, but must fall, over an undefined —but assumed small — distance at each end, to the value in the unbuckled sheet

at the toe (i.e. $N_{1toe} = q$, see Appendix C). When the tie-rod is connected to the tip of the cantilever the change in N_1 at each end of the tie-rod must be taken into account. The tensile end load transferred from the end of the tie-rod to the cantilever is therefore $N_{1toe} = q$ and <u>not</u> $N_1 = 2q - q_{cr}$. At first sight, it appears that equilibrium is being violated, but the change is assumed to occur over a short length at each end of the tie-rod and is brought about by local in-plane shear stresses in the skin near the toe. These local changes are assumed not to invalidate the solution of the tie-rod problem.

In Eq. (5) an additional moment (qz) has been added to M_{toe} to represent the moment due to the membrane stress resultant in the unbuckled skin at the toe (i.e. $N_{1toe} = q$) being offset a distance z from the centroid of the combined stack of the skin and flange layers (see Figure 1). z is given by

$$z = \frac{Et_{fr}\left(t_s + t_a + \frac{t_f}{2}\right) + Et_{sr}\frac{t_s}{2}}{Et_{fr} + Et_{sr}} - \frac{t_s}{2} \qquad (6)$$

where

Et_{fr} = membrane stiffness of the flange in the diagonal tension direction

Et_{sr} = membrane stiffness of the skin in the diagonal tension direction

t_f = flange thickness

t_s = skin thickness

t_a = adhesive thickness

G.4 <u>Determination of Bending Moment & Transverse Shear Force at Toe</u>

By enforcing the following conditions, obtained by comparing Figure 1 of this Appendix to Figure 1d of Appendix F:

$$\overline{M} = - M_{toe} \qquad (7)$$

$$R = + W_{toe} \qquad (8)$$

$$\theta = + \theta_{totr} \qquad (9)$$

we obtain the following expression for the bending moment in the skin at the toe:

$$M_{toe} = \frac{\frac{\pi \delta_{max}}{L}\left(1 - \frac{L_{fr}^2 N_1}{2 D_{totr}}\right) + \frac{L_{fr} q z}{D_{totr}}}{\left(\frac{\lambda - \pi/L}{N_1} + \frac{L_{fr}}{D_{totr}} + \frac{\pi}{2L}\frac{L_{fr}^2}{D_{totr}}\right)} \qquad (10)$$

where

$$c = \sqrt{1.5}\, L \left\{ \frac{\sqrt{\frac{N_2}{N_1}}}{1 + \sqrt{\frac{N_2}{N_1}}} \right\} \qquad \text{(from Eq. (7) of Appendix D)} \quad (11)$$

$$\delta_{max} = \frac{2}{\pi}\sqrt{Lc\left(\frac{q - q_{cr}}{Gt}\right)} \qquad \text{(from Eq. (6) of Appendix E)} \quad (12)$$

$$N_1 = 2q - q_{cr} \qquad \text{(from Eq. (7) of Appendix C)} \quad (13)$$

$$N_2 = q_{cr} \qquad \text{(from Eq. (5) of Appendix C)} \quad (14)$$

and

Gt = the in-plane shear stiffness of the skin referred to axes parallel and normal to the stiffener direction.

Also, from Eqs. (2), (7), and (8), we obtain the following expression for the transverse shear force in the skin at the toe:

$$W_{toe} = \frac{\pi}{L}\left(N_1 \delta_{max} + M_{toe}\right) \qquad (15)$$

Equation (10) is the full version of the expression for M_{toe} and is used in the code listed in Appendix M.

G.5 Parametric Study

In the course of applying SNAPPS, it was found in some cases that the moment in the skin at the toe reaches a maximum and then decreases. The following investigation of this behavior brought to light two dimensionless parameters which govern the magnitude of the maximum value of M_{toe} and the shear flow q^* at which it occurs, and which have practical design consequences.

Examination of typical magnitudes of the various terms in Eq. (10) reveals that M_{toe} may be roughly approximated by dropping terms in the numerator and denominator. The expression for M_{toe} then simplifies to

$$M_{toe} = \frac{\frac{\pi\delta_{max}}{L}\left(1 - \frac{L_{fr}^2 N_1}{2 D_{totr}}\right)}{\frac{\lambda}{N_1}} \qquad (16)$$

By substituting for δ_{max}, c, and N_1 and λ in terms of q and q_{cr}, it can be shown that M_{toe} can be expressed in terms of two dimensionless parameters and a function of q/q_{cr}.

$$\frac{M_{toe}}{q_{cr}}\sqrt{\frac{Gt}{D_{sr}}} = \left(1 - \frac{q_{cr} L_{fr}^2}{D_{totr}} \frac{q}{q_{cr}}\right) f\left(\frac{q}{q_{cr}}\right) \qquad (17)$$

The function $f(q/q_{cr})$ rises monotonically against q/q_{cr}, but the presence of the parameter $\frac{q_{cr} L_{fr}^2}{D_{totr}}$ makes it reach a maximum and then fall, as illustrated in Figure 3 where M_{toe} is plotted against q for panel C1. (Neither A1 or B1 reach the predicted maximum value of M_{toe}, as is shown in Figures 4 and 5.)

The form of Eq. (17) indicates that, for a specific panel, if we plot M_{toe} against q, and search for the maximum value of M_{toe}, and the value (q^*) of the shear flow at which it occurs, then we can plot both the maximum moment parameter $\frac{M_{toe}}{q_{cr}}\sqrt{\frac{Gt}{D_{sr}}}$, and the shear flow q^*/q_{cr} at which it occurs, against $\frac{q_{cr} L_{fr}^2}{D_{totr}}$.

Analyses, using the full version of the expression for M_{toe} given in Eq. (10), were done for the three test panels, A1, B1, and C1. In each case, several different values of $\frac{q_{cr} L_{fr}^2}{D_{totr}}$ were used, obtained by varying the bending stiffness of the combined skin and flange stack, D_{totr}. The resulting values of $\frac{M_{toe}}{q_{cr}}\sqrt{\frac{Gt}{D_{sr}}}$ and q^*/q_{cr} are plotted against $\frac{q_{cr} L_{fr}^2}{D_{totr}}$ in Figures 6 and 7. In each figure the solid symbols denote the nominal panel

and the open symbols are for the variations. Both figures show that the results from all three panels can be approximated by a single curve, as predicted by the approximate form of Eq. (16). It is apparent that both curves are fitted quite well by hyperbolae, and that the maximum toe moment can be approximated by

$$M_{toe,max} = 0.35\ (D_{totr}/L_{fr}^2)\ \sqrt{D_{sr}/Gt} \tag{18}$$

occurring at a shear flow

$$q^* = 0.59\ D_{totr}/L_{fr}^2 \tag{19}$$

G.6 Design Implications

From a design point of view it is desirable to reduce the toe moment as far as possible because the peel stress between the skin and the flange, the membrane stress in the critical skin ply, and, therefore, the maximum principal tensile stress depend on M_{toe}. The above results show that the maximum value of the toe moment increases as the skin/flange bending stiffness D_{totr} is increased, or as the flange length L_{fr} is made shorter. The term $\sqrt{D_{sr}/Gt}$ is approximately proportional to the skin thickness and consequently the toe moment also increases as the skin thickness t_s is increased.

In summary, these results confirm the need for compliant flanges which impose little restraint on the deformation of the buckled sheet (however, the stiffener must be sturdy enough to prevent the diagonal tension folds from progressing across the stiffener centerlines).

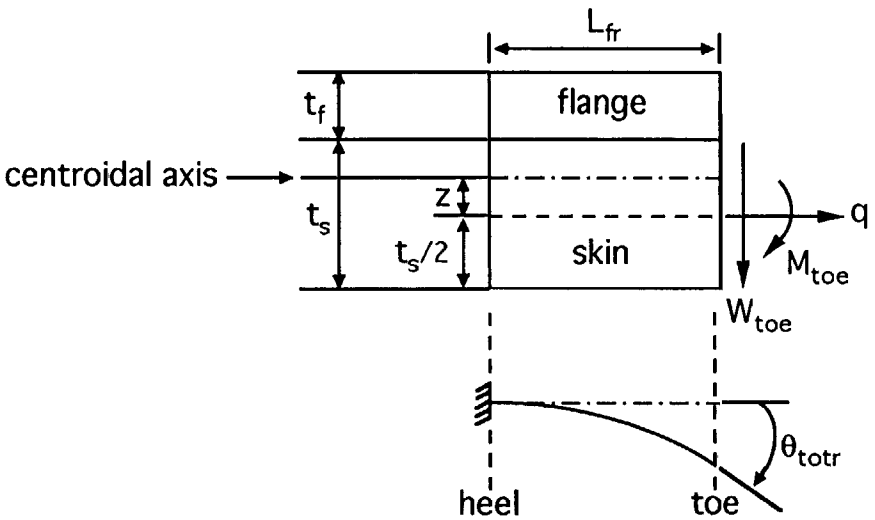

FIGURE 1 CANTILEVER BEAM MODEL OF COMBINED STACK OF SKIN, FLANGE AND ADHESIVE. THE BEAM RUNS BETWEEN THE HEEL (OR STIFFENER CENTERLINE) AND THE TOE OF THE FLANGE, AND IT IS IN THE DIRECTON OF THE DIAGONAL TENSION FOLD.

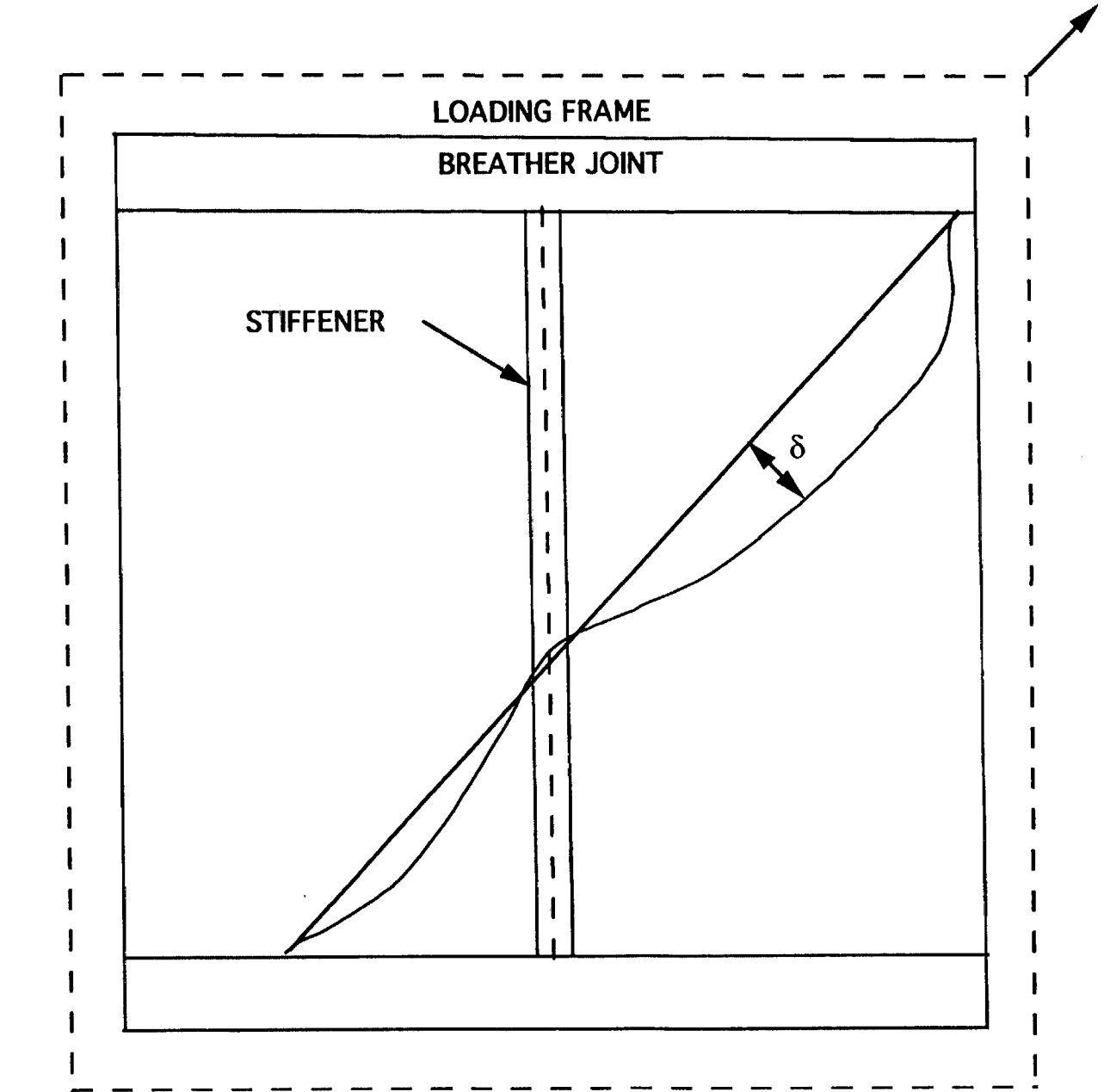

FIGURE 2 STAGS RESULTS FOR THE OUT-OF-PLANE DISPLACEMENT OF SKIN PLOTTED ALONG A DIAGONAL TENSION BUCKLE AT THE TEST FAILURE LOAD OF 64 Kips FOR PANEL C1.

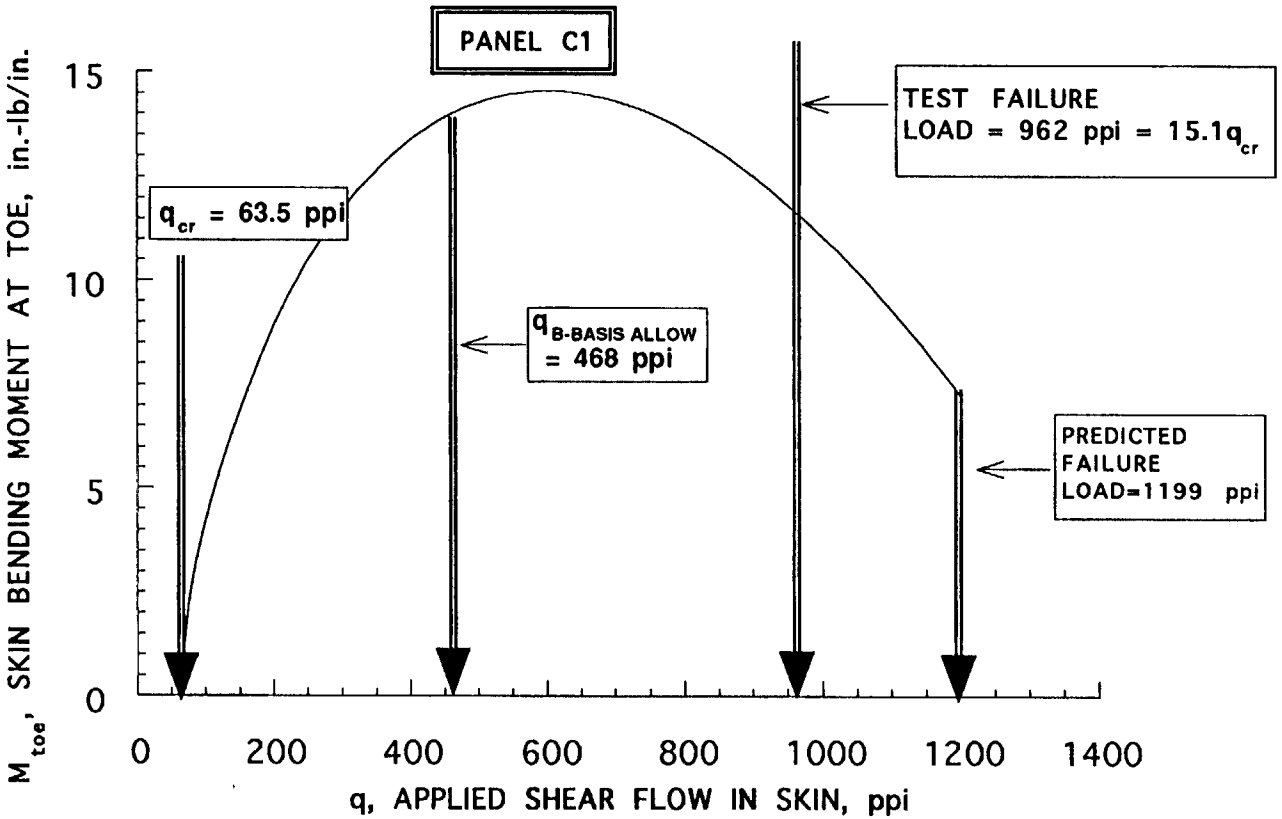

FIGURE 3 VARIATION OF SKIN BENDING MOMENT AT TOE OF FLANGE WITH APPLIED SHEAR LOAD. PANEL C1.

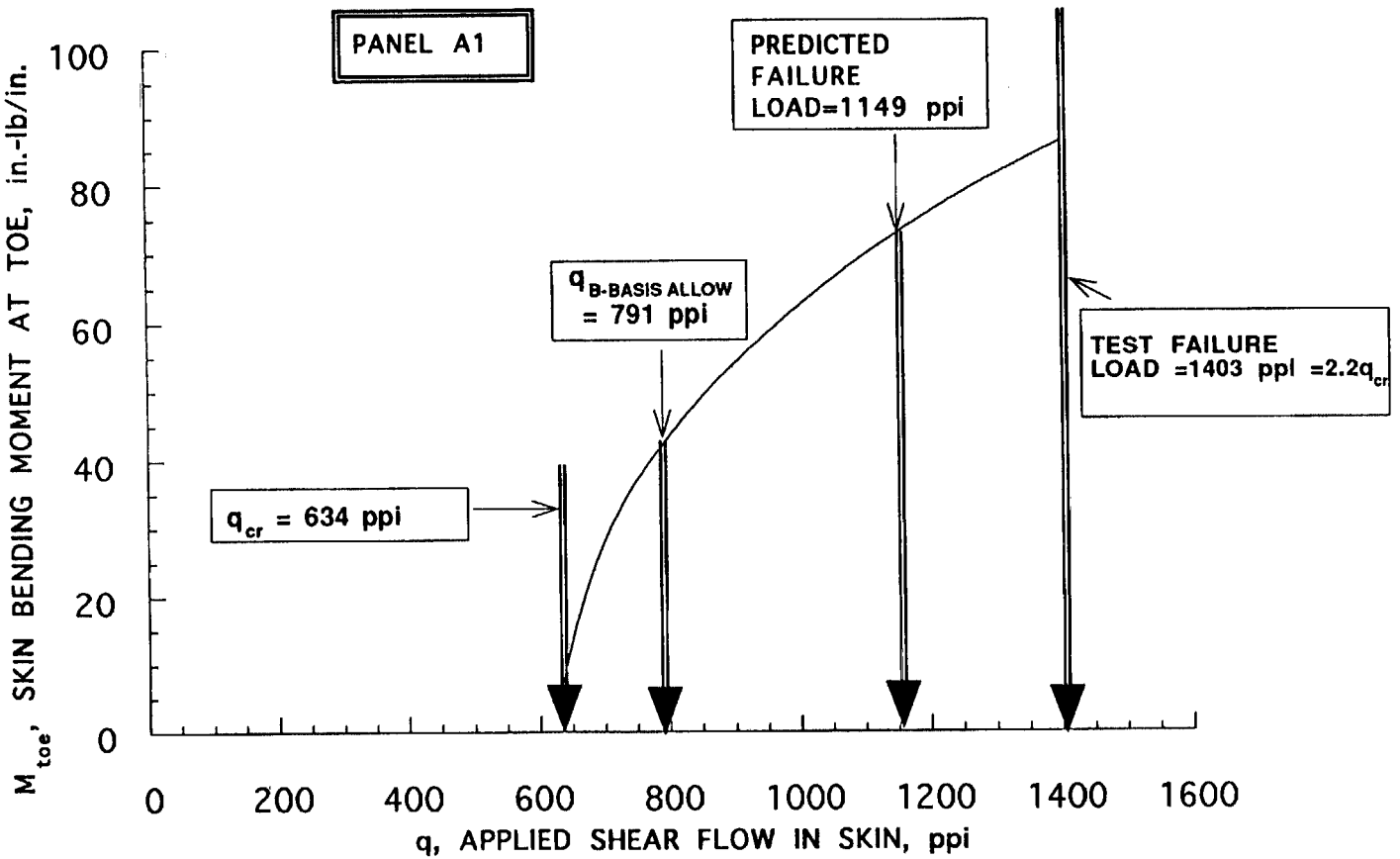

FIGURE 4 VARIATION OF SKIN BENDING MOMENT AT TOE OF FLANGE WITH APPLIED SHEAR LOAD. PANEL A1.

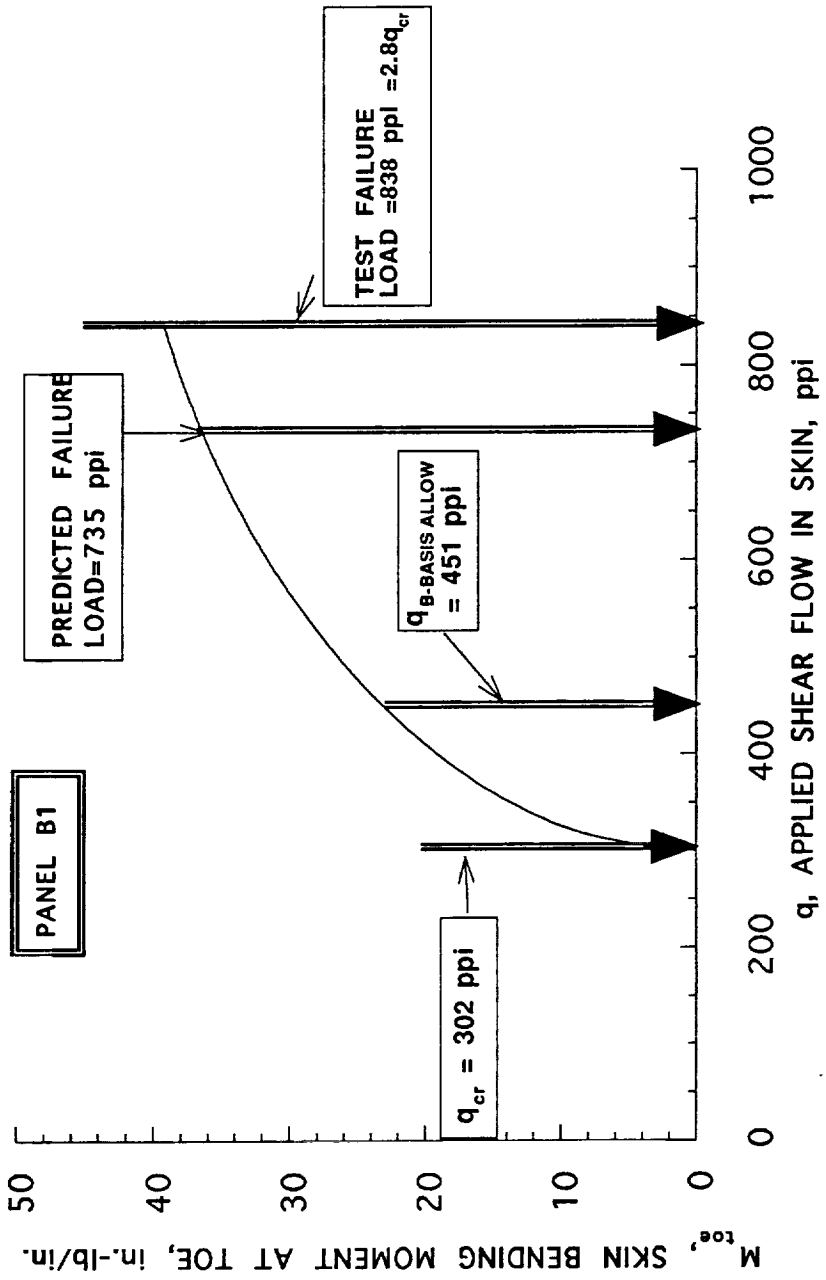

FIGURE 5 VARIATION OF SKIN BENDING MOMENT AT TOE OF FLANGE WITH APPLIED SHEAR LOAD. PANEL B1.

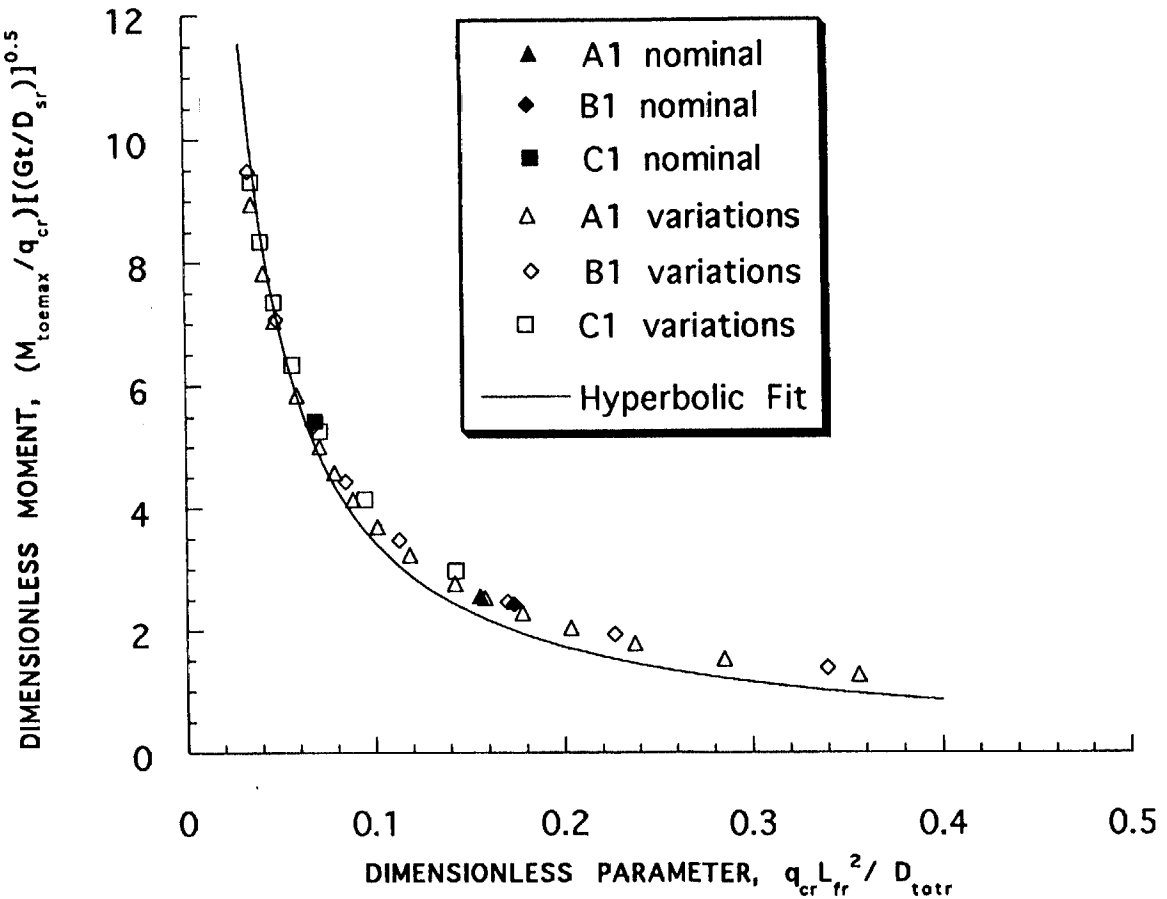

FIGURE 6 MAXIMUM MOMENT IN SKIN AT TOE

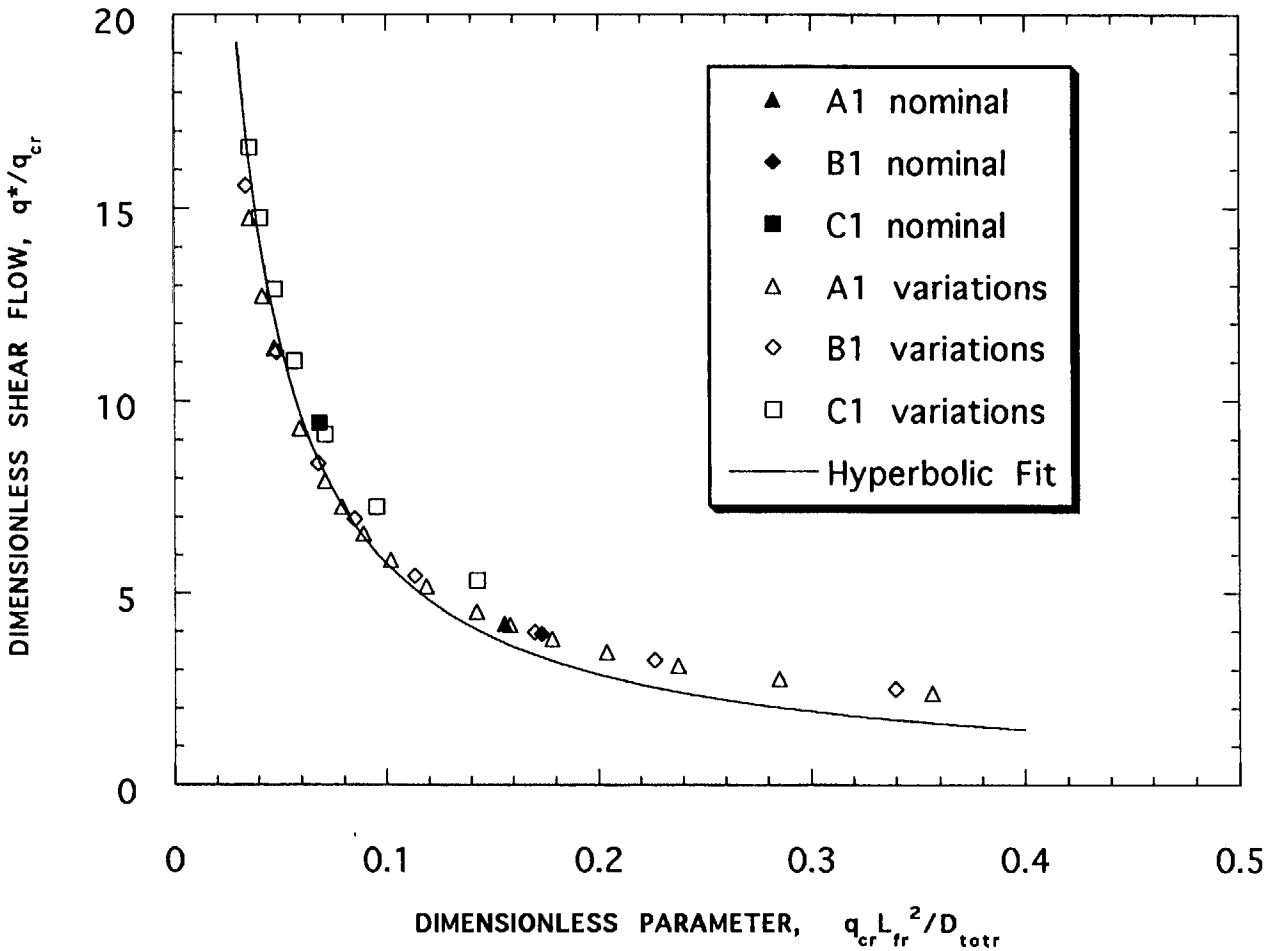

FIGURE 7 SHEAR FLOW, q*, AT WHICH THE MOMENT IN THE SKIN AT THE TOE, M_{toe}, IS A MAXIMUM

APPENDIX H

INTERLAMINAR SHEAR STRESS BETWEEN SKIN AND FLANGE

In this appendix, an expression is presented for the shear stress distribution along the interface between the skin and the flange, based on the "shear lag" analysis of Kuhn [1956]. The distribution is used in the peel stress analysis, described in Appendix I, and the maximum value of the shear stress, which occurs under the toe of the flange, is used in the failure criterion in Appendix L.

Figure 1a shows a section of the combined skin and flange model in the x-z plane, where x is in the direction of the diagonal tension fold, and z is normal to the plane of the skin. The section is of unit width in the inplane direction normal to the fold (i.e., of unit width normal to the plane of the paper). Following Kuhn, the skin-flange model is idealized as two axial load carrying bars joined by a shear carrying web, as indicated in Figure 1b. The boundary conditions are that at the toe, $x = 0$, the bar representing the skin is loaded by an axial tensile force P, and the bar representing the flange has zero load. A further assumption is made that the width of the flange L_{fr} is long enough for the shear stress to die away to zero at the heel. This assumption leads to Kuhn's Eq. (4.10) corresponding to Case 4 of Table 4.1. Adapting that equation to the Kuhn-type model of the layered model (Figure 1b) leads to the following equation for the distribution of the interlaminar shear stress between the skin and the flange:

$$\tau(x) = \frac{PK}{t}\left(\frac{E_f A_f}{E_f A_f + E_S A_S}\right) e^{-Kx} \tag{1}$$

where (Kuhn's Eq. (4.4))

$$K^2 = \frac{Gt}{b}\left(\frac{1}{E_f A_f} + \frac{1}{E_S A_S}\right) \tag{2}$$

In applying Eqs. (1) and (2) to a unit width w of the layered model, the axial stiffnesses $E_f A_f$ and $E_S A_S$ of the flange and skin in the Kuhn-type

model are replaced by wEt_{fr} and wEt_{sr} respectively (where Et denotes the product of modulus E and thickness t; the subscripts f and s denote the flange and skin, respectively, and the subscript r denotes that these quantities are measured in the [rotated] diagonal tension direction). The load P is replaced by wN_{1toe}, (where N_{1toe} is the end load in the skin immediately under the toe, as described in Appendix C), and the web thickness t is replaced by w. Further, because G is not uniform throughout the model, the quantity G/b in Eq. (2) must be replaced by a "modulus of foundation", denoted by ϕ_{xz}, which is given by Eq. (2) of Appendix J. With these substitutions, w nicely cancels out, and Eqs. (1) and (2) become

$$\tau(x) = N_{1toe}\, K \left(\frac{Et_{fr}}{Et_{fr} + Et_{sr}}\right) e^{-Kx} \tag{3}$$

and

$$K^2 = \phi_{xz} \left(\frac{1}{Et_{fr}} + \frac{1}{Et_{sr}}\right) \tag{4}$$

The maximum value of the shear stress occurs at the toe (x = 0), and is simply denoted by τ_{xz} (without any subscripts "toe"), i.e.,

$$\tau_{xz} = (\tau(x))_{x=0} = N_{1toe} K \left(\frac{Et_{fr}}{Et_{fr} + Et_{sr}}\right) \tag{5}$$

In the interest of keeping the model as simple as possible, a more exact analysis is not considered worthwhile at this time. However, the use of SUBLAM [Flanagan, 1993] to verify the distributions and magnitudes of the peel and shear stresses between the flange and the skin, should be part of any future work.

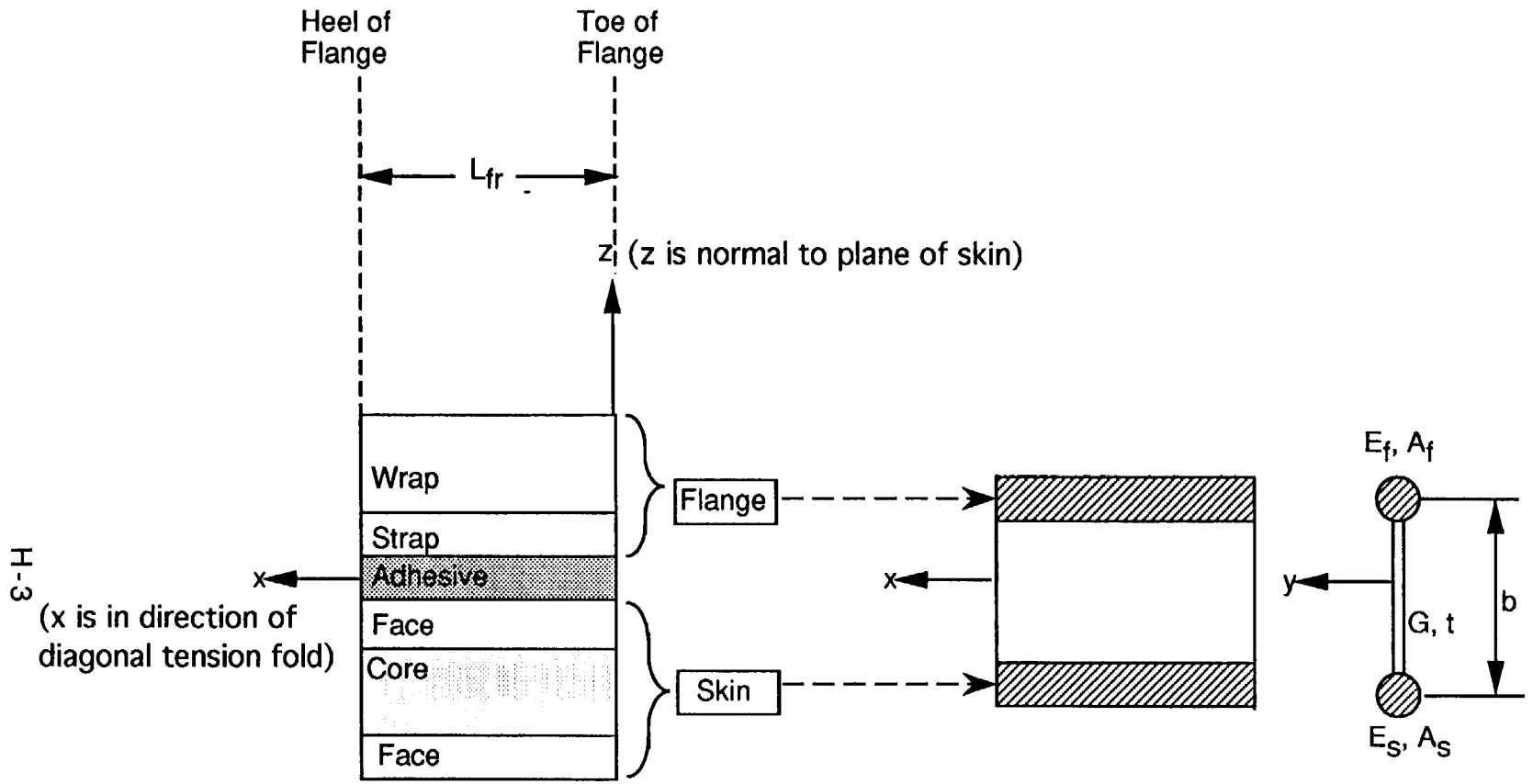

a) Section of Skin-Flange Model in the Direction of the Diagonal Tension Fold. The Section is of Unit Width in the Inplane Direction Normal to the Fold (i.e., of Unit Width Normal to the Plane of the Paper)

b) Skin-Flange Model is Idealized as Two Load Carrying Bars Joined by a Shear Carrying Web.

FIGURE 1 KUHN-TYPE SHEAR LAG MODEL FOR OBTAINING INTERLAMINAR SHEAR STRESS BETWEEN SKIN AND FLANGE

APPENDIX I

PEEL STRESS ANALYSIS

I.1 Introduction

A major contributor to stiffener disbonding is the peel stress between the skin and the flange immediately under the toe of the flange. Typical of the basic strength-of-materials approach adopted in SNAPPS, a simple beam model is used here to determine this stress. Figure 1 shows the model in which the skin and flange are idealized as beams that are coupled by an "elastic, Winkler-type, foundation" of modulus ϕ_z (determined in Appendix J). The peel stress is given by

$$\sigma_{peel}(x) = \phi_z[w_f(x)-w_s(x)] \qquad (1)$$

where w_f and w_s represent out-of-plane displacements of the flange and skin, respectively. The peel stress and displacements vary along the length of the coupled beams, as indicated in Eq. (1) by the axial coordinate x, which is measured from the toe of the flange to its heel, in the direction of the diagonal tension fold. The other coordinate used in this analysis is z, which is normal to the plane of the skin. The objective of the analysis is to obtain a closed-form expression for the peel stress at the toe of the flange. This stress is simply denoted by σ_z, (avoiding subscripts such as "toe"). That is,

$$\sigma_z = (\sigma_{peel})_{x=0}$$

The beams are assumed to be of length L_{fr} in the direction of the diagonal tension fold, and of unit width in the inplane direction normal to the fold. L_{fr} is the "rotated" flange (subscript "r" for rotated) width measured from the heel to the toe of the flange in the direction of the fold. The objective is to determine w_f and w_s, and hence ϕ_z, as a function of the following three loadings shown in Figure 1: the transverse shear force W_{toe} in the postbuckled skin; the bending moment M_{toe} in the skin; and the interlaminar shear stress distribution $\tau(x)$ at the skin-to-flange interface.

The interlaminar shear stress, whose presence complicates the analysis, arises from the diagonal tension field pull N_{1toe} unloading some of its load from the skin into the flange (see Figure 1). This shear stress causes a moment on each beam because it acts at a distance from the midplane of the flange and the skin. Thus, the present analysis may be regarded as being an extension of the classical "beam on an elastic foundation" method [Hetenyi, 1946] to the case in which two beams are elastically coupled together and are subjected to an offset shear traction on their interface surfaces.

We next make a reasonable assumption that greatly simplifies the analysis, and which is consistent with our objective of obtaining a closed-form expression for the peel stress at the toe, which is where the peel stress peaks and where failure has been observed in our tested shear panels. The assumption is based on results from detailed analyses [Cacho-Negrete, 1978] for thin laminates joined by a thin adhesive layer. The detailed results reveal that the peel stresses between the skin and the flange are highly localized under the heel and toe. Because they die-away so rapidly from each end of the flange, the two stress concentrations do not interact and are essentially uncoupled. Thus, for purposes of determining the peel stress at the toe, we may assume that the length (rotated flange width, L_{fr}) of the coupled beams is long enough so that conditions at one end (heel) do not affect the other end (toe). Analytically, it can be shown [Hetenyi, 1946] that this assumption is valid provided that the following equation involving the characteristic wave number β is satisfied:

$$\beta L_{fr} > \pi.$$

This condition is satisfied by our tested shear panels. For example, for panel C1, Figure 2 clearly shows that the rotated flange width

$$L_{fr} = (0.75") / \cos(45^\circ) = 1.06"$$

is "long enough" so that waves emanating from one end die out rapidly before they reach the other end. The decaying functions plotted in the

figure represent terms in the complementary solution for a beam on an elastic foundation. The assumption that conditions at one end of the flange do not affect conditions at the other end greatly simplifies the solution of the coupled beam equations and leads to an explicit closed-form formula for the peel stress at the toe in terms of the transverse shear force and bending moment in the skin, and the interlaminar shear stress between the skin and the flange. This formula requires an expression for the shear lag stress distribution $\tau(x)$ as a function of distance along the width of the rotated flange. This expression is given in the preceding appendix, and is repeated here for completeness:

$$\tau(x) = N_{1toe}\, K \left(\frac{Et_{fr}}{Et_{fr}+Et_{sr}} \right) e^{-Kx} \qquad (2)$$

where

N_{1toe} is the end load in the skin immediately under the toe. As described in Appendix C, $N_{1toe} = q$.

$$K = \sqrt{\phi_{xz} \left(\frac{1}{Et_{fr}} + \frac{1}{Et_{sr}} \right)}$$

and

ϕ_{xz} is the foundation modulus corresponding to the interlaminar shear stress, a closed-form expression for which is given in the next appendix,

Et_{sr} = membrane stiffness of the skin,

Et_{fr} = membrane stiffness of the flange.

Et_{sr} and Et_{fr} are measured in the direction of the diagonal tension fold.

I.2 Derivation of Equation for Peel Stress

Figures 3 and 4 display the notation, sign conventions, differential equations, and boundary conditions for the coupled beam analysis. The differential equations and boundary conditions differ from those of Hetenyi [1946] by the inclusion here of the interlaminar shear stress, τ, between the skin and the flange. They were derived here by writing equilibrium for the general differential element shown in Figure 3a, and using the constitutive equations given in Figure 3b. Specific forms of the differential equations and boundary conditions for the skin and flange are

summarized in Figure 4. It to be observed from that figure that the interlaminar shear stress appears in the boundary conditions, as well as in the differential equations, and that the differential equations are coupled. Because the solution of the coupled equations is straightforward, it is presented more-or-less in outline form.

- Coupled Differential Equations (DE)

$$DE_f: \quad D_{fr} w_f'''' + \phi_z(w_f - w_s) - \frac{t_f}{2}\tau' \tag{3}$$

$$DE_s: \quad D_{sr} w_s'''' - \phi_z(w_f - w_s) - \frac{t_s}{2}\tau' \tag{4}$$

where $(\,)' = \frac{d}{dx}(x)$; t_f and t_s are flange and skin thicknesses; and D_{fr} and D_{sr} are flange and skin bending stiffnesses in the direction of the diagonal tension fold (i.e., about an inplane axis normal to the direction of the fold).

- Boundary Conditions (BC) at x = 0

Note that, because the interaction between the damped waves emanating from the toe and heel is being neglected, boundary conditions at the heel are unnecessary.

BC(1): Flange: $M = 0 \Rightarrow w_f'' = 0$ (5)

BC(2): Flange: $V = 0 \Rightarrow$

$$w_f''' = \frac{t_f}{2\,D_{fr}}(\tau)_{x=0} = \frac{t_f}{2D_{fr}} N_{1toe} K \left(\frac{Et_{fr}}{Et_{fr} + Et_{sr}}\right)$$

or

$$w_f''' = \frac{\phi_z t_f}{KD_{fr}} C_n \tag{6}$$

where

$$C_n = \frac{N_{1toe}K^2}{2\phi_z}\left(\frac{Et_{fr}}{Et_{fr} + Et_{sr}}\right) \tag{7}$$

BC(3): Skin: $M = M_{toe} = -D_{sr}w_s''$

$$\Rightarrow w_s'' = -\frac{M_{toe}}{D_{sr}} \tag{8}$$

BC(4): Skin: $V = W_{toe}$

$$\Rightarrow w_s'''' = -\frac{W_{toe}}{D_{sr}} + \frac{\phi_z t_s}{KD_{sr}} C_n \qquad (9)$$

- Solution For w_f

Inserting

$$w_s = w_f + \frac{1}{\phi_z} D_{fr} w_f'''' - \frac{1}{\phi_z} \frac{t_f}{2} \tau'$$

from the DE for the flange (Eq. (3)) into the DE for the skin (Eq. (4)) produces the following 8^{th} order DE for w_f:

$$\frac{d^8 w_f}{dx^8} + 4\beta^4 \frac{d^4 w_f}{dx^4} = -\frac{\phi_z^2}{D_{fr} D_{sr}} \left[\frac{K^4}{\phi_z} t_f D_{sr} + t_f + t_s \right] C_n e^{-Kx} \qquad (10)$$

where

$$\beta = \left[\frac{\phi_z (D_{fr} + D_{sr})}{4 D_{fr} D_{sr}} \right]^{\frac{1}{4}} \qquad (11)$$

Complementary Solution of DE (Eq. (10)) for w_f

The solution of the homogeneous form of Eq. (10) is

$$w_f^{(C)} = Ae^{\beta x}\cos(\beta x) + Be^{\beta x}\sin(\beta x) + Ce^{-\beta x}\cos(\beta x) + De^{-\beta x}\sin(\beta x) + a + bx + cx^2 + dx^3$$

as may be verified by back-substitution into the DE.

Simplification: As described in detail above, we assume that the decaying waves emanating from the toe and heel die out rapidly, see Figure 1, so that there is no interaction between them. Thus, the first two terms in the above equation must vanish, and these conditions are satisfied by taking

$$A = B = 0$$

so that complementary solution for w_f simplifies to

$$w_f^{(C)} = Ce^{-\beta x}\cos(\beta x) + De^{-\beta x}\sin(\beta x) + a + bx + cx^2 + dx^3 \qquad (12)$$

Particular Solution of DE (Eq.(10)) for w_f

A particular solution of Eq. (10) is readily shown to be

$$w_f^{(p)} = -\left[\frac{1}{K^4(K^4+4\beta^4)}\right]\frac{\phi_z^2}{D_{fr}D_{sr}}\left[\frac{K^4}{\phi_z}t_f D_{sr} + t_f + t_s\right] C_n e^{-Kx}$$

Let

$$m = \frac{1}{K^4(K^4+4\beta^4)}\frac{\phi_z^2}{D_{fr}D_{sr}}\left[\frac{K^4}{\phi_z}t_f D_{sr} + t_f + t_s\right] \quad \text{(dimensions of length)} \qquad (13)$$

$$\therefore w_f^{(p)} = -mC_n e^{-Kx} \qquad (14)$$

Total Solution, $w_f = w_f^{(c)} + w_f^{(p)}$

$$w_f = Ce^{-\beta x}\cos(\beta x) + De^{-\beta x}\sin(\beta x) + a + bx + cx^2 + dx^3 - mC_n e^{-Kx} \qquad (15)$$

- Solution For w_s

From Eq. (3):

$$w_s = w_f + \frac{1}{\phi_z} D_{fr} w_f'''' - \frac{1}{\phi_z}\frac{t_f}{2}\tau'$$

By using Eq. (15) to eliminate w_f, and Eq. (11) to simplify the resulting expression, we obtain

$$w_s = -\frac{D_{fr}}{D_{sr}}\left[Ce^{-\beta x}\cos(\beta x) + De^{-\beta x}\sin(\beta x)\right] + a + bx + cx^2 + dx^3 - nC_n e^{-Kx} \qquad (16)$$

where

$$n = \left(1 + K^4\frac{D_{fr}}{\phi_z}\right)m - t_f \qquad (17)$$

- Determine Arbitrary Constants From BC's at x = 0

BC(1): Flange: M = 0 (Eq.(5)) ⇒

$$c = \beta^2 D + \frac{1}{2} m K^2 C_n \tag{18a}$$

BC(2): Flange: V = 0 (Eq. (6)) $\Rightarrow$

$$D = -\frac{M_{toe}}{2\beta^2(D_{fr}+D_{sr})} + (n - m)\frac{K^2}{2\beta^2}\left(\frac{D_{fr}+D_{sr}}{D_{sr}}\right)C_n \tag{18b}$$

BC(3): Skin: M = M_{toe} (Eq. (7)) $\Rightarrow$

$$d = -\frac{1}{3}\beta^3(C+D) + \frac{1}{6}\left(\frac{\phi_z t_f}{K D_{fr}} - mK^3\right)C_n \tag{18c}$$

BC(4): Skin: V = W_{toe} (Eq. (8)) $\Rightarrow$

$$C = \frac{1}{2\beta^2 (D_{fr}+D_{sr})}\left[M_{toe} + \frac{W_{toe}}{\beta}\right] + \left(\frac{D_{sr}}{D_{fr}+D_{sr}}\right)\left\{(n - m)\frac{K^2}{2\beta^2}\left[\frac{K}{\beta} - 1\right] + \frac{\phi_z}{2\beta^3 K}\left(\frac{t_f}{D_{fr}} - \frac{t_s}{D_{sr}}\right)\right\} C_n \tag{18d}$$

• Peel Stress At Toe (x=0)

The peel stress at the toe is given by

$$\sigma_z = (\sigma_{peel})_{x=0} = \phi_z[w_f(0)-w_s(0)]$$

which from Eqs. (15) and (16) becomes

$$\sigma_z = \phi_z\left[\left(\frac{D_{fr}+D_{sr}}{D_{sr}}\right)C\right] + (n - m)\, C_n$$

By substituting for C from Eq. (18d) into this equation, and performing some algebraic manipulation, we obtain the following expression for the peel stress:

$$\sigma_z = \frac{2\beta}{\left(1 + \frac{D_{sr}}{D_{fr}}\right)}\left[W_{toe} + \beta M_{toe}\right] + \phi_z t_f C_n\left\{\frac{2\beta}{K}\left[\frac{\left(\frac{D_{sr}}{D_{fr}} - \frac{t_s}{t_f}\right)}{\left(1 + \frac{D_{sr}}{D_{fr}}\right)}\right] - \left[1 \frac{K^4 D_{fr} m^*}{\phi_z}\right]\left[1 - \frac{K^2}{2\beta^2} + \frac{K^3}{2\beta^3}\right]\right\} \tag{19}$$

where the dimensionless parameter

$$m^* = \frac{m}{t_f} \tag{20}$$

has been introduced, and m is given by Eq. (13).

σ_z can be conveniently subdivided into two parts: the first, σ_{z1}, is due directly to the moment M_{toe} and the transverse shear W_{toe} applied from the skin; and the second, σ_{z2}, is caused by the shear along the interface between the skin and flange acting at half the laminate thickness away from the midplane of each laminate. The two parts of the peel stress are given by

$$\sigma_z = \sigma_{z1} + \sigma_{z2}$$

where

$$\sigma_{z1} = \frac{2\beta}{(1 + D_{sr}/D_{fr})}(W_{toe} + \beta M_{toe}) \tag{21}$$

and

$$\sigma_{z2} = C_n t_f \phi_z (F_1 + F_2) \tag{22}$$

and

$$F_1 = \left(1 - \frac{K^2}{2\beta^2} + \frac{K^3}{2\beta^3}\right)\left(\frac{m^* D_{fr} K^4}{\phi_z} - 1\right)$$

$$F_2 = \frac{2\beta D_{fr}}{K}\left(\frac{D_{sr}/D_{fr} - t_s/t_f}{D_{fr} + D_{sr}}\right)$$

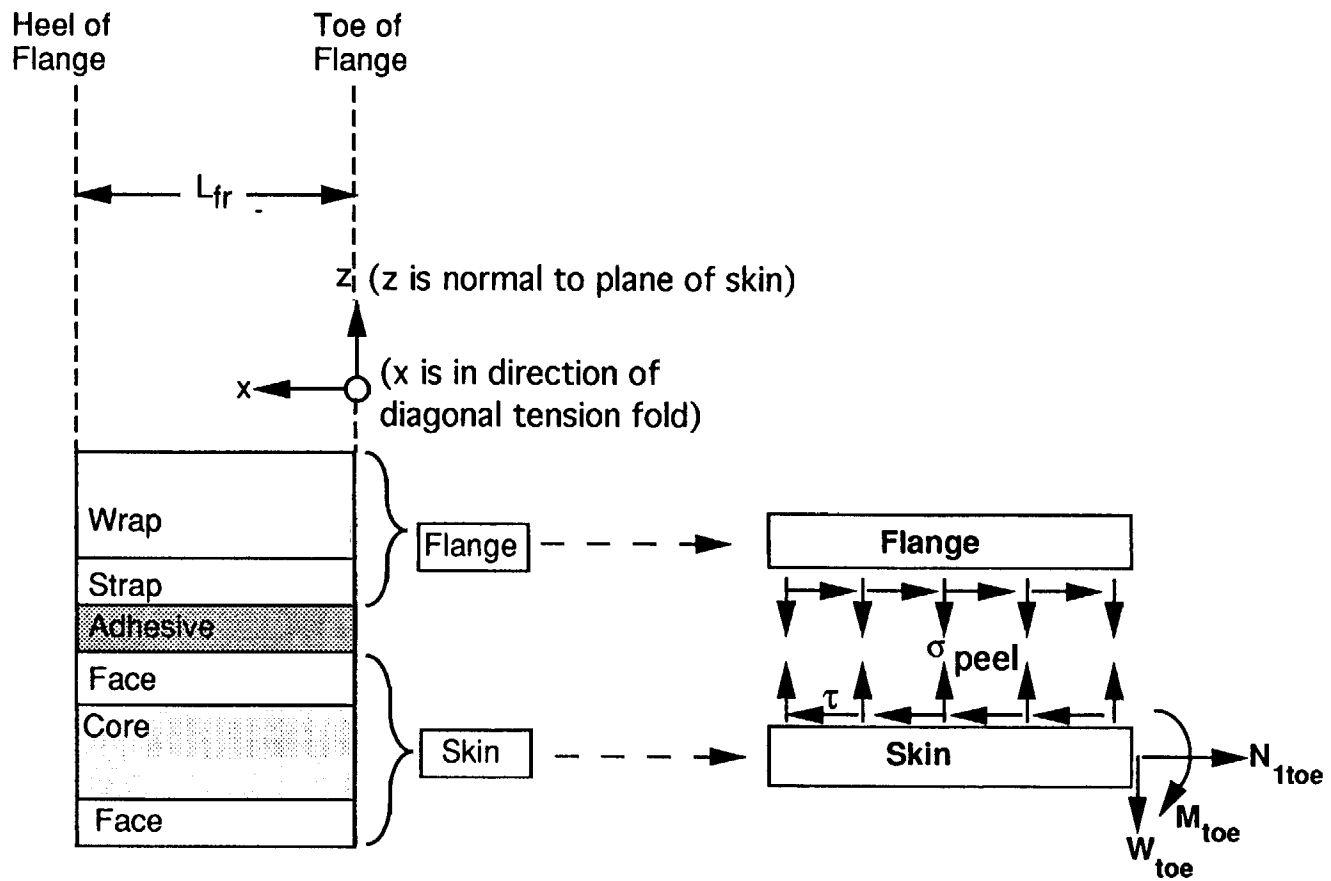

FIGURE 1 THE SKIN AND FLANGE ARE IDEALIZED AS BEAMS COUPLED BY AN ELASTIC FOUNDATION TO DETERMINE THE PEEL STRESS BETWEEN THE SKIN AND THE FLANGE.

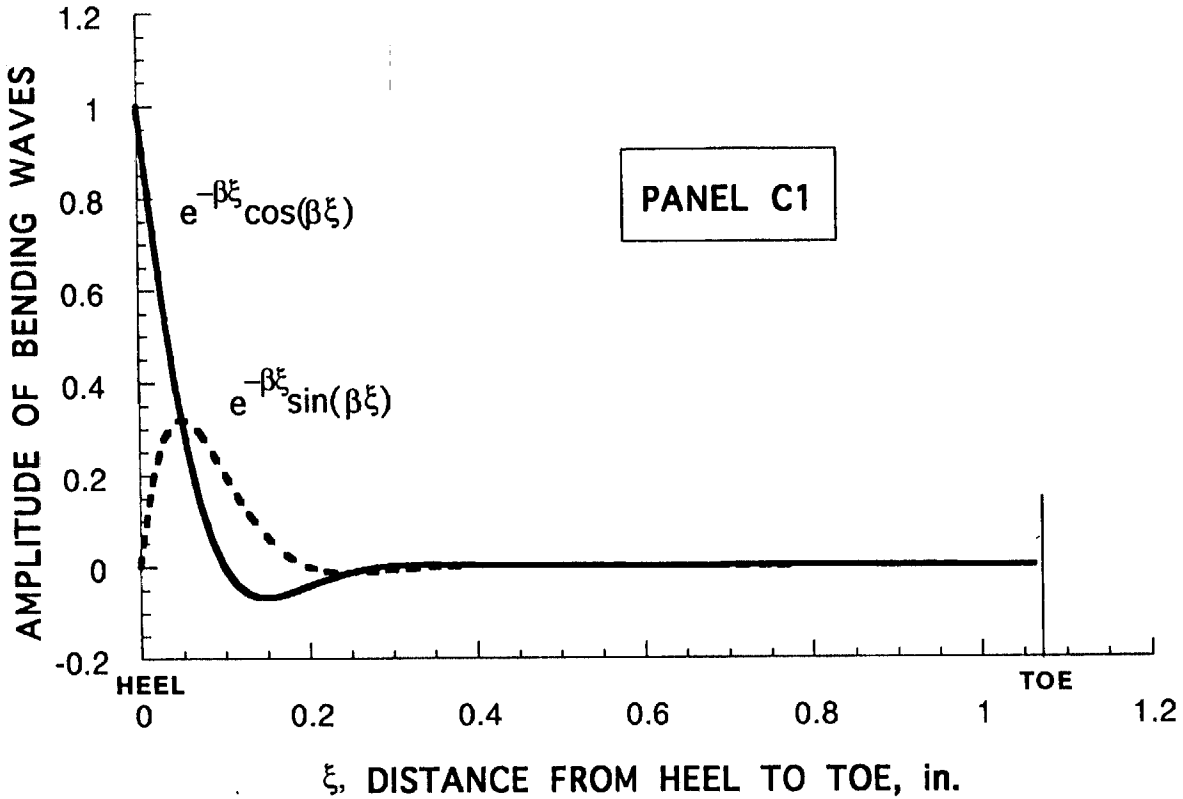

FIGURE 2 THE FLANGE IS LONG ENOUGH SO THAT WAVES EMANATING FROM THE HEEL DIE OUT BEFORE THEY REACH THE TOE (& vice versa). (ILLUSTRATED FOR PANEL C1)

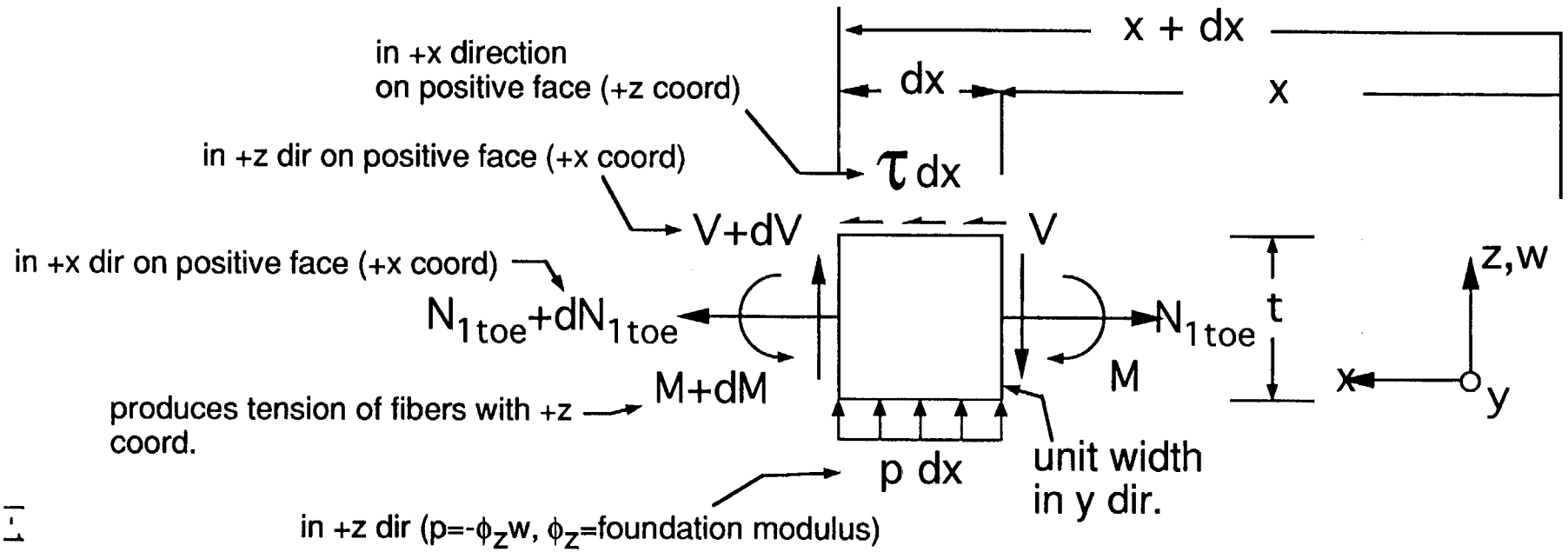

a) Free Body Diagram of Typical Beam Element

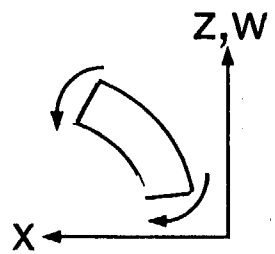

- pos M produces neg curvature

$$\Rightarrow \boxed{M = -D\frac{d^2w}{dx^2}}$$

- moment equilibrium

$$\Rightarrow \boxed{V = \frac{dM}{dx} + \frac{t}{2}\tau = -D\frac{d^3w}{dx^3} + \frac{t}{2}\tau}$$

b) Constitutive Equations

D=bending stiffness about neutral axis

FIGURE 3 NOTATION AND SIGN CONVENTION FOR TYPICAL BEAM ELEMENT

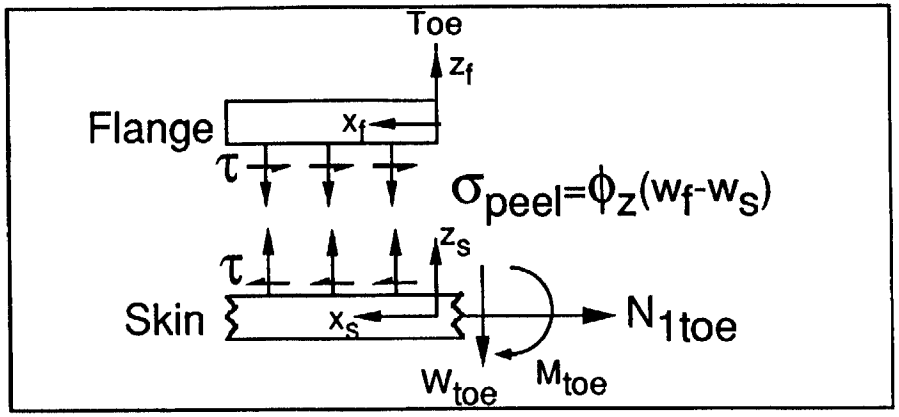

Beam Sign Convention

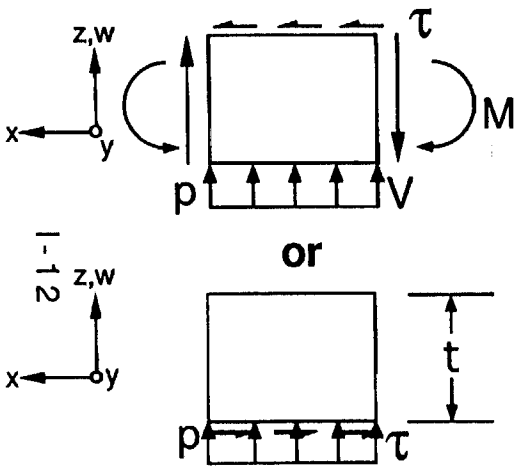

Skin

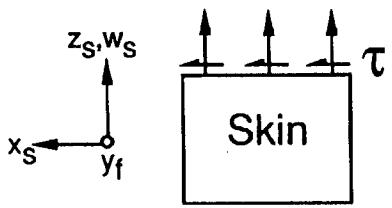

$p=+\phi_z(w_f-w_s)$

$\tau_{BEAM}=+\tau$

Flange

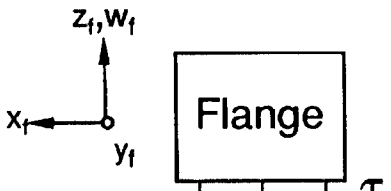

$p=-\phi_z(w_f-w_s)$

$\tau_{BEAM}=+\tau$

$$\text{DE}: D\frac{d^4w}{dx^4}-p-\frac{t}{2}\frac{d\tau}{dx}=0$$

$$D_{sr}\frac{d^4w_s}{dx^4}-\phi_z(w_f-w_s)-\frac{t_s}{2}\frac{d\tau}{dx}=0$$

$$D_{fr}\frac{d^4w_f}{dx^4}+\phi_z(w_f-w_s)-\frac{t_f}{2}\frac{d\tau}{dx}=0$$

BC at Toe:

$$V=+W_{toe}=-D_{sr}\frac{d^3w_s}{dx^3}+\frac{t_s}{2}\tau$$

$$M=+M_{toe}=-D_{sr}\frac{d^2w_s}{dx^2}$$

$$V=0$$

$$M=0$$

FIGURE 4 DIFFERENTIAL RELATIONS AND BOUNDARY CONDITIONS FOR COUPLED BEAM PROBLEM

APPENDIX J

FOUNDATION MODULI

Expressions for the interlaminar shear stress, τ_{xz}, and peel stress, σ_z, between the skin and the attached flange are derived in Appendices H and I, respectively. These expressions contain terms involving two "foundation modulii" corresponding to τ_{xz} and σ_z. A simple model is used in the present appendix to obtain closed-form equations for these modulii. This is done by summing up the flexibilities of the layers between the midplanes of the skin and flange under the assumption that the stresses are uniform between the midplanes. More complex derivations are not justified within the framework of the overall simple approach adopted in this work.

J.1 Foundation Modulus Corresponding to Peel Stress

Figure 1 depicts a cross section of the attached flange and skin. The cross section is in the diagonal tension direction, x, and is in the plane normal to the skin. A peel stress, σ_z, acts in the out-of-plane direction, z, on a unit area. Under the above assumptions, the extension of the midplane distance due to σ_z can be written as:

$$\delta_z = \sigma_z \left[\frac{1}{2}\left(\frac{t}{E_3}\right)_{flange} + \left(\frac{t}{E}\right)_{adhesive} + \left(\frac{t}{E_3}\right)_{face} + \frac{1}{2}\left(\frac{t}{E}\right)_{core} \right]$$

In this equation, t denotes laminate thickness, E is Young's modulus for the isotropic adhesive and core materials, and E_3 is the out-of-plane modulus for the flange and skin layers. (By assuming transverse isotropy for tape layers, we may take $E_3 = E_2$, where E_2 is the layer transverse modulus).

The foundation modulus corresponding to the peel stress is given by

$$\phi_z = \frac{\sigma_z}{\delta_z} = \frac{1}{\frac{1}{2}\left(\frac{t}{E_3}\right)_{flange} + \left(\frac{t}{E}\right)_{adhesive} + \left(\frac{t}{E_3}\right)_{face} + \frac{1}{2}\left(\frac{t}{E}\right)_{core}} \qquad (1)$$

J.2 Foundation Modulus Corresponding to Interlaminar Shear Stress

The foundation modulus corresponding to the shear stress τ_{xz} is found similarly. The displacement in the x direction of the skin relative to the flange is

$$\delta_x = \tau_{xz}\left[\frac{1}{2}\left(\frac{t}{G_{eff}}\right)_{flange} + \left(\frac{t}{G}\right)_{adhesive} + \left(\frac{t}{G_{eff}}\right)_{face} + \frac{1}{2}\left(\frac{t}{G}\right)_{core}\right]$$

In this equation, G denotes the usual shear modulus for the isotropic adhesive and core materials, and, for the laminates

$$t/G_{eff} = \sum_{i}^{n} t_i/G_{tti}$$

where G_{tti} is a through-the-thickness shear modulus for the i^{th} layer, and the summation is over the number of layers n in the laminate. In the case of tape layers, the values of G_{tti} depend on layer orientation. However, the value of τ_{xz} is not overly sensitive to this variation, and it is simplest to use G_{13} (subscript "1" pertains to the fiber direction) for all tape layers regardless of orientation. This simplification slightly overestimates the shear stiffness and so overpredicts τ_{xz}. For fabric layers $G_{13} = G_{12}$. Thus, for both tape and fabric layers, we take $G_{eff} = G_{13}$.

The foundation modulus corresponding to the interlaminar shear stress is

$$\phi_{xz} = \frac{\tau_{xz}}{\delta_x} = \frac{1}{\frac{1}{2}\left(\frac{t}{G_{13}}\right)_{flange} + \left(\frac{t}{G}\right)_{adhesive} + \left(\frac{t}{G_{13}}\right)_{face} + \frac{1}{2}\left(\frac{t}{G}\right)_{core}} \qquad (2)$$

J.3 Sensitivity Results

The effect of increasing ϕ_z by 30% for the C1 panel (the most significantly affected panel) is to increase the maximum principal tensile stress at the toe, σ_{mpt}, (used to calculate failure, see Appendix L) by only 1.3%. Increasing ϕ_{xz} for C1 by 30% increases σ_{mpt} by 5.4% The use of the simple formulae given above is therefore justified.

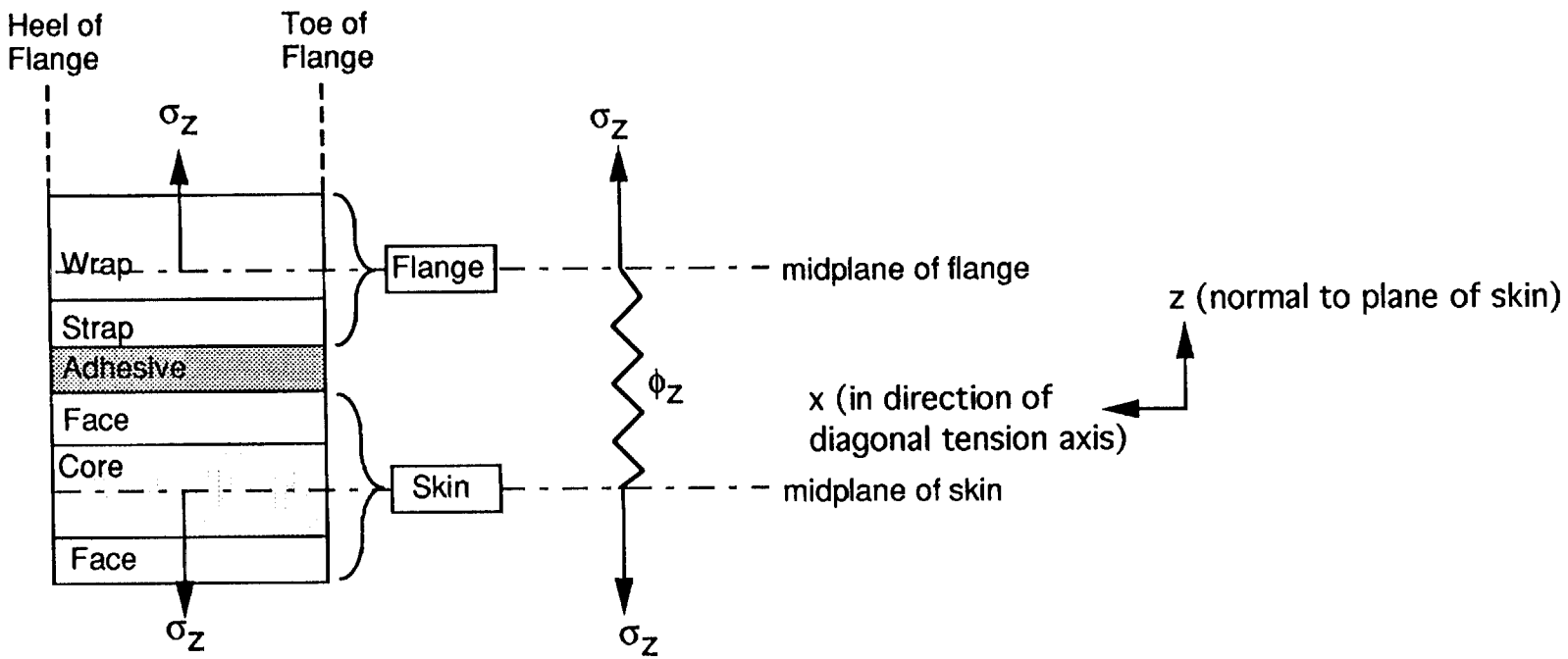

FIGURE 1 SIMPLE MODEL USED TO DETERMINE THE FOUNDATION MODULUS ϕ_z CORRESPONDING TO THE PEEL STRESS σ_z. σ_z ACTS ON A UNIT AREA NORMAL TO THE PLANE OF THE PAPER. (A SIMILAR MODEL IS USED FOR DETERMINING THE FOUNDATION MODULUS ϕ_{XZ} CORRESPONDING TO THE INTERLAMINAR SHEAR STRESS τ_{XZ}).

APPENDIX K

STRESS ANALYSIS OF THE CRITICAL PLY

The objective of this appendix is to determine the surface tension stress at the toe, σ_x, acting in the direction of the diagonal tension fold in the "critical ply" of the skin. The critical ply is defined as follows: it is on the stiffener side of the skin; it is put into tension along the diagonal tension fold by the membrane load, the bending moment, and the transverse shear force acting in the skin at the toe of the flange; and it's fibers lie across the direction of the diagonal tension fold. Finally, to be conservative, i.e., to obtain the highest possible value for σ_x, we assume that the critical ply is at the surface immediately under the toe of the attached flange. The stress σ_x is determined from the strain components derived next.

• Strains

We define a system of inplane axes (x, y) at the middle surface of the skin with the x axis parallel to the direction of the diagonal tension fold, and the y axis being normal to it. Therefore, the strain ε_x in the direction of the diagonal tension fold, on the surface of the skin, is the strain normal to the fiber direction of the "critical" ply. The strain ε_y normal to the diagonal tension fold, in the plane of the skin, on the surface of the skin, is the strain in the direction of the fiber of the "critical" ply.

The internal loads in the skin laminate near the toe are a tensile stress resultant N_{1toe} in the x direction, a compressive stress resultant N_{2toe} in the y direction, a moment M_{toe} about the y axis, and a transverse shear force W_{toe} (see Figure 1 of Appendix I). These loads cause membrane strains e_x and e_y in the midplane of the skin laminate and curvatures κ_x and κ_y. The surface strains in the x and y directions are

$$\varepsilon_x = e_x + \frac{t_s}{2}\kappa_x \tag{1}$$

and

$$\varepsilon_y = e_y + \frac{t_s}{2}\kappa_y \tag{2}$$

where t_s is the skin thickness.

From standard lamination theory [e.g., Grumman Advanced Composite Structures Manual], and with the assumptions that

- the skin laminate is balanced and symmetric,
- the bending/twisting coupling terms are small, and
- the curvature κ_y about the x axis is zero,

it is straight forward to show that curvature about the y axis is therefore

$$\kappa_x = \frac{M_{toe}}{D_{sr}} \tag{3}$$

The surface strains may then be written as

$$\varepsilon_x = \frac{N_{xtoe}}{Et_{sr}} - \nu_{sr}\frac{N_{ytoe}}{Et_{sr}} + \frac{M_{toe}}{D_{sr}}\frac{t_s}{2} \tag{4}$$

$$\varepsilon_y = \frac{N_{ytoe}}{Et_{sr}} - \nu_{sr}\frac{N_{xtoe}}{Et_{sr}} \tag{5}$$

In these equations, N_{xtoe} and N_{ytoe} are the stress resultants in the skin near the toe (see Figure 1 of Appendix B). The skin laminate properties are relative to the diagonal tension axis system, with subscript "r" pertaining to the "rotated" axis system (x, y), which makes an angle of 45° relative to the structural axis system. Et_{sr} is the skin membrane stiffness in the x direction, D_{sr} is the neutral axis bending stiffness of the skin about the y axis, and ν_{sr} is Poisson's ratio for the skin laminate. ($\nu_{sr} = \nu_{xy}$ is defined according to $\nu_{xy} E_y = \nu_{yx} E_x$, where E_x and E_y are engineering constants for the skin laminate).

- Stress

The stress σ_x in the critical ply, in the direction of the diagonal tension fold, and therefore normal to the fiber direction, is related to the above strains by

$$\sigma_x = \frac{E_2}{(1-\nu_{12}\nu_{21})}(\varepsilon_x + \nu_{12}\varepsilon_y) \tag{6}$$

where E_1, E_2, and ν_{12} are the in-plane Young's modulii and Poissons ratio for the face ply of the skin. The subscript "1" when affixed to a material property pertains to the fiber direction, and the Poisson's ratio ν_{12} is defined according to $\nu_{12} E_2 = \nu_{21} E_1$.

Substituting Eqs. (4) and (5) into Eq. (6), and recalling that the stress resultants in the skin at the toe are defined in Appendix C as

$N_{xtoe} = N_{1toe} = q$ (i.e., N_{xtoe} is tensile, and $q>0$)

and

$N_{ytoe} = -N_{2toe} = -q$ (i.e., N_{ytoe} is compressive, and $q>0$),

we can write the equation for σ_x as

$$\sigma_x = \frac{E_2}{(1-\nu_{12}\nu_{21})}\left\{(1-\nu_{12})(1+\nu_{sr})\frac{q}{Et_{sr}} + \frac{t_s}{2}\frac{M_{toe}}{D_{sr}}\right\} \qquad (7)$$

APPENDIX L

FAILURE CRITERION

Previous appendices describe a method whereby the state of stress in the critical ply under the toe of the stiffener flange may be rapidly, if approximately, estimated. It remains to develop a failure criterion for this ply in order to estimate the failing strength of the stiffened panel.

- **Maximum Principal Tensile Stress**

The three stress components τ_{xz}, σ_z and σ_x , derived in appendices H, I and K respectively, are combined to give the following maximum principal tensile stress in the surface ply immediately under the toe of the attached flange:

$$\sigma_{mpt} = \left(\frac{\sigma_z+\sigma_x}{2}\right) + \sqrt{\left(\frac{\sigma_z-\sigma_x}{2}\right)^2 + (\tau_{xz})^2} \qquad (1)$$

- **Failure Criterion**

Examination of photomicrographs of ply cross sections shows that for graphite/epoxy the placing of the fibers within such a section is random, and it is impossible to discern the orientation of the photographed section within the ply without other, external, clues. We may therefore assume transverse isotropy, and that the tensile strength at any orientation in the xz plane is equal to the transverse tensile strength F_2^{tu} of the layer, which can be more-or-less readily found from coupon tests on a laminate consisting of all 90° plies.

Failure is assumed to occur when the maximum principal tensile stress, from Eq. (1), in the critical layer in the skin immediately under the toe reaches the transverse tensile strength F_2^{tu} of the layer, i.e. when

$$\sigma_{mpt} = F_2^{tu} \qquad (2)$$

Failure of this layer constitutes failure of the joint, because cracking of the matrix allows the fibers to be pulled out of the skin surface. This type of failure was observed on all of the panels tested.

The following values used in the analysis of the test panels are based on statistical analysis of 19 coupon test results for transverse

tension of IM6/3501-6 graphite/epoxy tape, in the room temperature, ambient, moisture ("dry") condition [Shyprykevich, 1988]:

F_2^{tu} = Mean strength = 7150 psi
Standard Deviation = 1180 psi
"B-basis" allowable stress = 4460 psi

where the B-basis allowable strength is such that at least 90% of the transverse tensile strengths are expected to exceed the B-basis allowable value, with a confidence of 95%.

APPENDIX M

THE SNAPPS CODE

A Preliminary Design Code for Predicting the Nonlinear Response & Stiffener Separation of Postbuckled, Flat, Composite Shear Panels with Sandwich & Non-Sandwich Skins, Based on a Simplified Analysis Method

The analysis methodology described previously in this report is based on a number of modular "strength-of-materials-type" models. These models are used to derive simple, closed-form equations that can easily be used in a "hand analysis". For expediency, they have been programmed into a *preliminary design* code called SNAPPS using the True Basic language. Being such a simple language, True Basic readily permits users to modify SNAPPS to suit their individual needs such as, for instance, to echo more input data or to provide more output. Alternatively, because SNAPPS requires a minimum of input data, and consists of only a relatively small number of executable statements (less than four dozen) of coding of the equations, it should be an easy task for users to program SNAPPS in another language or spreadsheeet (such as MicroSoft Excel) of their choice.

The next portion of this appendix gives a listing of the True Basic code. This listing also serves as a self-contained "User's Guide" that has many annotations, along with cross-references to other appendices for further details. Also provided is the input data for three tested shear panels (A1, B1, C1), which are the sample problems. These panels are described fully in Appendix A, and are used in Section 3 to compare predicted and measured results. SNAPPS output for the test panels are presented in the remaining portions of the current appendix.

```
!M.1 SNAPPS Code Listing & "User'S Guide"
!
!
!  @@@@@@@@@@@@@@@@@@@@@@@@@@@@@@@@@@@@@@@@@@@@@@@@@@@@@@@@@@@@@@@@@@@@@@
!  @@               SNAPPS (Version 1.0, April 1997)                   @@
!  @@     (Speedy Nonlnear Analysis of Postbuckled Panels in Shear)    @@
!  @@                   BY DAVE SHARP & LARRY SOBEL                    @@
!  @@                                                                  @@
!  @@ A SIMPLIFIED ANALYSIS, PRELIMINARY DESIGN CODE FOR RAPIDLY       @@
!  @@ PREDICTING THE NONLINEAR RESPONSE & STIFFENER SEPARATION         @@
!  @@ OF POSTBUCKLED, FLAT, COMPOSITE SHEAR PANELS WITH SANDWICH       @@
!  @@ OR NON-SANDWICH SKINS                                            @@
!  @@@@@@@@@@@@@@@@@@@@@@@@@@@@@@@@@@@@@@@@@@@@@@@@@@@@@@@@@@@@@@@@@@@@@@
!
!--------------------------------------------------------------------------------
!
!*************************************************************
!******************DIMENSION & DATA STATEMENTS **************
!**********FOR GETTING RESPONSES FOR DIFF VALUES  of q *******
!*************************************************************
!   The argument in the following dimension statements is the number
!   of values of the shear flow, q. Response variables, such as stresses,
!   are computed for each value of q. The argument can be one,
!   if results for just one value of q are desired.
DIM q(30), qratio(30), c(30),Lb(30), Delta(30), Mtoe(30), Wtoe(30)
DIM N1(30), Lambda(30), ThetaTierodDeg(30), DeltaThetaDeg(30)
DIM SIGzTOE(30), TAUxzTOE(30), SIGxTOE(30), SIGmptTOE(30), STRAINx(30),STRAINy(30)
DIM STRAINxMICRO(30), STRAINyMICRO(30)
!--------------------------------------------------------------------------------
!
!*************************************************************
!******************READ IN VALUES OF SHEAR FLOW, q **********
!*************************************************************
!
MAT READ q                     ! NOTE: q must always be positive (App. C)
!DATA 634,700,791.2,800,850,900,950,1000,1050,1100,1149,1200,1300,1403,1500      !A1
!DATA 1550,1600,1650,1700,1750,1800,1850,1900,1950,2000,2050,2100,2150,2200,2250 !A1
!DATA 302,325,350,375,400,425,451.14,500,550,600,650,700,735,750,800,838,850     !B1
!DATA 900,950,1000,1050,1100,1150,1200,1250,1300,1350,1400,1450,1500             !B1
DATA 63.5,70,75,80,85,90,95,100,150,200,250,300,350,400,467.8,500,550           !C1
DATA 600,650,700,750,800,850,900,950,962,1000,1050,1100,1199                    !C1
!--------------------------------------------------------------------------------
!
!*************************************************************
!****************** READ IN REST OF INPUT DATA **************
!*************************************************************
!
!###############################################################################
!#                    COMMENT ON AXIS NOTATION (App. C)                        #
!#    The long (tension) direction of the diagonal tension (DT) fold is denoted #
!#    by x, and the in-plane direction normal to the DT fold is denoted by y.   #
!#    Most input laminate stiffness properties are referred to the DT x axis.  #
!#    These properties are called "rotated" properties, and are subscripted    #
!#    by "r" to so designate them (rather than use double subscripts "xy").    #
!#    For example, Dsr is the bending stiffness of the skin IN the DT          #
!#    direction (which is the x axis), or eqivalently, ABOUT the y axis.       #
!###############################################################################
!
READ qcr,btt,Lf
!                          qcr=Initial buckling value of shear flow
!                            qcr is always positive (see App. C).
!                          btt=Tot-to-Toe Width of Skin, measured normal
!                            to the direction of the stiffener
!                            (See Figure 1 of App. D).
!                          Lf=the heel-to-toe width of the attached flange,
!                            measured normal to the stiffener direction.
!                            (See Figure 1 of App. D).
READ tf,ts,tc,ta           ! Thicknesses for flange, skin, core, & adhesive.
READ E3f,E3faceply,Ec,Ea   ! Out-of-plane Young's Modulii for flange ply,
```

```
!                          face ply of skin, core, & adhesive.
!                          (E3 is in dir normal to plane of skin).
READ G13f,G13faceply,Gc,Ga ! Out-of-plane Shear Modulii for flange ply,
!                          face ply of skin, core, & adhesive.
!                          ("1" pertains to fiber direction).
READ E1faceply,E2faceply,NU12faceply
!                           In-plane Young's Modulii and Poisson's Ratio for face
!                           ply of skin (NU12 defined according to NU12E2=NU21E1.
!                           Thus, if E1>E2, then NU12 is the major Poisson ratio).
READ Gt,Etfr,Etsr,NUsr
!                         Gt=Skin shear stiffness in the global, structural axis
!                           system, x' ,y' (App. C). This system is
!                           parallel and normal to the stiffener direction.
!                         Etfr=rotated membrane stiffness of flange.
!                         Etsr=rotated membrane stiffness of skin.
!                              EA for a laminate is computed as follows:
!                                 • EA=(engineering constant for laminate)*
!                                      (laminate thickness)*(unit width)
!                         NUsr= rotated Poisson's ratio relative to DT direction.
!                          (NUsr=NUxy defined according to NUxyEy=NUyxEx).
READ Dfr,Dsr,Dtotr
!                         Dfr=rotated bending stiffness of flange
!                         about neutral axis.
!                         Dsr=rotated bending stiffness of skin
!                         about middle surface.
!                         Dtotr=rotated bending stiffness of combined (total)
!                         skin and flange laminates
!                         about neutral axis of total stack.
!-------------------------------------------------------------------------
!A1 Data, qfailtrest = 1403, qpred=1149, qallow=791.2
!DATA 634,9.5,0.75                        ! qcr,btt,Lf
!DATA 0.072,0.1172,0.050,0.008          ! tf,ts,tc,ta
!DATA 1.60E6,1.30E6,0.38E6,0.30E6       ! E3f,E3faceply,Ec,Ea
!DATA 0.64E6,0.80E6,0.15E6,0.12E6       ! G13f,G13faceply,Gc,Ga
!DATA 20.5E6,1.30E6,0.35                ! E1faceply,E2faceply,NU12faceply
!DATA 0.2612E6,0.4658E6,0.6302E6,0.206 ! Gt,Etfr,Etsr,NUsr
!DATA 248.1,1215,4574                   ! Dfr,Dsr,Dtotr
!B1 Data, qfailtest = 838, qpred=735.0, qallow=451.14
!DATA 302,9.5,0.75                        ! qcr,btt,Lf
!DATA 0.0576,0.0848,0.040,0.008         ! tf,ts,tc,ta
!DATA 1.60E6,1.30E6,0.38E6,0.30E6       ! E3f,E3faceply,Ec,Ea
!DATA 0.64E6,0.80E6,0.15E6,0.12E6       ! G13f,G13faceply,Gc,Ga
!DATA 20.5E6,1.30E6,0.35                ! E1faceply,E2faceply,NU12faceply
!DATA 0.1418E6,0.4080E6,0.3702E6,0.305 ! Gt,Etfr,Etsr,NUs
!DATA 132.5,479.9,1961                  ! Dfr,Dsr,Dtotr
!C1 Data, qfailtest= 962, qpred= 1199, qallow=467.8
DATA 63.5,15.5,0.75                      ! qcr,btt,Lf
DATA 0.0432,0.0648,0.020,0.008         ! tf,ts,tc,ta
DATA 1.60E6,1.30E6,0.38E6,0.30E6       ! E3f,E3faceply,Ec,Ea
DATA 0.64E6,0.80E6,0.15E6,0.12E6       ! G13f,G13faceply,Gc,Ga
DATA 20.5E6,1.30E6,0.35                ! E1faceply,E2faceply,NU12faceply
DATA 0.1388E6,0.3454E6,0.3626E6,0.306  ! Gt,Etfr,Etsr,NUsr
DATA 58.5,249,1038                     ! Dfr,Dsr,Dtotr
!-------------------------------------------------------------------------
PRINT
PRINT  "&&&&&&&&&&&&&&&&&&&&&&&&&&&&&&&&&&&&&&&&&&&&&&&&&&&&&&&&&&&&&&&&&&"
PRINT  "&&&&&&&&&&&&&&&&     SNAPPS ANALYSIS OF PANEL C1     &&&&&&&&&&&&&&&"
PRINT  "&&&&&&&&&&&&&&&&     (Version 1.0, April 1997)       &&&&&&&&&&&&&&&"
PRINT  "&&&&&&&&&&&&&&&&&&&&&&&&&&&&&&&&&&&&&&&&&&&&&&&&&&&&&&&&&&&&&&&&&&"
PRINT
PRINT
PRINT "************************************************"
PRINT "************* ECHO  SELECTED INPUT  **************"
PRINT "************************************************"
PRINT
PRINT "Initial Buckling Shear Flow, qcr                ";qcr;"lb/in."
PRINT "Toe-to-Toe Width of Skin, btt                   ";btt;"in."
PRINT "Flange Width (normal to stiff dir.), Lf         ";Lf;"in."
PRINT "Thickness of Flange, tf                         ";tf;"in."
```

```
PRINT "Thickness of Skin, ts                                    ";ts;"in."
PRINT "Thickness of Core, tc                                    ";tc;"in."
PRINT "Thickness of Adhesive, ta                                ";ta;"in."
PRINT "Shear Stiff of Skin relative to global axes, Gt";Gt;"lb"
PRINT "Memb Stiff of Flange in dir of DT fold, Etfr   ";Etfr;"lb"
PRINT "Memb Stiff of Skin in dir of DT fold, Etsr     ";Etsr;"lb"
PRINT "Bend Stiff of Flange in dir of DT fold, Dfr    ";Dfr;"lb-in."
PRINT "Bend Stiff of Skin in dir of DT fold, Dsr      ";Dsr;"lb-in."
PRINT
!-------------------------------------------------------------------------
!
!*************************************************************
!******** Compute Geometric Variables (independent of q) *****
!*************************************************************
!
LET cosdt = 1/sqr(2)          ! Assumed angle of diagonal tension is 45°
LET L = btt/cosdt             ! L = toe-to-toe length of buckle in direction of
!                             diagonal tension fold.
LET Lfr = Lf/cosdt            ! Lfr is width of flange in direction of
!                             diagonal tension fold.
!-------------------------------------------------------------------------
!
!*************************************************************
!**********GET RESPONSES FOR DIFF VALUES OF q ****************
!*************************************************************
!
!-------------------------------------------------------------------------
! The upper range for the index i in the following "DO" LOOP must be the same as
!      the DIMENSION statement for q. The upper range can be one,
!      if results for just one value of q are desired (change
!      DIMENSION & MATRIX DATA statements accordingly).
!         ##########################################################
!         #       CHANGE UPPER RANGE OF INDEX FOR i                #
!         #       TO MAKE IT EQUAL TO THE NUMBER OF q VALUES       #
!         ##########################################################
!                                  |
   FOR i =1 to 30 step 1 !         |
!                |                 |
!                |_________________|
!
! ******************** STRESS RESULTANTS N1, N2, (App. C)**************************
!
LET qratio(i) = q(i)/qcr                ! Computed for printout only
LET N1(i) = 2*q(i)-qcr ! N1 is the diagonal tension pull in the direction of
!                        the DT fold.
LET N2 = qcr           ! N2 is the compressive resultant normal to the fold.
!                        Recall that qcr is always positive.  Thus, N2 is positive
!                        when it is in compression.
!
! ******** WAVEWIDTH c & WAVELENTH Lb, (App. D); Max Disp, Delta (App. E)*********
!
LET c(i) = sqr(1.5)*L*sqr(N2/N1(i))/(1+sqr(N2/N1(i)))  ! c is width of DT fold.
LET Lb(i) = c(i)/cosdt       ! Lb is axial wavelength, computed for printout.
LET Delta(i) = (2/pi)*sqr(c(i)*L*(q(i)/Gt-qcr/Gt))     ! Max out-of-plane disp.
! ****BENDING MOMENT Mtoe, & TRANSVERSE SHEAR FORCE AT TOE, Wtoe (App. G)********
LET Lambda(i) = sqr(N1(i)/Dsr)
LET ztotr = (Etfr*(ts+ta+tf/2) + Etsr*ts/2)/(Etfr+Etsr)
!        ztotr is distance of neutral axis of skin + flange model
!        from skin outer face (skin side of panel).
LET z = ztotr - ts/2
!        z is "eccentricity" distance from middle surface of skin to
!        neutral axis of skin + flange model.
LET NUM = (pi*Delta(i)/L)*((N1(i)*Lfr^2)/(2*Dtotr)-1.0)-(q(i)*Lfr*z)/Dtotr
LET DEN = Lambda(i)/N1(i) + Lfr/Dtotr + pi/(N1(i)*L)*((N1(i)*Lfr^2)/(2*Dtotr)-1.0)
LET Mbar = NUM/DEN ! moment on tierod at toe
LET Wtoe(i)= (pi/L)*(N1(i)*Delta(i)-Mbar)
LET Mtoe(i) = -Mbar
!
! ******************** ROTATION AT TOE, Theta (for printout), (App. G) ***********
```

```
!
LET ThetaFlangeRad = -(Mbar+q(i)*z)*Lfr/Dtotr+(Wtoe(i)*Lfr^2)/(2*Dtotr)
LET ThetaTierodRad = (Lambda(i)*Mbar)/N1(i)+Wtoe(i)/N1(i)
LET ThetaFlangeDeg = (180/pi)*ThetaFlangeRad
LET ThetaTierodDeg(i) = (180/pi)*ThetaTierodRad
LET DeltaThetaDeg(i) = ThetaFlangeDeg - ThetaTierodDeg(i) ! check on compatibility
!
! ***************** INTERLAMINAR SHEAR STRESS AT TOE, TAUxzTOE (App. H) *************
!
LET tface=0.5*(ts-tc)  ! Thickness of face sheet. (This equation applies to
!                        laminates without a core in which case
!                        the "face" thickness is half the skin thickness).
LET Phixz=1/[0.5*(tf/G13f)+(ta/Ga)+(tface/G13faceply)+0.5*(tc/Gc)]
!    Phixz is foundation modulus corresponding to shear stress (App. J).
LET K = sqr(Phixz*(1/Etfr+1/Etsr))
LET TAUxzTOE(i) = q(i)*K*Etfr/(Etfr+Etsr)        !In DT axex.
!
! ********************* PEEL STRESS AT TOE, SIGzTOE (App. I) ***********************
!
LET Phiz=1/[0.5*(tf/E3f)+(ta/Ea)+(tface/E3faceply)+0.5*(tc/Ec)]
!     Phiz is foundation modulus corresponding to Peel Stress (App. J)
LET Beta = (Phiz*(Dsr+Dfr)/4/Dsr/Dfr)^0.25
LET SIGz1 = 2*Beta*(Wtoe(i)+Beta*Mtoe(i))/(1+Dsr/Dfr)
!                              SIGz1 = Peel Stress due to Mtoe & Wtoe
LET Cn = q(i)*K^2*Etfr/2/Phiz/(Etsr+Etfr)
LET mstar = (Phiz/Dsr/Dfr/K^4)*(Dsr*K^4+Phiz*(1+ts/tf))/(K^4+4*Beta^4)
LET F1 = (1-K^2/2/Beta^2+K^3/2/Beta^3)*(mstar*K^4*Dfr/Phiz-1)
LET F2 = 2*Beta*Dfr*(Dsr/Dfr-ts/tf)/K/(Dfr+Dsr)
LET SIGz2 = Cn*tf*Phiz*(F1+F2)    ! Peel Stress due to shear stress.
LET SIGzTOE(i) = SIGz1 + SIGz2      ! Total Peel Stress.
!
! ********* STRAINS AT TOE IN CRITICAL PLY, STRAINx, STRAINx (App. K) *************
!
! In what follows, (1) the x axis is in the direction of the DT fold, (2) the
! in-plane y axis is in the direction normal to the direction of the DT fold,
! and (3) the CRITICAL PLY is defined as follows:  its fibers are normal to the
! direction of the DT fold, it is the outermost skin ply on the stiffener side
! of the skin, and it is conservatively assumed to be at the surface of the skin.
LET STRAINx(i) = q(i)/Etsr-NUsr*(-q(i))/Etsr+(Mtoe(i))*ts/2/Dsr
!                              STRAINx is the tension strain in the critical ply.
!                              It is in the direction of the DT fold,
!                              and is normal to the fiber direction.
LET STRAINy(i) = -q(i)/Etsr-q(i)*NUsr/Etsr
!                              STRAINy is the comp strain in the critical ply.
!                              It is in the direction normal to the DT fold,
!                              and it is in the fiber direction.
LET STRAINxMICRO(i)=STRAINx(i)*1.0E6    !in units of microstrain for printout
LET STRAINyMICRO(i)=STRAINy(i)*1.0E6    !in units of microstrain for printout
!
! *************** TENSION STRESS AT TOE IN CRITICAL PLY, SIGxTOE (App. K)***********
!
LET NU21faceply = NU12faceply*(E2faceply/E1faceply)
LET Q22faceply = E2faceply/(1-NU12faceply*NU21faceply)
LET SIGxTOE(i) = Q22faceply*STRAINx(i)+NU12faceply*Q22faceply*STRAINy(i)
!                              SIGxTOE is the  tension stress in the critical ply.
!                              It is in the direction of the DT fold,
!                              and is normal to the fiber direction.
!
! ***************** MAX PRIN TENSION STRESS AT TOE, SIGmptTOE (App. L)**************
!
LET SIGmptTOE1=(SIGzTOE(i)+SIGxTOE(i))/2
LET SIGmptTOE2=SQR(((SIGzTOE(i)-SIGxTOE(i))/2)^2+TAUxzTOE(i)^2)
LET SIGmptTOE(i)=SIGmptTOE1+ SIGmptTOE2
!      SIGmptTOE is the max prin tension stress at the toe of the flange.
!      It acts in a plane in the DT direction that is normal to the skin.
!
!-------------------------------------------------------------------------
   NEXT i
!-------------------------------------------------------------------------
```

```
!
!************************************************************
!******************** PRINT OUTPUT RESULTS ********************
!************************************************************
!
! Note the following output variables (and others not shown) do not depend on q.
! Hence, for maximum efficiency they could have been computed outside the
! DO loop on the q values.  However, this was not done because (1) we prefer to
! compute them in the analysis sections where they belong, and (2) the code
! runs very fast, so it really doesn't matter.
PRINT
PRINT "*****************************************************"
PRINT "*******  SELECTED SCALAR OUTPUT RESULTS   ********"
PRINT "******* (Quantities That Don't Vary with q)********"
PRINT "*****************************************************"
PRINT
PRINT "Toe-to-toe Length of Diagonal Tension Fold     ";L;"in."
PRINT "Thickness of Face                              ";tface;"in."
PRINT "Thru-Thickness Foundation Modulus              ";Phiz;"lb/sq in./in."
PRINT "Interlaminar Shear Foundation Modulus          ";Phixz;"lb/sq in./in."
PRINT "Beta, Die-away Rate for Flatwise Tensile Stress";Beta;"1/in."
PRINT "K, Parameter in Kuhn Shear-lag Analysis        ";K;"1/in."
PRINT
PRINT
PRINT "*****************************************************"
PRINT "*******  SELECTED MATRIX OUTPUT RESULTS   ********"
PRINT "*******  (Quantities That Vary with q)    ********"
PRINT "*****************************************************"
PRINT
PRINT
PRINT "Applied Shear Flow, q, lb/in."
PRINT "-----------------------------"
MAT PRINT q
PRINT "Ratio of Applied Shear Flow to its Critical Value, q/qcr"
PRINT "-------------------------------------------------------"
MAT PRINT qratio
PRINT "Transverse Width of Buckle, c, in."
PRINT "----------------------------------"
MAT PRINT c
PRINT "Buckle Wavelength (projected along stiffener), Lb, in."
PRINT "------------------------------------------------------"
MAT PRINT Lb
PRINT "Maximum Out-of-Plane Displacement of Skin, Delta,in."
PRINT "----------------------------------------------------"
MAT PRINT Delta
PRINT "Axial Load in Tie-Rod model,N1,lb/in."
PRINT "--------------------------------------"
MAT PRINT N1
PRINT "Lambda, Wave Number in Tie-Rod Analysis, 1/in."
PRINT "---------------------------------------------"
MAT PRINT Lambda
PRINT "Skin Bending Moment at Toe, Mtoe, in.-lb/in."
PRINT "--------------------------------------------"
MAT PRINT Mtoe
PRINT "Transverse Shear Force in Skin at Toe, Wtoe, lb/in."
PRINT "---------------------------------------------------"
MAT PRINT Wtoe
PRINT "Rotation at End of Tie-rod Model, ThetaTierodDeg, deg."
PRINT "------------------------------------------------------"
MAT PRINT ThetaTierodDeg
PRINT "Compat. Check: Tie-rod Rotation-Skin/flange Rotation, DeltaThetaDeg, deg."
PRINT "-------------------------------------------------------------------------"
MAT PRINT DeltaThetaDeg
PRINT " In-plane Tens Strain in Critical Ply, STRAINx, micro in."
PRINT "---------------------------------------------------------"
MAT PRINT STRAINxMICRO
PRINT " In-plane Comp Strain in Critical Ply, STRAINy, micro in."
PRINT "---------------------------------------------------------"
MAT PRINT STRAINyMICRO
```

```
PRINT "In-plane Tens Stress in Critical Ply, SIGxTOE, lb/sq in."
PRINT "-------------------------------------------------------"
MAT PRINT SIGxTOE
PRINT "Peel Stress at Toe, SIGzTOE, lb/sq in."
PRINT "--------------------------------------"
MAT PRINT SIGzTOE
PRINT "Shear Lag Stress at Toe, TAUxzTOE, lb/sq in."
PRINT "-------------------------------------------"
MAT PRINT TAUxzTOE
PRINT "Maximum Principal Tensile Stress Under Toe, SIGmptTOE, lb/sq in."
PRINT "-----------------------------------------------------------------"
MAT PRINT SIGmptTOE
!-------------------------------------------------------------------------
END
```

M.2 SNAPPS Output for Panel A1

```
&&&&&&&&&&&&&&&&&&&&&&&&&&&&&&&&&&&&&&&&&&&&&&&&&&&&&&&&&&&&&&&&&&&&&&&&
&&&&&&&&&&&&&&&&      SNAPPS ANALYSIS OF PANEL A1      &&&&&&&&&&&&&&&&
&&&&&&&&&&&&&&&&      (Version 1.0, April 1997)        &&&&&&&&&&&&&&&&
&&&&&&&&&&&&&&&&&&&&&&&&&&&&&&&&&&&&&&&&&&&&&&&&&&&&&&&&&&&&&&&&&&&&&&&&
```

```
************************************************
************* ECHO  SELECTED INPUT  **************
************************************************
```

Initial Buckling Shear Flow, qcr	634 lb/in.
Toe-to-Toe Width of Skin, btt	9.5 in.
Flange Width (normal to stiff dir.), Lf	.75 in.
Thickness of Flange, tf	.072 in.
Thickness of Skin, ts	.1172 in.
Thickness of Core, tc	.05 in.
Thickness of Adhesive, ta	.008 in.
Shear Stiff of Skin relative to global axes, Gt	261200 lb
Memb Stiff of Flange in dir of DT fold, Etfr	465800 lb
Memb Stiff of Skin in dir of DT fold, Etsr	630200 lb
Bend Stiff of Flange in dir of DT fold, Dfr	248.1 lb-in.
Bend Stiff of Skin in dir of DT fold, Dsr	1215 lb-in.

```
************************************************
*******  SELECTED SCALAR OUTPUT RESULTS   ********
******* (Quantities That Don't Vary with q)*******
************************************************
```

Toe-to-toe Length of Diagonal Tension Fold	13.435 in.
Thickness of Face	.0336 in.
Thru-Thickness Foundation Modulus	7.10216e+6 lb/sq in./in.
Interlaminar Shear Foundation Modulus	3.01583e+6 lb/sq in./in.
Beta, Die-away Rate for Flatwise Tensile Stress	9.63497 1/in.
K, Parameter in Kuhn Shear-lag Analysis	3.3556 1/in.

```
************************************************
*******  SELECTED MATRIX OUTPUT RESULTS   ********
*******  (Quantities That Vary with q)    ********
************************************************
```

Applied Shear Flow, q, lb/in.

634	700	791.2	800	850
900	950	1000	1050	1100
1149	1200	1300	1403	1500
1550	1600	1650	1700	1750
1800	1850	1900	1950	2000
2050	2100	2150	2200	2250

Ratio of Applied Shear Flow to its Critical Value, q/qcr

1	1.1041	1.24795	1.26183	1.34069
1.41956	1.49842	1.57729	1.65615	1.73502
1.8123	1.89274	2.05047	2.21293	2.36593
2.44479	2.52366	2.60252	2.68139	2.76025
2.83912	2.91798	2.99685	3.07571	3.15457
3.23344	3.3123	3.39117	3.47003	3.5489

Transverse Width of Buckle, c, in.

8.22724	7.83852	7.4017	7.36427	7.16445
6.98366	6.81882	6.66755	6.52794	6.39846
6.28018	6.16509	5.95972	5.77166	5.61241
5.53612	5.46335	5.39381	5.32727	5.2635
5.2023	5.1435	5.08693	5.03245	4.97993
4.92924	4.88028	4.83295	4.78714	4.74279

Buckle Wavelength (projected along stiffener), Lb, in.

11.6351	11.0853	10.4676	10.4147	10.1321
9.87639	9.64327	9.42933	9.23189	9.04878
8.88152	8.71875	8.42831	8.16236	7.93715
7.82926	7.72634	7.628	7.5339	7.44371
7.35717	7.27401	7.19401	7.11696	7.04269
6.971	6.90176	6.83482	6.77004	6.70731

Maximum Out-of-Plane Displacement of Skin, Delta,in.

0	.103849	.155742	.159636	.17961
.196786	.211939	.225547	.237929	.249312
.259659	.269706	.287649	.304177	.318307
.325135	.331689	.337993	.344068	.349931
.355599	.361085	.366402	.371561	.376574
.381447	.386191	.390812	.395318	.399715

Axial Load in Tie-Rod model,N1,lb/in.

634	766	948.4	966	1066
1166	1266	1366	1466	1566
1664	1766	1966	2172	2366
2466	2566	2666	2766	2866
2966	3066	3166	3266	3366
3466	3566	3666	3766	3866

Lambda, Wave Number in Tie-Rod Analysis, 1/in.

.722365	.794011	.883502	.891662	.936678
.979628	1.02077	1.06032	1.09845	1.13529
1.17028	1.20561	1.27205	1.33703	1.39547
1.42465	1.45325	1.4813	1.50882	1.53585
1.56242	1.58854	1.61424	1.63953	1.66444
1.68899	1.71318	1.73703	1.76056	1.78379

Skin Bending Moment at Toe, Mtoe, in.-lb/in.

6.21677	29.3103	42.4791	43.5241	49.0105
53.893	58.3166	62.3698	66.112	69.5855
72.7592	75.8452	81.3274	86.2848	90.3948
92.3213	94.126	95.8145	97.392	98.8631
100.232	101.503	102.678	103.763	104.759
105.669	106.496	107.242	107.91	108.502

Transverse Shear Force in Skin at Toe, Wtoe, lb/in.

1.4537	25.455	44.472	46.237	56.2317
66.2565	76.3782	86.6284	97.0223	107.566
118.048	129.112	151.256	174.665	197.243
209.074	221.031	233.112	245.313	257.632
270.066	282.611	295.266	308.028	320.894
333.863	346.932	360.098	373.361	386.718

Rotation at End of Tie-rod Model, ThetaTierodDeg, deg.

-.274466	.163239	.419363	.440586	.554935

.661474	.762598	.859706	.953696	1.04517
1.1328	1.22222	1.39315	1.56429	1.72178
1.80177	1.88103	1.95962	2.03759	2.11497
2.1918	2.26811	2.34393	2.41929	2.49421
2.56871	2.64282	2.71654	2.7899	2.86291

Compat. Check: Tie-rod Rotation-Skin/flange Rotation, DeltaThetaDeg, deg.

0	-1.11022e-16	1.11022e-16	1.11022e-16	-2.22045e-16
2.22045e-16	-6.66134e-16	4.44089e-16	5.55112e-16	-8.88178e-16
-4.44089e-16	4.44089e-16	4.44089e-16	-2.22045e-16	-6.66134e-16
8.88178e-16	6.66134e-16	4.44089e-16	4.44089e-16	-8.88178e-16
8.88178e-16	0	0	0	4.44089e-16
-8.88178e-16	-4.44089e-16	0	-4.44089e-16	4.44089e-16

In-plane Tens Strain in Critical Ply, STRAINx, micro in.

1513.11	2753.22	3562.89	3630.13	3990.42
4321.6	4630.63	4921.8	5197.97	5461.19
5708.03	5954.46	6410.24	6846.45	7230.3
7418.9	7601.63	7778.75	7950.51	8117.15
8278.86	8435.82	8588.22	8736.2	8879.92
9019.5	9155.07	9286.76	9414.66	9538.88

In-plane Comp Strain in Critical Ply, STRAINy, micro in.

-1213.27	-1339.57	-1514.1	-1530.94	-1626.63
-1722.31	-1817.99	-1913.68	-2009.36	-2105.05
-2198.82	-2296.41	-2487.78	-2684.89	-2870.52
-2966.2	-3061.89	-3157.57	-3253.25	-3348.94
-3444.62	-3540.3	-3635.99	-3731.67	-3827.36
-3923.04	-4018.72	-4114.41	-4210.09	-4305.78

In-plane Tens Stress in Critical Ply, SIGxTOE, lb/sq in.

1426.08	2992.93	3973.71	4054.08	4482.25
4872.27	5233.28	5570.89	5888.85	6189.83
6470.24	6748.36	7257.75	7738.87	8156.67
8359.89	8555.42	8743.6	8924.77	9099.21
9267.2	9428.98	9584.77	9734.77	9879.19
10018.2	10151.9	10280.6	10404.3	10523.2

Peel Stress at Toe, SIGzTOE, lb/sq in.

490.27	1325.93	1844.36	1887.05	2115.29
2324.62	2519.82	2703.78	2878.42	3045.08
3201.65	3358.27	3648.93	3928.59	4176.1
4298.26	4417.01	4532.5	4644.89	4754.31
4860.89	4964.74	5065.97	5164.67	5260.92
5354.8	5446.4	5535.78	5623.	5708.13

Shear Lag Stress at Toe, TAUxzTOE, lb/sq in.

904.166	998.291	1128.35	1140.9	1212.21
1283.52	1354.82	1426.13	1497.44	1568.74
1638.62	1711.36	1853.97	2000.86	2139.19
2210.5	2281.81	2353.11	2424.42	2495.73
2567.03	2638.34	2709.65	2780.95	2852.26
2923.57	2994.87	3066.18	3137.48	3208.79

Maximum Principal Tensile Stress Under Toe, SIGmptTOE, lb/sq in.

1976.24	3459.93	4460.39	4543.99	4992.9
5406.77	5793.91	6159.45	6506.84	6838.56
7150.25	7462.03	8040.44	8596.52	9088.26

9330.83	9566.51	9795.66	10018.6	10235.6
10446.9	10652.8	10853.4	11049.	11239.9
11426.	11607.7	11785.	11958.1	12127.2

M.3 SNAPPS Output for Panel B1

```
&&&&&&&&&&&&&&&&&&&&&&&&&&&&&&&&&&&&&&&&&&&&&&&&&&&&&&&&&&&&&&&&&&&&&&&&
&&&&&&&&&&&&&&&&      SNAPPS ANALYSIS OF PANEL B1      &&&&&&&&&&&&&&&&
&&&&&&&&&&&&&&&&      (Version 1.0, April 1997)        &&&&&&&&&&&&&&&&
&&&&&&&&&&&&&&&&&&&&&&&&&&&&&&&&&&&&&&&&&&&&&&&&&&&&&&&&&&&&&&&&&&&&&&&&
```

```
************************************************
************* ECHO  SELECTED INPUT  **************
************************************************
```

Initial Buckling Shear Flow, qcr	302 lb/in.
Toe-to-Toe Width of Skin, btt	9.5 in.
Flange Width (normal to stiff dir.), Lf	.75 in.
Thickness of Flange, tf	.0576 in.
Thickness of Skin, ts	.0848 in.
Thickness of Core, tc	.04 in.
Thickness of Adhesive, ta	.008 in.
Shear Stiff of Skin relative to global axes, Gt	141800 lb
Memb Stiff of Flange in dir of DT fold, Etfr	408000 lb
Memb Stiff of Skin in dir of DT fold, Etsr	370200 lb
Bend Stiff of Flange in dir of DT fold, Dfr	132.5 lb-in.
Bend Stiff of Skin in dir of DT fold, Dsr	479.9 lb-in.

```
************************************************
*******  SELECTED SCALAR OUTPUT RESULTS   ********
******* (Quantities That Don't Vary with q)*******
************************************************
```

Toe-to-toe Length of Diagonal Tension Fold	13.435 in.
Thickness of Face	.0224 in.
Thru-Thickness Foundation Modulus	8.73141e+6 lb/sq in./in.
Interlaminar Shear Foundation Modulus	3.663e+6 lb/sq in./in.
Beta, Die-away Rate for Flatwise Tensile Stress	12.0413 1/in.
K, Parameter in Kuhn Shear-lag Analysis	4.34426 1/in.

```
************************************************
*******  SELECTED MATRIX OUTPUT RESULTS   ********
*******  (Quantities That Vary with q)    ********
************************************************
```

Applied Shear Flow, q, lb/in.

302	325	350	375	400
425	451.14	500	550	600
650	700	735	750	800
838	850	900	950	1000
1050	1100	1150	1200	1250
1300	1350	1400	1450	1500

Ratio of Applied Shear Flow to its Critical Value, q/qcr

1	1.07616	1.15894	1.24172	1.3245
1.40728	1.49384	1.65563	1.82119	1.98675
2.15232	2.31788	2.43377	2.48344	2.64901
2.77483	2.81457	2.98013	3.1457	3.31126
3.47682	3.64238	3.80795	3.97351	4.13907
4.30464	4.4702	4.63576	4.80132	4.96689

Transverse Width of Buckle, c, in.

8.22724	7.93576	7.66041	7.41872	7.20381
7.01068	6.82801	6.52883	6.26708	6.0397
5.83934	5.66075	5.54656	5.50004	5.35425
5.252	5.22109	5.09874	4.98575	4.88092
4.78327	4.69197	4.60634	4.52578	4.4498
4.37795	4.30986	4.24519	4.18367	4.12502

Buckle Wavelength (projected along stiffener), Lb, in.

11.6351	11.2229	10.8335	10.4917	10.1877
9.9146	9.65626	9.23315	8.86299	8.54143
8.25808	8.00551	7.84402	7.77823	7.57205
7.42745	7.38373	7.21071	7.05092	6.90266
6.76456	6.63545	6.51435	6.40042	6.29297
6.19136	6.09506	6.00361	5.9166	5.83367

Maximum Out-of-Plane Displacement of Skin, Delta,in.

0	8.37181e-2	.118825	.144207	.164648
.181968	.197745	.222798	.244298	.262892
.27934	.29413	.303681	.307598	.319982
.32878	.331461	.342171	.35222	.361693
.370659	.379176	.387291	.395045	.402472
.409602	.41646	.423069	.429448	.435615

Axial Load in Tie-Rod model,N1,lb/in.

302	348	398	448	498
548	600.28	698	798	898
998	1098	1168	1198	1298
1374	1398	1498	1598	1698
1798	1898	1998	2098	2198
2298	2398	2498	2598	2698

Lambda, Wave Number in Tie-Rod Analysis, 1/in.

.793283	.851558	.910681	.966192	1.01868
1.0686	1.11841	1.20601	1.28951	1.36793
1.44208	1.51261	1.56008	1.57999	1.64461
1.69207	1.70678	1.76677	1.82479	1.88102
1.93562	1.98872	2.04043	2.09087	2.14012
2.18826	2.23537	2.2815	2.32672	2.37108

Skin Bending Moment at Toe, Mtoe, in.-lb/in.

2.7567	10.4579	14.0668	16.8592	19.2241
21.3055	23.2567	26.4384	29.2109	31.5974
33.6624	35.4497	36.553	36.9913	38.3118
39.1797	39.4308	40.364	41.1247	41.7243
42.1723	42.4772	42.6464	42.6866	42.6035
42.4026	42.0887	41.6661	41.1389	40.5107

Transverse Shear Force in Skin at Toe, Wtoe, lb/in.

.644616	9.25799	14.348	19.0492	23.6685
28.2997	33.1951	42.5468	52.4168	62.5919
73.0605	83.8079	91.4888	94.8189	106.079
114.796	117.576	129.296	141.23	153.368
165.7	178.219	190.916	203.786	216.821
230.017	243.367	256.867	270.512	284.298

Rotation at End of Tie-rod Model, ThetaTierodDeg, deg.

-.292593	5.80309e-2	.221353	.352984	.470019

.578464	.685752	.875172	1.05896	1.23581
1.40751	1.57519	1.69058	1.73959	1.90124
2.02249	2.06052	2.21772	2.37309	2.52681
2.67903	2.82988	2.97947	3.12788	3.27521
3.42151	3.56685	3.71128	3.85486	3.99762

Compat. Check: Tie-rod Rotation-Skin/flange Rotation, DeltaThetaDeg, deg.

-1.11022e-16	-6.45317e-16	-1.38778e-16	-3.88578e-16	-6.10623e-16
1.11022e-16	-3.33067e-16	-8.88178e-16	-6.66134e-16	6.66134e-16
2.22045e-16	-4.44089e-16	0	2.22045e-16	8.88178e-16
-4.44089e-16	0	0	4.44089e-16	4.44089e-16
-1.33227e-15	0	8.88178e-16	0	0
-4.44089e-16	-8.88178e-16	8.88178e-16	0	0

In-plane Tens Strain in Critical Ply, STRAINx, micro in.

1308.15	2069.64	2476.62	2811.46	3108.53
3380.55	3645.1	4098.44	4519.65	4906.76
5265.46	5599.63	5820.49	5912.09	6205.02
6415.65	6480.13	6738.84	6982.31	7211.53
7427.37	7630.57	7821.77	8001.58	8170.5
8329.	8477.52	8616.44	8746.12	8866.87

In-plane Comp Strain in Critical Ply, STRAINy, micro in.

-1064.59	-1145.66	-1233.79	-1321.92	-1410.05
-1498.18	-1590.32	-1762.56	-1938.82	-2115.07
-2291.33	-2467.59	-2590.96	-2643.84	-2820.1
-2954.05	-2996.35	-3172.61	-3348.87	-3525.12
-3701.38	-3877.63	-4053.89	-4230.15	-4406.4
-4582.66	-4758.91	-4935.17	-5111.43	-5287.68

In-plane Tens Stress in Critical Ply, SIGxTOE, lb/sq in.

1225.72	2186.24	2679.04	3077.33	3426.13
3742.12	4046.46	4561.44	5032.48	5458.84
5847.97	6204.96	6437.76	6533.52	6836.48
7051.02	7116.11	7374.24	7612.4	7831.9
8033.86	8219.26	8388.95	8543.7	8684.2
8811.04	8924.81	9025.99	9115.06	9192.45

Peel Stress at Toe, SIGzTOE, lb/sq in.

360.01	902.069	1170.22	1385.13	1572.78
1742.71	1906.54	2184.61	2440.4	2673.57
2888.09	3086.64	3217.17	3271.15	3443.09
3566.07	3603.6	3753.64	3893.97	4025.24
4148.01	4262.79	4369.98	4469.97	4563.09
4649.66	4729.93	4804.17	4872.61	4935.44

Shear Lag Stress at Toe, TAUxzTOE, lb/sq in.

687.847	740.233	797.174	854.115	911.056
967.997	1027.53	1138.82	1252.7	1366.58
1480.47	1594.35	1674.06	1708.23	1822.11
1908.66	1935.99	2049.88	2163.76	2277.64
2391.52	2505.4	2619.29	2733.17	2847.05
2960.93	3074.81	3188.69	3302.58	3416.46

Maximum Principal Tensile Stress Under Toe, SIGmptTOE, lb/sq in.

1605.58	2524.06	3022.18	3433.48	3798.98
4133.97	4459.96	5019.	5538.93	6017.35
6461.36	6875.81	7150.29	7264.29	7629.54

7892.96	7973.76	8298.75	8605.99	8896.79
9172.23	9433.28	9680.78	9915.51	10138.1
10349.2	10549.4	10739.2	10919.	11089.2

M.4 SNAPPS Output for Panel C1

```
&&&&&&&&&&&&&&&&&&&&&&&&&&&&&&&&&&&&&&&&&&&&&&&&&&&&&&&&&&&&&&&&&&&&&&&&
&&&&&&&&&&&&&&&&      SNAPPS ANALYSIS OF PANEL C1      &&&&&&&&&&&&&&&&
&&&&&&&&&&&&&&&&      (Version 1.0, April 1997)        &&&&&&&&&&&&&&&&
&&&&&&&&&&&&&&&&&&&&&&&&&&&&&&&&&&&&&&&&&&&&&&&&&&&&&&&&&&&&&&&&&&&&&&&&
```

```
************************************************
************* ECHO  SELECTED INPUT  **************
************************************************
```

Initial Buckling Shear Flow, qcr	63.5 lb/in.
Toe-to-Toe Width of Skin, btt	15.5 in.
Flange Width (normal to stiff dir.), Lf	.75 in.
Thickness of Flange, tf	.0432 in.
Thickness of Skin, ts	.0648 in.
Thickness of Core, tc	.02 in.
Thickness of Adhesive, ta	.008 in.
Shear Stiff of Skin relative to global axes, Gt	138800 lb
Memb Stiff of Flange in dir of DT fold, Etfr	345400 lb
Memb Stiff of Skin in dir of DT fold, Etsr	362600 lb
Bend Stiff of Flange in dir of DT fold, Dfr	58.5 lb-in.
Bend Stiff of Skin in dir of DT fold, Dsr	249 lb-in.

```
************************************************
*******  SELECTED SCALAR OUTPUT RESULTS   ********
******* (Quantities That Don't Vary with q)*******
************************************************
```

Toe-to-toe Length of Diagonal Tension Fold	21.9203 in.
Thickness of Face	.0224 in.
Thru-Thickness Foundation Modulus	1.19455e+7 lb/sq in./in.
Interlaminar Shear Foundation Modulus	5.12601e+6 lb/sq in./in.
Beta, Die-away Rate for Flatwise Tensile Stress	15.8456 1/in.
K, Parameter in Kuhn Shear-lag Analysis	5.38309 1/in.

```
************************************************
*******  SELECTED MATRIX OUTPUT RESULTS   ********
*******  (Quantities That Vary with q)    ********
************************************************
```

Applied Shear Flow, q, lb/in.

63.5	70	75	80	85
90	95	100	150	200
250	300	350	400	467.8
500	550	600	650	700
750	800	850	900	950
962	1000	1050	1100	1199

Ratio of Applied Shear Flow to its Critical Value, q/qcr

1	1.10236	1.1811	1.25984	1.33858
1.41732	1.49606	1.5748	2.3622	3.14961
3.93701	4.72441	5.51181	6.29921	7.36693
7.87402	8.66142	9.44882	10.2362	11.0236
11.811	12.5984	13.3858	14.1732	14.9606
15.1496	15.748	16.5354	17.3228	18.8819

Transverse Width of Buckle, c, in.

13.4234	12.7988	12.3881	12.0241	11.6977
11.4024	11.1332	10.8861	9.16312	8.13046
7.41248	6.87201	6.44424	6.09372	5.70489
5.54649	5.32658	5.13268	4.95991	4.8046
4.66393	4.53567	4.41808	4.3097	4.20938
4.18639	4.11614	4.02916	3.94777	3.80088

Buckle Wavelength (projected along stiffener), Lb, in.

18.9835	18.1003	17.5195	17.0046	16.543
16.1254	15.7447	15.3953	12.9586	11.4982
10.4828	9.71849	9.11354	8.61783	8.06794
7.84393	7.53292	7.2587	7.01437	6.79473
6.59579	6.41441	6.2481	6.09484	5.95296
5.92045	5.8211	5.6981	5.58299	5.37525

Maximum Out-of-Plane Displacement of Skin, Delta,in.

0	.072971	9.54906e-2	.112688	.126875
.139069	.149821	.159475	.225236	.266522
.297461	.322527	.343761	.362279	.384224
.39365	.407263	.419822	.431499	.442422
.452694	.462398	.471601	.480358	.488717
.490668	.496715	.504388	.511764	.525587

Axial Load in Tie-Rod model,N1,lb/in.

63.5	76.5	86.5	96.5	106.5
116.5	126.5	136.5	236.5	336.5
436.5	536.5	636.5	736.5	872.1
936.5	1036.5	1136.5	1236.5	1336.5
1436.5	1536.5	1636.5	1736.5	1836.5
1860.5	1936.5	2036.5	2136.5	2334.5

Lambda, Wave Number in Tie-Rod Analysis, 1/in.

.504995	.554282	.589398	.622535	.653996
.684011	.712764	.7404	.974576	1.1625
1.32401	1.46786	1.59882	1.71983	1.87147
1.93934	2.04026	2.13641	2.22842	2.31678
2.40189	2.48409	2.56365	2.64081	2.71579
2.73348	2.78875	2.85985	2.92922	3.06194

Skin Bending Moment at Toe, Mtoe, in.-lb/in.

.288823	1.88333	2.4554	2.93106	3.35245
3.73731	4.09503	4.43131	7.10387	9.06279
10.5862	11.7862	12.7255	13.4448	14.1185
14.3305	14.5351	14.5998	14.5356	14.3518
14.056	13.6552	13.1552	12.5611	11.8777
11.7008	11.109	10.2588	9.33037	7.27322

Transverse Shear Force in Skin at Toe, Wtoe, lb/in.

4.13938e-2	1.06996	1.53571	1.97858	2.41703
2.85761	3.30313	3.75489	8.65248	14.1524
20.126	26.4885	33.1825	40.1669	50.047
54.8888	62.582	70.4739	78.5507	86.8008
95.214	103.781	112.495	121.349	130.335
132.511	139.449	148.685	158.04	176.892

Rotation at End of Tie-rod Model, ThetaTierodDeg, deg.

-9.42543e-2	1.95239e-2	5.86234e-2	9.13684e-2	.120798

.148156	.174078	.198939	.41893	.615842
.801965	.981229	1.15552	1.32595	1.5521
1.65782	1.82012	1.9804	2.13888	2.29573
2.45109	2.60509	2.75783	2.9094	3.05986
3.09582	3.2093	3.35776	3.5053	3.79489

Compat. Check: Tie-rod Rotation-Skin/flange Rotation, DeltaThetaDeg, deg.

0	-1.07553e-16	6.93889e-18	-1.66533e-16	1.52656e-16
-3.60822e-16	1.11022e-16	-4.44089e-16	5.55112e-17	5.55112e-16
-1.11022e-16	-9.99201e-16	0	0	-8.88178e-16
0	-4.44089e-16	-6.66134e-16	0	8.88178e-16
0	-4.44089e-16	-4.44089e-16	4.44089e-16	0
-8.88178e-16	-4.44089e-16	8.88178e-16	0	0

In-plane Tens Strain in Critical Ply, STRAINx, micro in.

266.294	497.183	589.63	669.532	742.373
810.459	875.015	936.781	1464.62	1899.61
2277.93	2614.16	2916.47	3190.14	3522.02
3665.57	3872.29	4060.8	4232.53	4388.69
4530.3	4658.23	4773.26	4876.05	4967.21
4987.42	5047.28	5116.73	5176.01	5264.91

In-plane Comp Strain in Critical Ply, STRAINy, micro in.

-228.712	-252.124	-270.132	-288.141	-306.15
-324.159	-342.168	-360.177	-540.265	-720.353
-900.441	-1080.53	-1260.62	-1440.71	-1684.91
-1800.88	-1980.97	-2161.06	-2341.15	-2521.24
-2701.32	-2881.41	-3061.5	-3241.59	-3421.68
-3464.9	-3601.77	-3781.85	-3961.94	-4318.52

In-plane Tens Stress in Critical Ply, SIGxTOE, lb/sq in.

244.014	535.784	648.647	745.076	832.251
913.198	989.52	1062.19	1671.17	2158.5
2571.58	2929.52	3243.02	3519.	3841.84
3976.74	4164.99	4329.39	4471.81	4593.83
4696.77	4781.81	4849.93	4902.02	4938.88
4945.53	4961.2	4969.61	4964.7	4917.66

Peel Stress at Toe, SIGzTOE, lb/sq in.

77.9546	241.615	303.021	355.08	401.926
445.295	486.102	524.898	849.204	1108.97
1329.98	1522.44	1691.99	1842.27	2019.72
2094.57	2199.96	2293.18	2375.2	2446.83
2508.76	2561.58	2605.81	2641.89	2670.24
2675.93	2691.21	2705.13	2712.29	2707.55

Shear Lag Stress at Toe, TAUxzTOE, lb/sq in.

166.761	183.831	196.962	210.092	223.223
236.354	249.485	262.616	393.923	525.231
656.539	787.847	919.155	1050.46	1228.52
1313.08	1444.39	1575.69	1707.	1838.31
1969.62	2100.92	2232.23	2363.54	2494.85
2526.36	2626.16	2757.46	2888.77	3148.76

Maximum Principal Tensile Stress Under Toe, SIGmptTOE, lb/sq in.

347.272	624.13	737.862	836.719	927.127
1011.81	1092.21	1169.22	1829.47	2376.19
2854.35	3282.24	3670.12	4024.63	4460.25

4651.14	4929.35	5187.27	5426.7	5649.13
5855.82	6047.87	6226.24	6391.76	6545.17
6580.26	6687.13	6818.24	6939.04	7149.65

REFERENCES

Almroth, B. O., Brogan, F. A., and Stanley, G. M., [1982], "Structural Analysis of General Shells, Vol. II, User's Instructions for STAGSC-1", LMSC-D633873, December 1982.

Cacho-Negrete, C., et al., [1978], "Advanced Composite Wing Cover-To-Substructure Attachment (CTSA) Development Program", Second Quarterly Progress Report, WPAFB Contract No. F-33615-77-C-3071, February 1978.

Cox, B., and Flanagan, G., [1997], "Handbook of Analytical Methods for Textile Composites", NASA Contractor Report 4750, March, 1997.

Dastin, S., [1996], Personal Communication, October, 1996.

Flanagan, G., [1993], "A Sublaminate Analysis Method For Predicting Delamination Loads In Composite Structures", J. of Reinforced Plastics and Composites, Vol. 12, pp. 876-887, August 1993.

Flanagan, G., [1991], "MACLAMINATE", Grumman Aircraft Systems Report.

Flanagan, G., [1988], Personal Communication, September, 1988.

Hetenyi, M., [1946], "Beams on Elastic Foundation", University of Michigan Press, Ann Arbor.

Housner, J. M., and Stein, M., [1975], "Numerical Analysis and Parametric Studies of the Buckling of Composite Orthotropic Compression and Shear Panels", NASA TN D-7996. (1975)

Kuhn, P., Peterson, J. P., and Levin, L.R., [1952], "A Summary of Diagonal Tension. Part I-Methods of Analysis", NACA TN 2661.

Kuhn, P., [1956], "Stresses in Aircraft Structures", McGraw-Hill Book Company, Inc.

Li, J., O'Brien, T. K., and Rousseau, C. Q., [1996], "Test and Analysis of Composite Hat Stringer Pull-off Test Specimens", NASA Technical Memorandum 110263, June 1996.

Minguet, P. J., and O'Brien, T. K., [1996], "Analysis of Test Methods for Characterizing Skin/Stringer Debonding Failures in Reinforced Composite Panels", Composite Materials: Testing and Design (12th Volume), ASTM STP 1274, pp.105-124, American Society for Testing and Materials, 1996.

Minguet, P. J., and O'Brien T. K., [1995], "Analysis of Composite Skin/Stringer Bond Failure Using a Strain Energy Release Rate Approach", Tenth International Conference on Composite Materials. Vancouver, Canada, Volume 1, pp. 245-252, August 1995.

Nemeth, M. P., [1997], "Buckling Behavior of Long Symmetrically Laminated Plates Subjected to Shear and Linearly Varying Axial Edge Loads", NASA Technical Paper 3659, July 1997.

Perry, D. J., [1950], "Aircraft Structures", McGraw-Hill Book Company, Inc.

Ranalli, E. R., and Bunce, F. R., [1977], "The Analyses of Shear Panel Stiffeners with Emphasis on Forced Crippling", Report No. SAR-77-2, Grumman Aerospace Corporation, December, 1977.

Seydel, E., [1933], "Uber das Ausbeulen von rechteckige isotroper oder orthogonal-anisotropen Platten bei Schubbeanspruchung", Ing. Archiv, Bd.4, S. 169-191, 1933.

Sharp, D. and Sobel, L. [1989], "To Extend and Refine the Current Procedures for Disbond Analysis of Buckled, Stiffened Composite Panels", May, 1989.

Sharp, D. [1989], "DISBON Failure Analysis of Composite Shear Panels-Another Approach", Presented at Structural Sciences Technical Review, Grumman Corp., Nov.,1989.

Shyprykevich, P. [1988], "test results, Carbon Materials Allowables Program", Grumman Aerospace Corp. Report C17A-10-RP-022, 1988.

Sobel, L. [1990], "Buckling and Postbuckling Analyses of Stiffened Composite Shear Panels using the STAGSC-1 Computer Code", Report SMR-90-1, Grumman Corp., Oct., 1990.

Sobel, L., and Sharp, D., [1994], "Comparison of Analytical and Experimental Results for the Postbuckling Behavior of a Stiffened, Flat, Composite Shear Panel", Paper Number 94-1365, presented at the 35th Structures, Structural Dynamics and Materials Conference, Hilton Head, South Carolina. April 18-21 1994.

Tsai, H. C., [1983], "Approximate Solution for Skin/Stiffener Separation Including Effect of Interfacial Shear Stiffness in Composite Tension Field Panel", Report No. NADC-83131-60m Nov. 1983.

Timoshenko, S. P., [1956], "Strength of Materials, Part II", 3rd Edition, Robert E. Kreiger Publishing Company.

Timoshenko, S. P., & Gere, J. M., [1961], "Theory of Elastic Stability", 2nd Edition, McGraw-Hill Book Company, Inc.

Visconti, J., [1988], "Empirical Data Base for Postbuckled Damage Tolerant Composite Structures", AD-RDRT-88-1, Grumman Aircraft Systems Division, Nov. 1988,

- Vol. I, "Coupon Test Results"
- Vol. II, "Pull-off and Twist-off Element Test Results"
- Vol. III, "Shear Panel Test Results"

Wang, J. T., Davila, C. G., Sleight, D. W., & Krishnamurthy, T., [1994], "Crown Panel Stiffener-Frame Intersections Structural Integrity Analyses", 5th NASA/DoD Advanced Composites Technology Conference, Seattle, Wa., Aug. 1994.

REPORT DOCUMENTATION PAGE

Form Approved
OMB No. 0704-0188

1. AGENCY USE ONLY *(Leave blank)*	2. REPORT DATE	3. REPORT TYPE AND DATES COVERED
	October 1997	Contractor Report

4. TITLE AND SUBTITLE
Novel Composites for Wing and Fuselage Applications -
Speedy Nonlinear Analysis of Postbuckled Panels in Shear (SNAPPS)

5. FUNDING NUMBERS
C NAS1-18784
TA 6
WU 538-10-11-02

6. AUTHOR(S)
Dave Sharp and Larry Sobel

7. PERFORMING ORGANIZATION NAME(S) AND ADDRESS(ES)
Northrop Grumman Corporation
M/S A01-26
South Oyster Bay Road
Bethpage, NY 11714-3581

8. PERFORMING ORGANIZATION REPORT NUMBER

9. SPONSORING/MONITORING AGENCY NAME(S) AND ADDRESS(ES)
NASA Langley Research Center
Hampton, VA 23681-0001

10. SPONSORING/MONITORING AGENCY REPORT NUMBER
NASA/CR-97-206256

11. SUPPLEMENTARY NOTES
Dave Sharp: Retired Consultant
NASA Langley Technical Monitor: H. Benson Dexter
Final Report: Task 6

12a. DISTRIBUTION/AVAILABILITY STATEMENT
Unclassified - Unlimited
Subject Category 24
Distribution: Nonstandard
Availability: NASA CASI (301) 621-0390

12b. DISTRIBUTION CODE

13. ABSTRACT *(Maximum 200 words)*

A simple and rapid analysis method, consisting of a number of modular, "strength-of-materials-type" models, is presented for predicting the nonlinear response and stiffener separation of postbuckled, flat, composite, shear panels. The analysis determines the maximum principal tensile stress in the skin surface layer under the toe. Failure is said to occur when this stress reaches the mean transverse tensile strength of the layer. The analysis methodology consists of a number of closed-form equations that can easily be used in a "hand analysis". For expediency, they have been programmed into a preliminary design code called SNAPPS [Speedy Nonlinear Analysis of Postbuckled Panels in Shear], which rapidly predicts the postbuckling response of the panel for each value of the applied shear load. SNAPPS response and failure predictions were found to agree well with test results for three panels with widely different geometries, laminates and stiffnesses. Design guidelines are given for increasing the load-carrying capacity of stiffened, composite shear panels.

14. SUBJECT TERMS	15. NUMBER OF PAGES
Postbuckled Shear Panels, Diagonal Tension	144
	16. PRICE CODE A07

17. SECURITY CLASSIFICATION OF REPORT	18. SECURITY CLASSIFICATION OF THIS PAGE	19. SECURITY CLASSIFICATION OF ABSTRACT	20. LIMITATION OF ABSTRACT
Unclassified	Unclassified	Unclassified	